ฟลูออเรสเซนซ์เซ็นเซอร์ชนิดคัดเลือกสูงสำหรับไบโอเจนิกแอมีนและคอปเปอร์ (II) ไอออน

นายอนุศักดิ์ ไชยแจ่ม

วิทยานิพนธ์นี้เป็นส่วนหนึ่งของการศึกษาตามหลักสูตรปริญญาวิทยาศาสตรดุษฎีบัณฑิต
สาขาวิชาเคมี ภาควิชาเคมี
คณะวิทยาศาสตร์ จุฬาลงกรณ์มหาวิทยาลัย
ปีการศึกษา 2559

HIGHLY SELECTIVE FLUORESCENCE SENSORS FOR BIOGENIC AMINES AND COPPER (II) ION

Mr. Anusak Chaicham

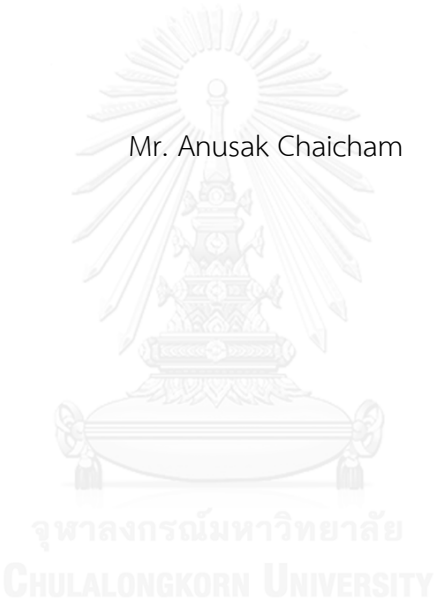

A Dissertation Submitted in Partial Fulfillment of the Requirements
for the Degree of Doctor of Philosophy Program in Chemistry
Department of Chemistry
Faculty of Science
Chulalongkorn University
Academic Year 2016

Thesis Title	HIGHLY SELECTIVE FLUORESCENCE SENSORS FOR BIOGENIC AMINES AND COPPER (II) ION
By	Mr. Anusak Chaicham
Field of Study	Chemistry
Thesis Advisor	Assistant Professor Boosayarat Tomapatanaget, Ph.D.

Accepted by the Faculty of Science, Chulalongkorn University in Partial Fulfillment of the Requirements for the Doctoral Degree

.....Dean of the Faculty of Science
(Associate Professor Polkit Sangvanich, Ph.D.)

THESIS COMMITTEE

.....Chairman
(Associate Professor Vudhichai Parasuk, Ph.D.)

.....Thesis Advisor
(Assistant Professor Boosayarat Tomapatanaget, Ph.D.)

.....Examiner
(Associate Professor Nongnuj Muangsin, Ph.D.)

.....Examiner
(Professor Sanong Ekgasit, Ph.D.)

.....External Examiner
(Professor Sujittra Youngme, Ph.D.)

อนุศักดิ์ ไชยแจ่ม : ฟลูออเรสเซนซ์เซ็นเซอร์ชนิดคัดเลือกสูงสำหรับไบโอเจนิกแอมีนและคอปเปอร์ (II) ไอออน (HIGHLY SELECTIVE FLUORESCENCE SENSORS FOR BIOGENIC AMINES AND COPPER (II) ION) อ.ที่ปรึกษาวิทยานิพนธ์หลัก: ผศ. ดร.บุษยรัตน์ ธรรมพัฒนกิจ, 122 หน้า.

งานวิจัยนี้มีจุดมุ่งหมายเพื่อที่จะออกแบบและสังเคราะห์โมเลกุลเซ็นเซอร์สำหรับตรวจวัดไบโอจินิกเอมีน และสร้างอุปกรณ์ไมโครฟลูอิดิกแบบสามมิติ ในส่วนของการตรวจวัดไบโอจินิกเอมีนได้จำแนกออกเป็น 2 กลุ่ม คือ การตรวจวัดสารจำพวกแคติคอลเอมีน และอีกกลุ่มหนึ่งคือตรวจวัดฮีสตามินและฮีสทิดีน สำหรับการตรวจวัดแคติคอลเอมีนนั้นได้นำเอาโมเลกุลคูมารินแอลดีไฮด์ (CA) และกรดไพรีนโบโรนิก (PBA) มารวมตัวกันโดยมีสารสื่อประสาทเป็นตัวเชื่อม ซึ่งจะเหนี่ยวนำให้เกิด FRET จาก PBA ไปยัง CA ผลการทดลองแสดงให้เห็นว่า DA และ NE สามารถเป็นตัวเชื่อมระหว่าง CA กับ PBA ทำให้เกิดกระบวนการ FRET ในส่วนของการตรวจวัดฮีสทิดีนและฮีสตามิน ผู้วิจัยได้ออกแบบเซ็นเซอร์ที่ประกอบด้วยฮีสตามีนบลู (HB) ที่บรรจุอยู่ในซิลิกาที่มีรูพรุนในระดับนาโน และปรับปรุงพื้นผิวของซิลิกาด้วยฟลูออเรสซีนไอโซไทโอไซยาเนต จากผลการทดลองพบว่าฮีสตามินจะเหนี่ยวนำให้เกิดการเพิ่มขึ้นของสัญญาณฟลูออเรสเซนต์ที่ 525 นาโนเมตร (กระตุ้นที่ 340 นาโนเมตร) โดยเกิดจากการถ่ายโอนพลังงานจาก HB ไปยัง FC แต่จะไม่พบการเปลี่ยนแปลงนี้ในกรณีของฮีสทิดีน เนื่องจากแรงผลักทางไฟฟ้าของหมู่คาร์บอซิลเลตในฮีสทิดีน

ในส่วนของอุปกรณ์ไมโครฟลูอิดิกแบบสามมิติ ผู้วิจัยได้พัฒนาอุปกรณ์ตรวจวัดเชิงปริมาณโดยการใช้ FBA ยึดติดบนกระดาษ งานวิจัยนี้ได้ออกแบบอุปกรณ์ออกเป็น 2 ส่วนคือ ส่วนตรวจวัดและส่วนควบคุม เพื่อใช้กำจัดปัจจัยที่มีผลต่อการเคลื่อนที่ของสารตัวอย่าง เครื่องมือนี้สามารถใช้ตรวจวัดความเข้มข้นของคอปเปอร์ไอออนได้ในช่วง 10-100 ไมโครโมลาร์ และยังถูกนำมาประยุกต์ใช้ในการตรวจวัดไอออน Cu^{2+} ในตัวอย่างเลือด พบว่าได้ร้อยละของผลได้เท่ากับ 103.38%

ภาควิชา เคมี ลายมือชื่อนิสิต .....

สาขาวิชา เคมี ลายมือชื่อ อ.ที่ปรึกษาหลัก .....

ปีการศึกษา 2559

5373929823 : MAJOR CHEMISTRY

KEYWORDS: MOLECULAR SENSOR, BIOGINIC AMINES, 3D MICROFLUICDIC DEVICE, FRET, NANOPOROUS SILICA

ANUSAK CHAICHAM: HIGHLY SELECTIVE FLUORESCENCE SENSORS FOR BIOGENIC AMINES AND COPPER (II) ION. ADVISOR: ASST. PROF. BOOSAYARAT TOMAPATANAGET, Ph.D., 122 pp.

This research aims to design and synthesize the molecular sensors for biogenic amine sensing and fabricate 3D microfluidic device. In the case of biogenic amine, it can be classified into two group, the first group is catecholamine and the second group is histamine and histidine. For catecholamine sensing, coumarin aldehyde (CA) and pyrene boronic acid (PBA) formed intermolecular assembly in the presence of neurotransmitters and induced FRET on process from PBA to CA. The result showed DA and NE performed a guest linker including intermolecular assembly of CA and PBA resulting in FRET on/off process. In the case of histidine and histamine sensing, we designed histamine sensor, consisting of histamine blue (HB) loaded in nanoporous silica modified surface by fluorescein isothiocyanate (FC). The result showed that histamine induced an increasing fluorescent intensity at 525 nm (ex. 340 nm) by energy transfer process from HB to FC. No fluorescence response was observed in the case of histidine due to the electronic repulsion between negative charge on carboxylate based fluorescein dye on the surface and carboxylate group in histidine.

In the case of 3D microfluidic device, we developed the quantitative assay by fabrication of FBA and fluorescein dye on the paper. This research designed the device into two part of assay zone and control zone for normalization the factor of flow-through rate of the sample. This device provided the linear range from 10-100 micro molar of copper ions concentration and it was applied to measure Cu^{2+} ion in blood sample with an acceptable value of 103.38% recovery.

Department: Chemistry Student's Signature .....

Field of Study: Chemistry Advisor's Signature .....

Academic Year: 2016

ACKNOWLEDGEMENTS

The accomplishment of this thesis could not occur without the kindness, personal friendship, encouragement, suggestions, assistance and the extensive supports throughout my Ph. D career from my thesis advisor, Assist. Prof. Dr. Boosayarat Tomapatanaget. In addition, I would like to thank Assoc. Prof. Dr. Vudhichai Parasuk, Assoc. Prof. Dr. Nongnuj Muangsin, Prof. Dr. Sanong Ekgasit and Prof. Dr. Sijittra Youngme for their input, interest, value suggestions and comments as committee members and thesis examiners.

This thesis would not be successful without kindness and helps of a number of people. First, I am grateful to the Scientific and Technological Research Equipment Center of Chulalongkorn University, particularly, Miss Chiraporn Chaicham for synthesis and characterization silica nanoparticles. I would like to express my appreciation to former and the current staffs in the Supramolecular Chemistry Research Unit.

Financial supported by the Thailand Research Fund (TRF), the Commission on Higher Education (CHE) (RSA5680015 and RTA5380003) and the Higher Education Research Promotion and National Research University Project of Thailand, Office of the Higher Education Commission (AM1006A-56), and the Ratchadaphiseksomphot Endowment Fund of Chulalongkorn University (RES560530126-AM), The Royal Golden Jubilee Program (PHD/0235/2552) of the TRF and CHE and National of Center of Excellence for Petroleum, Petrochemical, and Advance Materials (NCE-PPAM).

Finally, I would like to express my deepest gratitude to my family for their love, care, kindness, encouragement and other assistance throughout my life.

CONTENTS

Page

Page

Page

Page

List of Figure

Chapter I

Appendix

List of Table

Chapter I

Introduction and literature reviews

Biogenic amines are biological molecules compose of amine group in their structures which can be functionally classified in two groups. The first group composes of catechol group in the molecules (such as dopamine, epinephrine and norepinephrine) called catecholamines (Figure 1.1) which can be found in a variety of central nervous system functions [1]. Thus their malfunction directly relates to central nerve diseases such as Parkinson's disease [2]. The patient has a low concentration of dopamine in the central nervous system as a result of the death of dopamine-generating cell. Hypertension or high blood pressure results from the high level of epinephrine in the central nervous [3]. The second biogenic amines group composes of imidazole group in their structures to participate enzyme catalyzed reaction. For example, histidine is an essential amino acid for growth and repair of tissues in humans and other mammals [4-6]. However, the high level of histidine caused by deficiency of the enzyme histidase leads to histidinemia disease [7-11]. Moreover, Basophils bacteria can decarboxylate histidine to form a toxic compound of histamine which is an indicator of freshness of seafood [12, 13]. Consequently, the quantitative detection and discrimination of biogenic amines are very important for clinical diagnosis and food industry.

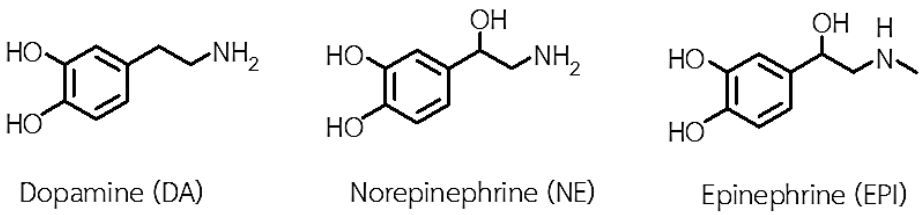

Figure 1.1 Structure of catecholamines

In general, catecholamines have been detected and discriminated from the other biogenic amines by electrochemical technique due to the favorable redox properties of catechol group [14-17]. For detection of histamine and histidine, the chromatographic methods are commonly available for analyzing their concentrations [18-21]. However, there have been only few reports regarding to optical technique for analyzing biogenic amine. Consequently, this research aims to design molecular chemosensor and create new strategy for biogenic amine detection by using fluorescence method.

In order to increase quantitative detection and discrimination of biogenic amines, the technique of Fluorescence Resonance Energy Transfer (FRET) will be applied to sensing purposes. The mechanism of FRET involves an excited energy transfer of donor chromophore to a nearby acceptor chromophore in a non-radiative fashion through long-range dipole-dipole interactions. Thus, the energy transfer requires the overlap of donor emission spectrum and reabsorption spectra of acceptor chromophore (Figure 1.2) and the chromophore molecules concerned must be in close proximity (10 – 100 Å). Moreover, the approximately parallel transition dipole orientations support energy transfer [22, 23].

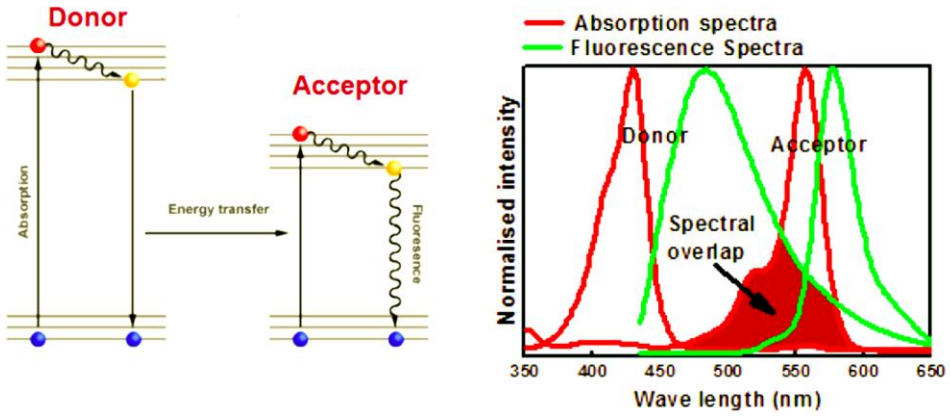

Figure 1.2 Schematic representation of the FRET spectral overlap integral [22, 23]

Concerning about catecholamine molecular sensor, the molecular sensor normally composes of the receptor unit for both ortho-hydroxy (or catechol) and amine group regarding chemical structure of catecholamine (as show in Figure 1.1). The receptor for ortho-hydroxy commonly uses boronic acid because it can form boronate ester under the optimal pH condition [24]. In the second receptor for amine binding, the aldehyde moiety is normally used to form schiff-base with primary amine. Notable examples reported by Secor and co-workers [25] included coumarin derivative containg boronic acid and aldehyde group as a selective sensor for catecholamine (Figure 1.3).

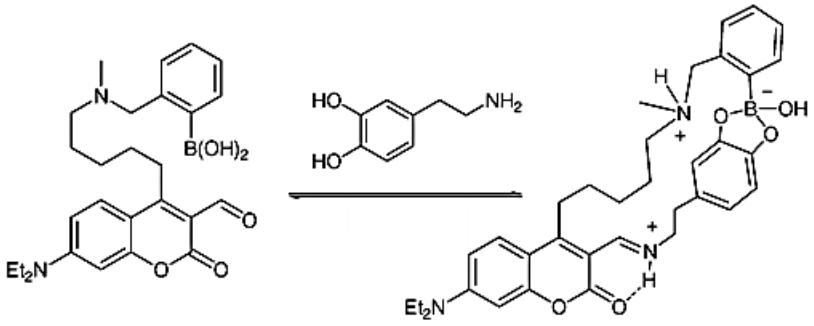

Figure 1.3 The molecular sensor based on cumarin derivative for dopamine detection [25]

Moreover, Jang and coworker synthesized the anthrancene fluorophore bearing boronic acid and aldehyde group as a fluorescence chemosensor for catecholamine as shown in Figure 1.4. Both reported that sensors bind to catecholamine by forming an iminium bond with primary ammonium moiety as well as a boronate ester with catachol moiety. However, the results cannot clearly distinguish type of catecholamine such as epinephrine, dopamine and norepinephine.

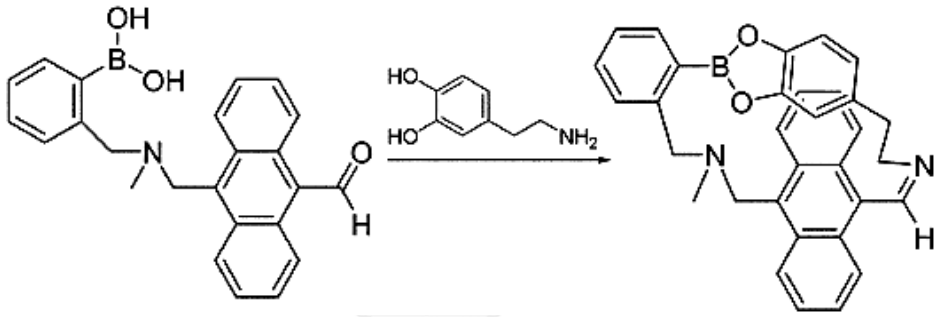

Figure 1.4 The molecular sensor based on antrancene derivative for dopamine detection

In the case of histamine and histidine chemosensor, the metal complex is normally applied to detect via ligand exchange process. Actually, Ni^{2+} [20] and Cu^{2+} [26, 27] can be used to form complex with histidine and histamine with a high association constant. If the metal binds to chromogenic ligand with lower association constant value, histamine and histidine will replace and induce the change in optical properties. For example, Seto and coworkers [28] reported the Nile Res derivative which contains an iminodiatetic acid as a binding unit for metal. This sensor complexed with Ni^{2+} and Cu^{2+} exhibited a high lipophilic character in aqueous. In the part of

sensing of biogenic amines, the fluorescent spectra of Ni^{2+} complex gave a higher selectivity for histamine than Cu^{2+} complex. Compared to other biogenic amines, the Ni^{2+} complex showed significantly spectral change to histamine (as show in Figure 1.5).

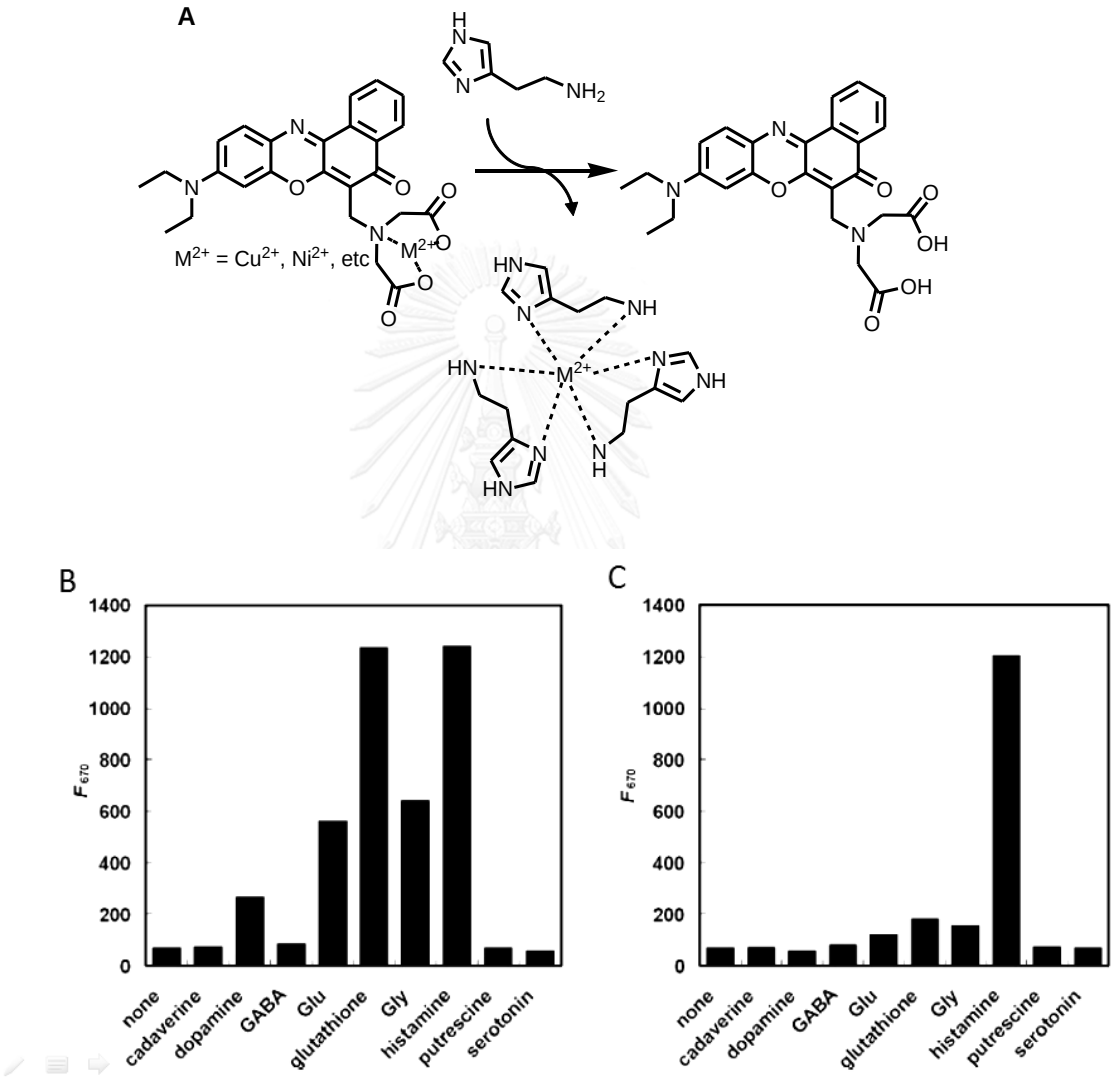

Figure 1.5 Selectivity of copper and nickel complex for histamine (A) Molecular structures of the biogenic amines tested. Fluorescence responses of copper complex (B) and nickel complex (C) to various biogenic amines under excitation wavelength at 600 nm [28]

In the case of histidine sensor, Wu and Yan [29] reported a turn-on photoluminescent sensor for histidine based on Ni^{2+}-modulated homocysteine-capped CdTe quantum dots (DQs). The high affinity and stable complex of histidine with Ni^{2+} in aqueous solution enables Ni^{2+} to dissociate from the surface of CdTe QDs. This process induced the change in photoluminescence of CdTe QDs as shown in Figure 1.6.

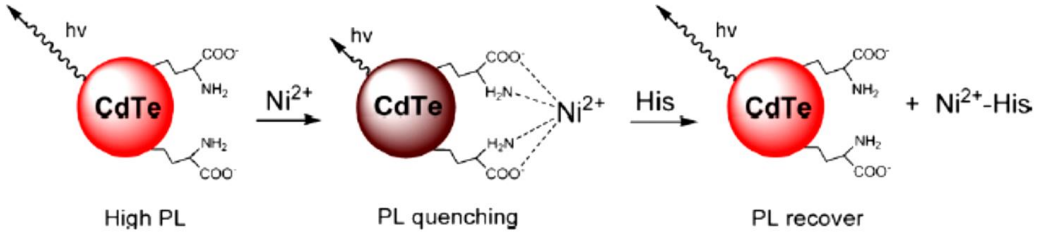

Figure 1.6 Schematic illustration for the signal transduction mechanism for the developed turn-on photoluminescent sensor for histidine based on Ni^{2+}modulated homocuteine-capped CdTe QDs [29].

For the application of molecular sensor in biological system, the high selectivity and low detection limit for target analyst is required. Therefore, the fluorescence technique is widely used due to a high sensitive method and a low concentration for detection[30, 31] . However, the fluorescence signal from biological system can interfere the measuring of analytes. To overcome this problem, the FRET is applied for detection [32-36].

The development of molecular sensor to be a device in functional simple and inexpensive platforms for reproducible and rapid quantitative assays of analytes in

variety of environments is a challenge for scientist. The key of quantitative assay should be inexpensive, be easy to operate, and provide rapid and high precision without the requirement of specialized electronic devices to measure the output of the assay. To achieve this goal, measurement of time is performed by using a time. For examples reported by Gregory and co-worker in 2013 [37, 38], demonstrated quantitative assays based on hydrophobic oligomers- to- hydrophilic switch of hydrogen- peroxide-responsive. This research applies the switching of water-insoluble poly(carbamate) oligomers to hydrophilic product (Figure1.7) to fabricate 3D paper-based microfluidic device for quantitative measurement hydrogen peroxide by time required for an analyst to pass through a 3D paper-based microfluidic device (Figure 1.8). The assay gave high selective for hydrogen peroxide based on the reaction between the aryl boronate with hydrogenperoxide and quantitative of analyst is measured from rate of depolymerization of oligomer which an insoluble oligomer into water-soluble products in response to hydrogen peroxide.

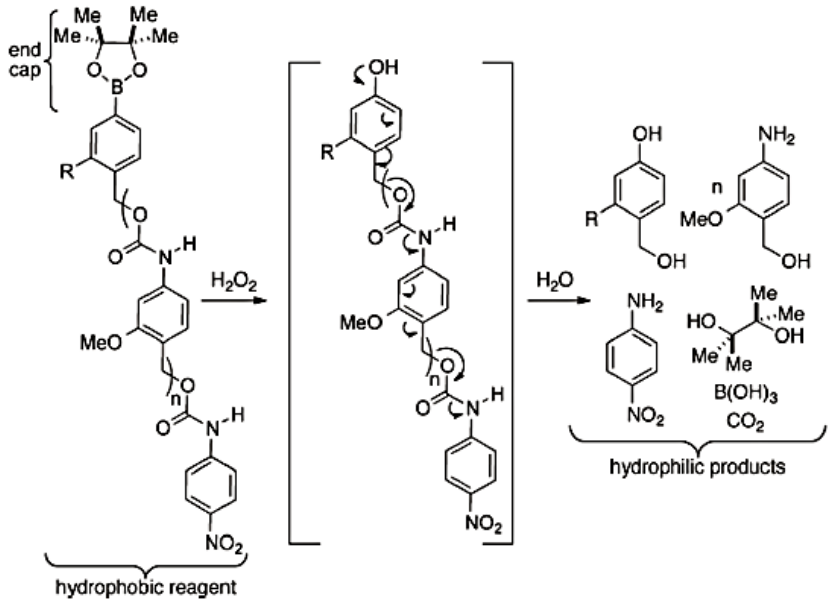

Figure 1.7 Hydrophobic oligomer is used and the depolymerization responses to hydrogen peroxide [37].

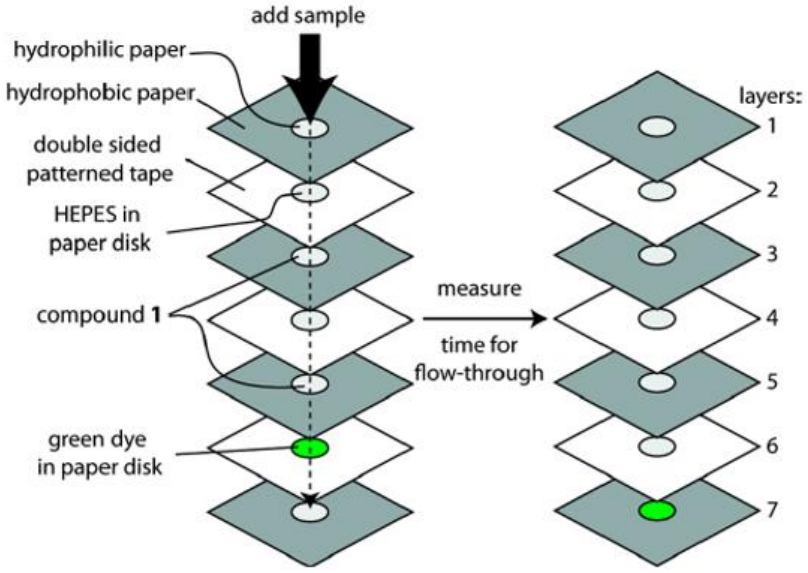

Figure 1.8 Graphical representation of the device, including the dry reagents that are included in each layer [38].

However, the factors of temperature, humidity, and sample viscosity effects toward sample distribution rates resulting in low precision in this design. Thus Gregory and co-worker had been developed 3D microfluidic device by adding the control zone to normalize the affected factors.[37] The challenge of the aim is the control zone should be similar to assay zone but analyst need to remove out of the sample. Thus they designed the new device that composed the left-hand channel (the assay region) in Figure 1.9a. This region was deposited a target enzyme glucose oxidase in layer 3 to react with glucose analyte and yielded hydrogen peroxide as a product. The control region (right-hand channel in the cross-section in Figure 1.9b) contains the same reagents and the same order as the assay region but no deposit enzyme. In this control region, hydrogen peroxide will not be generated; therefore, hydrogen peroxide will not be present to react with oligomer. Hence, the time required for the sample to pass through this control region (and carry the green color to the top of the device) depends on the temperature and humidity under which the assay is conducted, as well as on the viscosity of the sample. These factors will affect sample distribution rates in the assay region as well (the left-hand channel); therefore, this control region normalizes the output of the assay for the effects of these variables on sample distribution. This normalization is implemented by measuring the time required for the control region to turn green relative to when the assay region (the left-hand region) turns green.

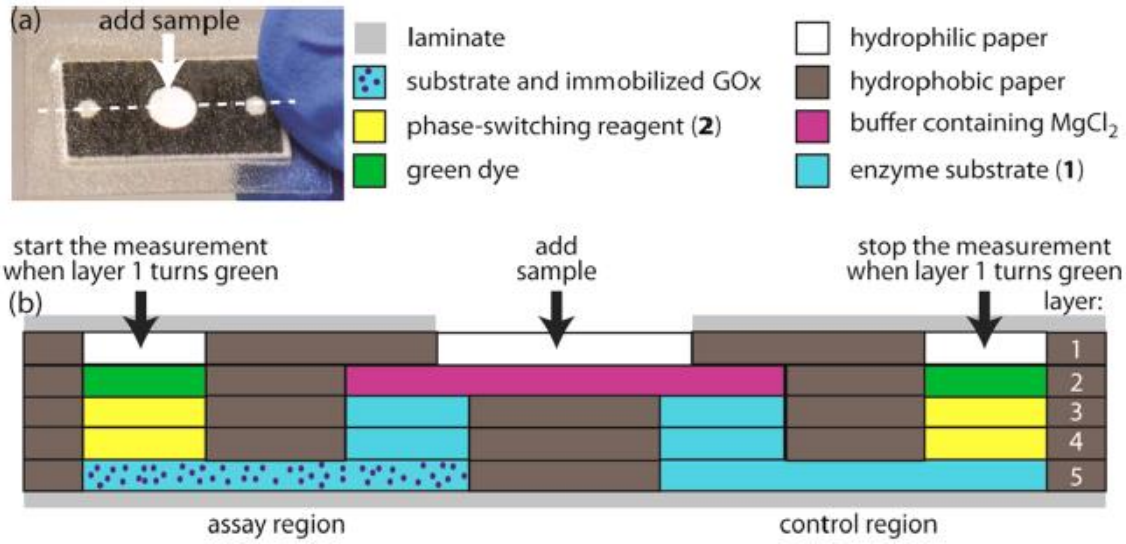

Figure 1.9 (a) Photograph of a three-dimensional paper-based microfluidic device for quantifying active enzyme analytes by measuring the relative time required for a sample to turn a control region green (right-hand region) relative to when an assay region (left-hand region) turns green. (b) The left channel is the assay region and the right channel is the control region [37].

Moreover, Gregory and co-worker [39] also designed quantitative assays that operate by measuring flow-through time or by counting the number of colored bars at a fixed assay time as show in Figure 1.10. The device was designed into 8 layers and 16 bars. All bar was deposited the same reagent in each layer but the various amount of hydrophobic molecule was deposited in layer 3 and layer 5 in each bar. Thus the flow through rate of analyte would pass layer 3 and 5 in different rate resulting in the appearance of the green bar on the top layer was different. The number of green bar

depended on concentration of analyte, thus, this device could be used to determine the concentration of analyte.

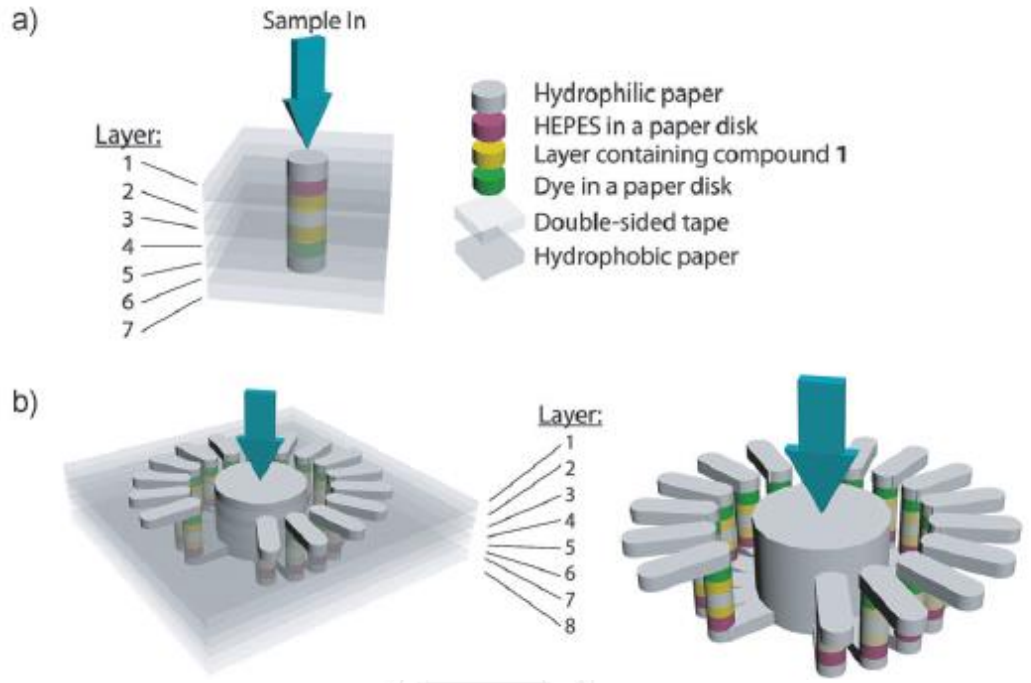

Figure 1.10 a) Digital assays that use a single conduit device to report the concentration of hydrogen peroxide by measuring the time required for the sample to flow through the device. b) Analog assays that use a radial paper-based microfluidic device for quantifying the level of hydrogen peroxide by using a fixed assay time and by counting the number of bars that become colored as a function of the concentration of hydrogen peroxide in the sample [39].

However, the oligomers need many steps for synthesis and provide a high limited of detection in the range of millimolar of analyst. Herein, we describe an

approach for substantially improving the sensitive model assay by using small molecule and also reducing the waste from synthesis and saving cost.

In our work, we have paid attention to study the sensing purposes both of types of biogenic amines and design the microfluidic device to detect Cu^{2+} in sample. The different approaches including:

(i) Molecular chemosensor for catecholamines amines,

(ii) Molecular chemosensor for histidine and histamine

(iii) 3D microfluidic device for sensing Copper ions

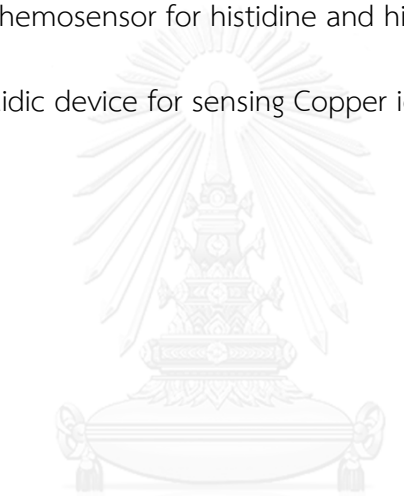

Chapter II

Catecholamine Sensors

2.1 Introduction

Catecholamines including epinephrine, norepinephine and dopamine, are an important role in number of neurotransmitters. Most of them are involved in a variety of central nervous system functions thus malfunction of them directly relates to central nerve diseases such as Parkinson's disease and hypertension. Sensitive and selective detection of catecholamine neurotransmitters have been accomplished using electrochemical technique due to the favorable redox properties of the catechol. Regarding to optical techniques, there have been only few reports based on the chemosensor of catecholamine, particularly, bearing boronic acid and aldehyde for covalently binding with catechol and amine groups producing the formation of a boronate ester and an iminium bond of catecholamine, repectively. However, most fluorescent chemosensors previously reported displayed chelation- enhanced fluorescent quenching (CHEQ) effect upon adding catecholamines. Concerning the discrimination of the kind of catecholamines, many reports regarding to fluorescent chemosensors exhibited a non- specific binding among epinephrine, dopamine and norepinephine. None of fluorescence chemosensors for catecholamine sensing showed the fluorescence performance regarding to the Fluorescence Resonance Energy Transfer (FRET) process. This approach alerts us to develop the fluorescence sensor for a highly selective detection and discrimination of the different kind of catecholamines (such as dopamine, epinephrine and norepinephrine) under the significant emission changes via FRET process upon the intermolecular self-assembled reaction. The intermolecular self- assembled complex is expected to offer the promising advantages of reducing the complicated design and synthesis of the fluorescence compound containing both donor and acceptor fluorophores. Herein, we demonstrated the conceptually self- assembled complexation between coumarin aldehyde (CA) and pyrene boronic acid (PBA) with catecholamine as a guest linker

2.2 Experiment

2.1.1 Materials

All reagents were standard analytical grade, purchased from Fluka, Sigma-aldrich, Merck and TCI and used without further purification. Commercial grade organic solvents such as dichloromethane, hexane, methanol acetone and ethyl acetate were distilled prior to use. DMF was dried over CaH_2 and freshly distillation under nitrogen. Thin layer chromatography was performed using Merck silica gel 60 (70-230 mesh). All solvents were freshly distilled before use.

2.1.2 Synthesis of Coumarin aldehyde (CA)

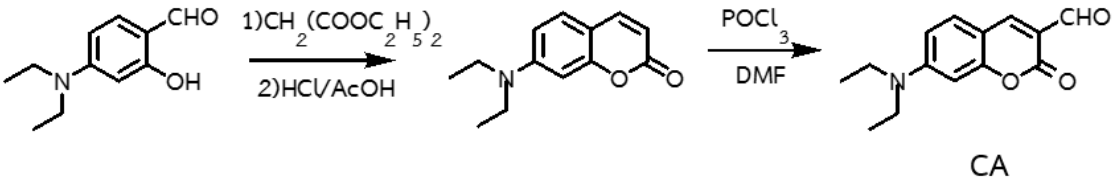

CA

Figure 2.1 Synthesis pathway of **CA**

Coumarin aldehyde (**CA**) was synthesized according to the literature method [40]. Diethylmalonate (13.0 mL, 85.5 mmol), 4-dimethylaminosalicylaldehyde (8.236 g, 42.62 mmol), and piperidine (4.2 mL, 42 mmol) were combined with 120 mL absolute ethanol in a 250 mL round bottom flask equipped with a stir bar and condenser. After refluxing for 8 h, the solution was cooled to room temperature and the solvent was then removed by rotatory evaporator. The crude product was dissolved in 50 mL

HCl/AcOH (2:3) and returned to reflux for 12 h. After the reaction complete, the mixture was cooled to room temperature and the ice was then added in to the solution. The solution was filtered and the solid was washed with water and then followed by extraction with CH_2Cl_2 for 3 times. The organic layer was combined and solvent was removed by vacuum to yield a brown solid. 47 g (85%).

2.1.3. Complexation studies

*2.1.3.1 Fluorescence studies of pyrene boronic acid (**PBA**) sensor with biogenic amines*

Typically, 0.5 M HEPES buffer (pH 7.4) containing 100 mM $Na_2S_2O_3$ was prepared in Milli-Q water with sodium chloride as supporting electrolyte. Stock solution of 1 x 10^{-3} M **PBA** in DMSO was prepared. A solution of 0.001 M biogenic amines (dopamine, norepinephrine, epinephrine, lysine, tyramine and glutamic acid) in 0.5 M HEPES buffer was prepared. The solution of 1 mM NaOH 2 μL was added directly to 2.00 μL of **PBA** in a 1-cm quartz and stirred for 2 min followed by addition of the solution of biogenic and stirred for 1 min. After 1796 μM of 0.5 M HEPES was added to adjust pH of the solution and the solution was stirred for 1 min. Fluorescence spectra of sensor **PBA** and complexation of sensor **PBA** with biogenic amines were recorded from 350–800 nm at ambient temperature with excitation wavelength of 340 nm.

*2.1.3.2 Fluorescence studies of intermolecular assembly of sensor **PBA** and **CA** with biogenic amines*

Initially, the stock solutions of 1 mM **PBA** and **CA** was prepared in DMSO. A solution of 0.001 M biogenic amines (dopamine, norepinephrine, epinephrine, lysine, tyramine and glutamic acid) in 0.5 M HEPES buffer (pH 7.4) containing 100 mM $Na_2S_2O_3$ were prepared. 2 μL of sensor **PBA** solution was pipetted into a 1-cm quartz and 2 μL 1 mM of NaOH was added directly to the solution of sensor **PBA**. The mixture was stirred for 2 min followed by addition of 60 μL of sensor **CA** to the mixture and 200 μL of biogenic amine solution was then added. After the reaction mixture was stirred for 1 min, 1736 μL of 0.5 M HEPES was directly added to adjust pH of the solution and stirred. Fluorescence spectra of the combined sensors (**PBA** and **CA**) and the biogenic amines were recorded from 350–800 nm at ambient temperature with excitation wavelength of 340 nm.

2.1.4 Determination of binding constant of PBA with catecholamines

Binding constant was performed by fluorescent titration. For all complexation studies, the stock solution (1 mM) of guests was prepared in a buffer solution (100 mM Na_2SO_3, 50 mM HEPES and 20 mM NaCl, pH 7.4 in Milli-Q water) and the stock solution of sensor **PBA** (1 mM) was prepared in DMSO and then was diluted to 1×10^{-6} M by the buffer solution. For all measurements, the fluorescence spectra were recorded under the excitation wavelength at 340 nm, and the emission slit widths of 0.5 nm.

The association constants (K) for 1:1 formation were determined from the fluorescence spectral changes using Benesi-Hildebrand equation [41, 42].

$$\frac{Y_0}{Y_0 - Y} = \frac{\propto}{K[G]} + \propto \qquad (1.1)$$

Where Y_0 = Fluorescence intensity of host

Y = Fluorescence intensity of host-guest

[G] = Concentration of guest

The plot of $Y_0/(Y_0-Y)$ versus 1/[G] provided the intercept (α) and the slope (α/K). Then, the binding constant was determined by intercept/slope.

2.1.5 Determination of detection limit of PBA and combined sensors toward catecholamines

*2.1.5.1 Determination of the detection limit of sensor **PBA** with catecholamine*

Typically, 0.5 M HEPES buffer (pH 7.4) containing 100 mM $Na_2S_2O_3$ was prepared in Milli-Q water with sodium chloride as supporting electrolyte. Stock solution of sensor **PBA** (1×10^{-6} M) was prepared in a volumetric flask (25 mL). Fluorescence spectra of **PBA** were monitored for 10 times and all data were used to calculate the standard deviation. The stock solution of guest (1×10^{-3} M) was added in portions (2-150 mL) to the stock solution of sensor **PBA** and then fluorescence spectra of each portion were

recorded with the excitation wavelength of 340 nm for 3 times. All data were used to construct the calibration curve for the calculation of the detection limit by using following equation [43].

$$\text{Detection limit} = Y_B + 3S_B \qquad (1.2)$$

When Y_B = the average fluorescence intensities of blank (free sensor **PBA**)

S_B = standard deviation of blank

2.1.5.2 Determination of the detection limit of the combined sensors with dopamine

Initially, 25 mL of 1 x 10^{-6} M **PBA** and 3 x 10^{-5} M **CA** solution were prepared in 0.5 M HEPES buffer (pH 7.4) containing 100 mM $Na_2S_2O_3$. Fluorescence spectra of the mixture were recorded with the excitation of 340 nm for 10 times. The fluorescence intensities at 487 nm of all data were used to calculate the standard deviation. The stock solution of DA (1 x 10^{-3} M) was prepared in 0.5 M HEPES buffer (pH 7.4) containing 100 mM $Na_2S_2O_3$ and then was added in portions (2-150 mL) to the 2 mL of the mixture solution of host. The fluorescence spectra were recorded with the excitation wavelength of 340 nm for 3 times. All data were used to construct the calibration curve for the calculation of the detection limit according to the equation 1.2.

2.1.6 Interference of foreign in dopamine detection

Typically, 0.5 M HEPES buffer (pH 7.4) containing 100 mM $Na_2S_2O_3$ was prepared in Milli-Q water with sodium chloride as supporting electrolyte. Stock solution of **PBA**

(1×10^{-3} M) in DMSO was prepared. A solution of 1 mM dopamine (DA) and 0.1 M other biogenic amines (lysine, tyramine and glutamic acid) in 0.5 M HEPES buffer were prepared. The 2 μL of 1 mM NaOH solution was added directly to 2.00 μL of sensor **PBA** solution in a 1-cm quartz and stirred for 2 min followed by addition of the solution of 200 μL of DA and 200 μL of the other biogenic amines and the mixture were stirred for 1 min. After 1596 μL of 0.5 M HEPES was added to adjust pH of the solution and the mixture solution was stirred for 1 min. Fluorescence spectra of sensor **PBA** and complexation of sensor **PBA** with biogenic amines were recorded from 350–800 nm at ambient temperature with excitation wavelength of 340 nm.

2.1.7 Determination of % recovery of dopamine in urine

Firstly, the synthetic urine [44-46] was prepared as a solvent as indicated in Table 2.1. The solution of 2 μL of 1×10^{-3} M **PBA** solution was pipetted into a 1-cm quartz and 2 μL of 1 mM NaOH was added directly to the solution of sensor **PBA**. The mixture was stirred for 2 min and followed by addition of 60 μL of sensor **CA**. The solution of dopamine in various concentrations from 5 -25 μM was then added into the solution mixture. After the reaction mixture was stirred for 1 min, the synthetic urine was directly added to adjust the volume of the solution mixture and then the solution was stirred until the reaction completed. Fluorescence spectra of the combined sensor (**PBA** and **CA**) and dopamine were recorded from 350–800 nm at ambient temperature with excitation wavelength of 340 nm.

Table 2.1 Composition of synthetic urine[45]

Species	Concentration (gl^{-1})
$CaCl_2.H_2O$	0.65
$MgCl_2.6H_2O$	0.651
NaCl	4.6
Na_2SO_4	2.3
$Na_3C_6H_8O_7.2H_2O$	0.65
Na_2CO_3	0.020
KH_2PO_4	2.8
KCl	1.6
NH_4Cl	1
$CO(NH_2)_2$	25
$C_4H_7N_3O$	1.1

2.2 Result and discussion

2.2.1 Conceptual design

Catecholamines including epinephrine (EPI), norepinephrine (NE) and dopamine (DA) are important neurotransmitters which have a similar structure consisting of catechol and amino groups in their structures. Catecholamines are normally involved in a variety of central nervous system functions thus the malfunction of them directly relates to neurologic diseases. For example, the deficiency amount of DA in body fluids is generally an essential indicator for patients suffering Parkinson's disease in the clinical diagnosis. However, a critically elevated amount of EPI in the human blood certainly leads to the increase of blood pressure and heart failure. Furthermore, the patients suffering in tumors of 20 adrenal glands are found to have the large amounts of EPI and NE in their blood and urine. Specific detection of each catecholamine species is a challenge task for sensing purpose. Regarding the optical detection, there are only few reports concerning the chemosensor of catecholamine, particularly, bearing boronic acid and aldehyde for covalently binding with catechol and amine groups of catecholamine species to form a boronate ester and an iminium ion, repectively. However, most fluorescent chemosensors reported previously displayed chelation-enhanced fluorescent quenching (CHEQ) effect [47-52] upon adding catecholamines. Concerning the discrimination of each catecholamines, many reports regarding fluorescent chemosensors showed a nonspecific binding among EPI, DA and NE. None of fluorescence chemosensors for catecholamine sensing employed the

Fluorescence Resonance Energy Transfer (FRET) process as a tool in detection. This alerts us to develop the fluorescence sensor for a highly selective detection and discrimination among DA, EPI and NE under the significant emission changes via the FRET process induced by the intermolecular assembled complex. This conceptual system is expected to offer the promising advantages not only reducing the complicated design and synthesis of the fluorescence compound containing both donor and acceptor fluorophores but also reducing the waste from synthesis and saving cost. Herein, we demonstrated a FRET-on process induced by an intermolecular assembly of coumarin aldehyde (**CA**) and pyrene boronic acid (**PBA**) with catecholamine as a guest linker, as shown in Figure 2.2.

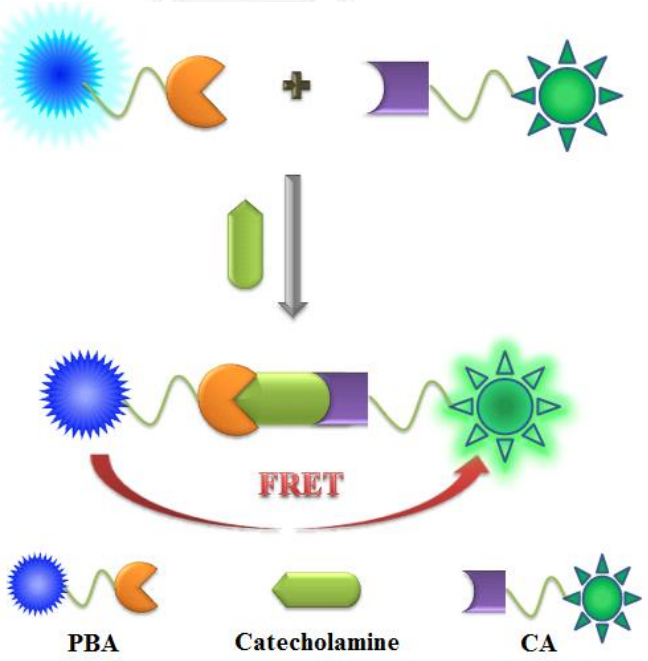

Figure 2.2 Conceptual design for sensing catecholamine

2.2.2 Determination of pKa of pyrene boronic acid (PBA)

Prior to verification of the covalent binding affinity of sensor **PBA** with catecholamine, the pH profile of sensor **PBA** should be firstly examined by fluorescence spectroscopy to indicate the pK_a value. The pH profile (Figure 2.3) revealed the approximately small pK_a value of 6.5. The small value of pK_a implied that the high electron density in pyrene ring would stabilize the electron deficient boronic acid to preferentially rearrange in the sp^3- hybidized orbital around boron atom. Therefore, sensor **PBA** could be applied to detect catecholamine based on reaction between sp^3- hybridized boronic acid of sensor **PBA** and catechol moiety of catecholamine in normal condition (pH 7.4).

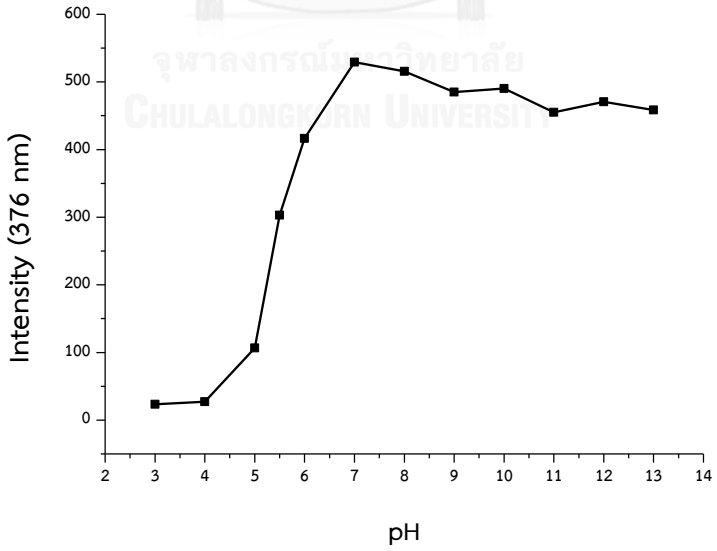

Figure 2.3 The pH profile of sensor **PBA** (0.75 μM) at 376 nm in various pH under excitation wavelength of 340 nm.

2.2.3 Binding properties of sensor PBA and catecholamines

The fluorescence spectra feature of sensor **PBA** in HEPES buffer pH 7.4 exhibited a strong emission band in the region of 375-425 nm assigned to monomeric pyrene species under excitation wavelength of 340 nm. Upon the addition of dopamine (DA), norepinephrine (NE) and epinephrine (EPI), a large red shift at 451 nm corresponding to excimer band of pyrene was observed as shown in Figure 2.4. As a result of the similar emission spectra, it is hypothesized that the reaction between catechol moiety based catecholamine and sp^3-hybidized boronic acid group in sensor **PBA** producing the boronate ester induced the excimer emission spectrum of sensor **PBA**. Consequently, the similar structures of DA, NE and EPI lead to the similar excimer fluorescence band centered at 451 nm as shown in Figures 2.4 and 2.5.

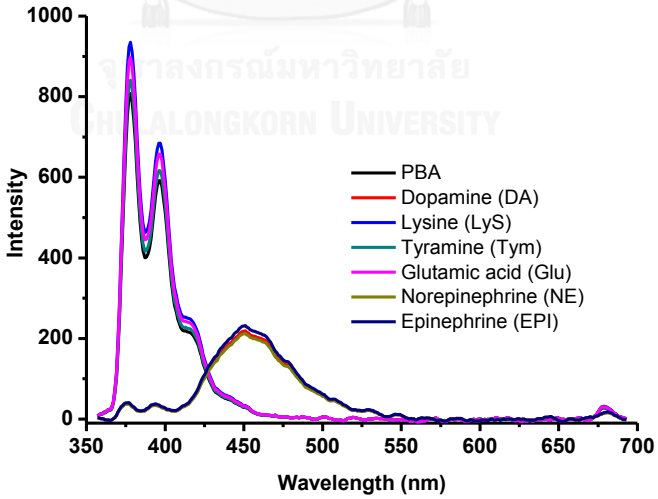

Figure 2.4 Fluorescence spectra of sensor **PBA** in HEPES buffer solution in the presence of various biogenic amines.

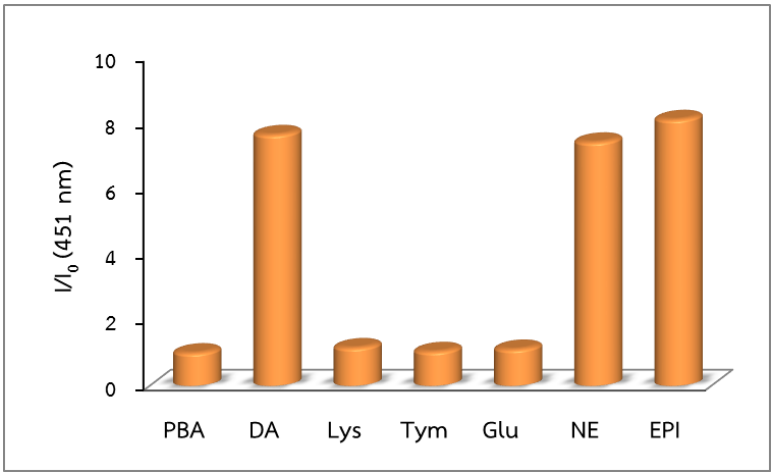

Figure 2.5 Relative fluorescence intensity at 451 nm of sensor **PBA** (1 μM) in the presence of various biogenic amines.

To investigate the binding affinity between sensor **PBA** and catelamines, the stoichiometry of sensor **PBA** and catecholamines including DA, NE and EPI were firstly estimated by Job's method [34, 53, 54]. The result showed the binding mode at 1:1 ratio of sensor **PBA** and catecholamines (Figure 2.6 – 2.8).

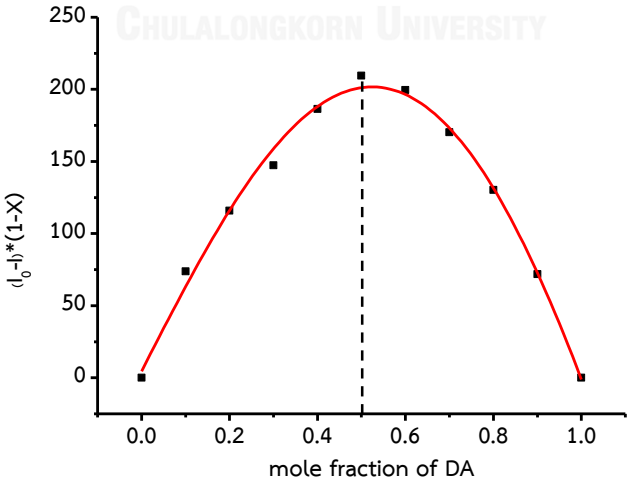

Figure 2.6 Job' plot of sensor **PBA** and DA monitoring fluorescence intensity at 376 nm under excitation wavelength at 340 nm

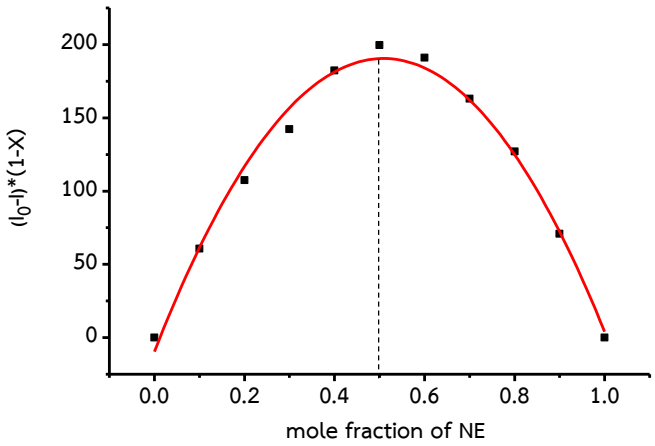

Figure 2.7 Job' plot of sensor **PBA** and NE monitoring the fluorescence intensity at 376 nm under excitation wavelength at 340 nm

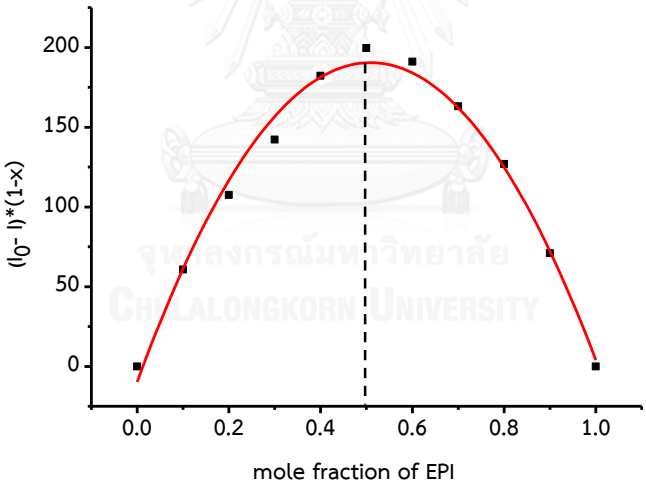

Figure 2.8 Job' plot of sensor **PBA** and EPI monitoring the fluorescence intensity at 376 nm under excitation wavelength at 340 nm

Fluorescence titration technique was used to evaluate the binding constant (log K value) of sensor **PBA** toward DA, NE and EPI. The result showed dramatically decrease of the fluorescence intensity of momomeric pyrene with concomitant of an enhancement of excimer band upon increasing of cathecholamines concentration as illustrated in Figure 2.9-2.11. From Benesi plot, the log K values of sensor **PBA** with DA, NE and EPI were evaluated to be 4.23, 4.10 and 4.35 M^{-1}, respectively. Considering the small difference log K values, it is possibly caused by the same reaction between catecholamine and boronic acid group resulting in the similar binding affinity.

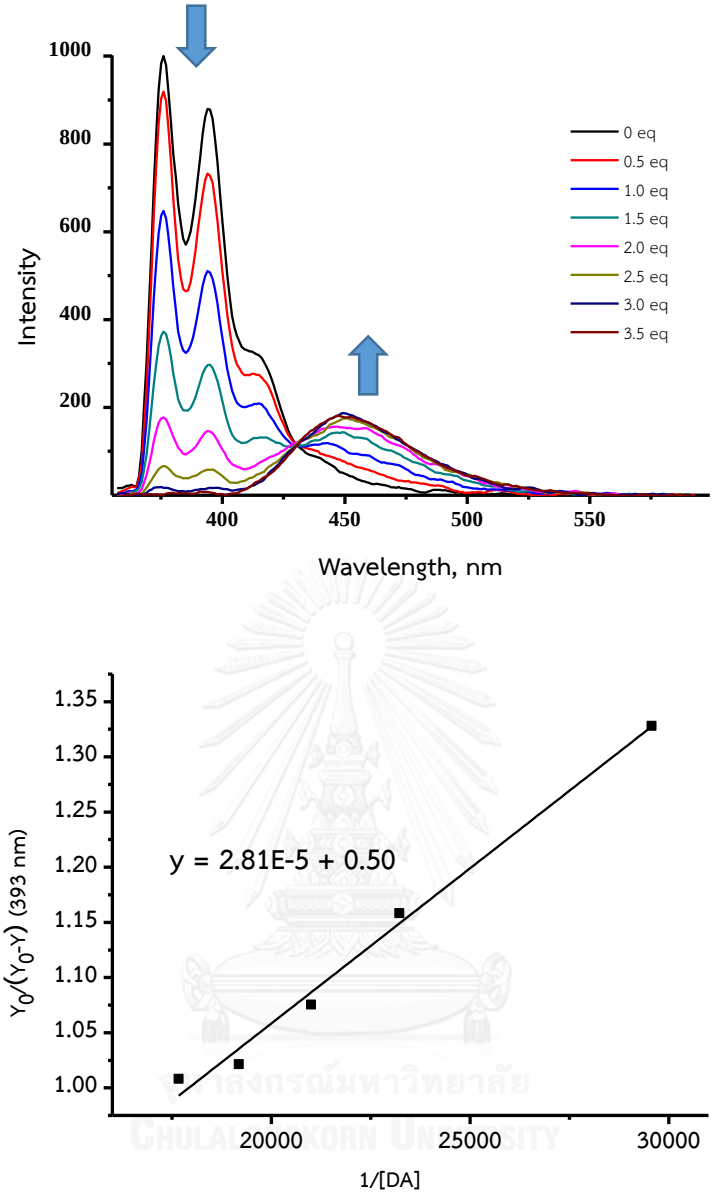

Figure 2.9 (a) Fluorescence titration spectra of sensor **PBA** (1 mM) with various concentration of DA in HEPES buffer pH 7.4 under excitation wavelength of 340 nm and (b) Benesi plot of sensor **PBA** (1 mM) with various concentration of DA at the fluorescence intensity of 393 nm.

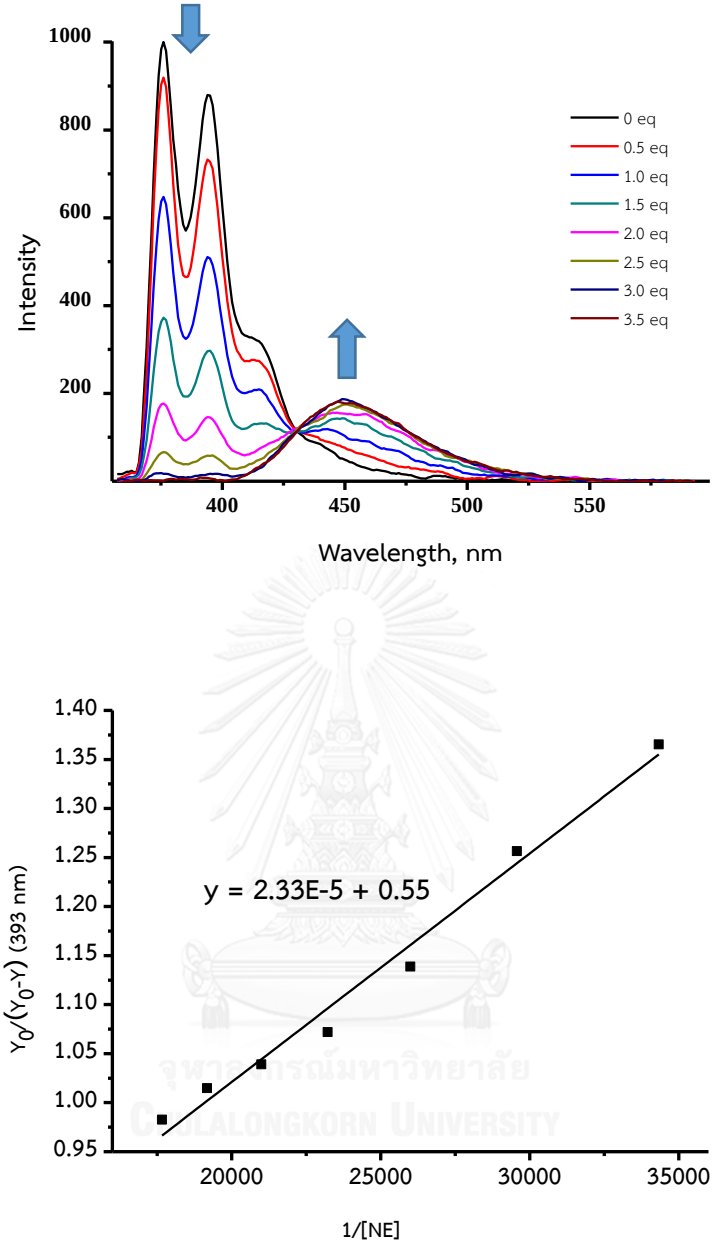

Figure 2.10 (a) Fluorescence titration spectra of sensor **PBA** (1 μM) with various concentration of NE in HEPES buffer pH 7.4 under excitation wavelength of 340 nm and (b) Benesi plot of sensor **PBA** (1 mM) with various concentration of NE at fluorescence intensity of 393 nm.

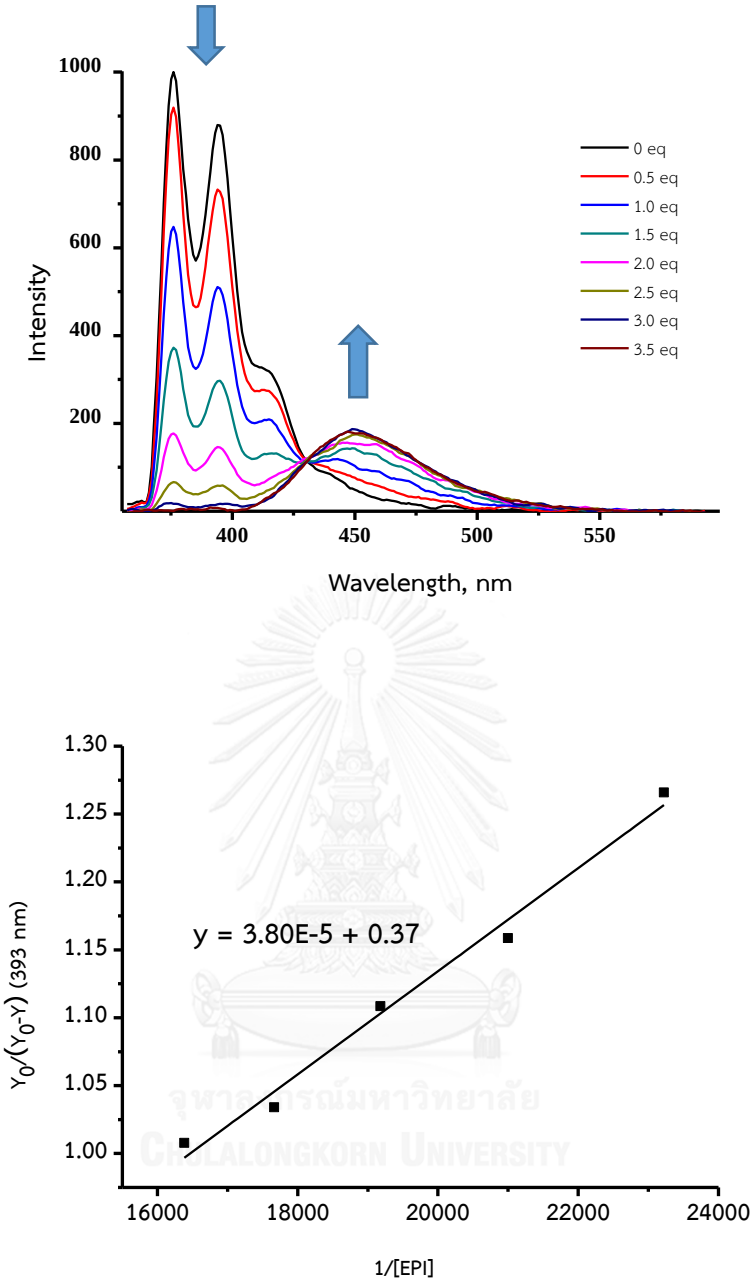

Figure 2.11 (a) Fluorescence titration spectra of sensor **PBA** (1 μM) with various concentration of EPI in HEPES buffer pH 7.4 under excitation wavelength of 340 nm and (b) Benesi plot of sensor **PBA** (1 μM) with various concentration of EPI at fluorescence intensity of 393 nm.

2.2.4 The intermolecular assembly of sensor PBA and CA

As comprehensive studies on discrimination of catecholamine derivatives, the proper primary amine sensor should act an acceptor fluorescence sensor whose absorption band overlaps with emission excimer band of sensor **PBA**, to sequentially provide FRET- on process. As anticipated, the fitting acceptor sensor containing aldehyde receptor based coumarin (**CA**) was chosen. The reaction between primary amine and aldehyde receptor produced an iminium ion initiating intermolecular assembly of donor and acceptor fluorescence sensor via catecholamine as a linker. The optimization of FRET efficiency for the couple of sensors **PBA** and **CA** was firstly estimated by varying concentration of sensor **CA** in the solution mixture of sensors **PBA** and DA. The fluorescence spectra exhibited a dramatically decreased fluorescence excimer band centered at 451 nm with a concomitant of the appearance emission band at 487 nm upon increasing of **CA** concentration as shown in Figure 2.12. The FRET efficiency was estimated and the result showed the highest FRET efficiency at 3×10^{-5} M of sensor **CA** as evidenced from the highest fluorescence intensity at 487 nm as summarized in Table 2.2.

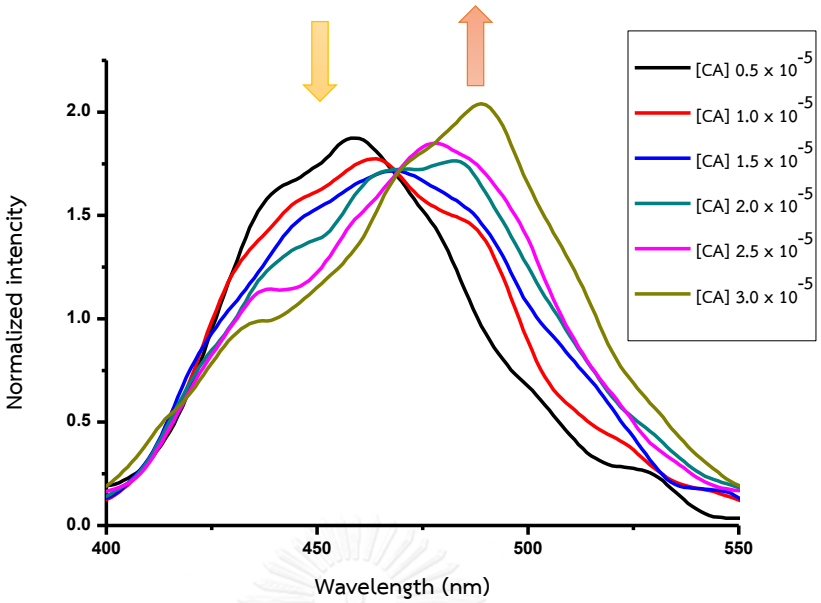

Figure 2.12 Normalized fluorescence titration spectra of sensor **PBA** (1 μM) with sensor **CA** in HEPES buffer pH 7.4 solution.

Table 2.2 FRET efficiency of catecholamine induced intermolecular assembly with fluorescence sensor **PBA** (1 μM) and various concentration of sensor **CA** in the presence of dopamine (100 μM).

	0.5	1.0	1.5	2.0	2.5	3.0	3.5	4
FERT efficiency	0.42	0.39	0.40	0.44	0.57	0.73	0.59	0.60

In addition, time-resolved FRET (trFRET) was performed to insist the FRET mechanism. The trFRET spectra revealed that fluorescence intensity of excimer band

centered at 451 nm rapidly decreased and simultaneously increased in emission band at 487 nm assigned to fluorescence band of sensor **CA** (Figure 2.13 and 2.14). This result is a strong evidence to support the energy transfer mechanism from donor excimer **PBA** to an acceptor **CA**.

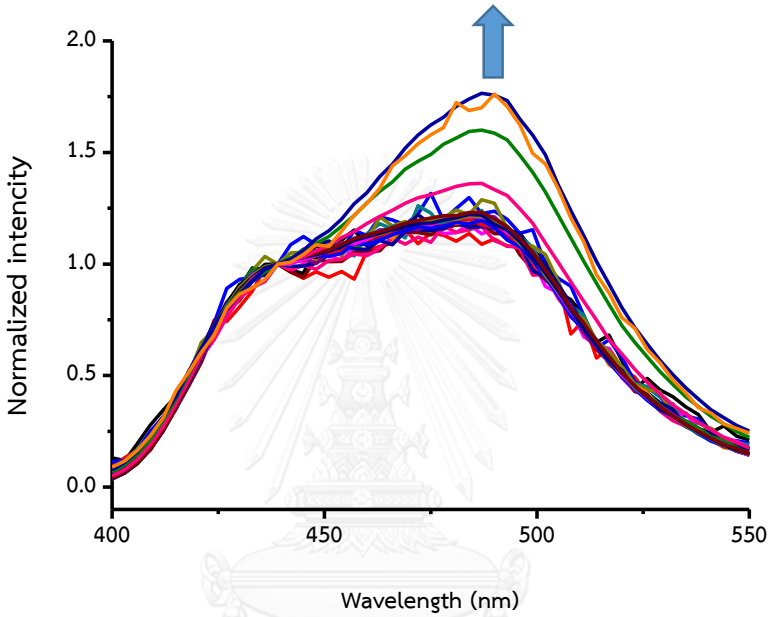

Figure 2.13 Time-resolved emission spectra of complexation sensor **PBA** (1 μM) + **CA** (30 μM) in the presence of 100 μM of DA in HEPES buffer solution pH 7.4 upon the normalized intensity of excimer band of sensor **PBA**.

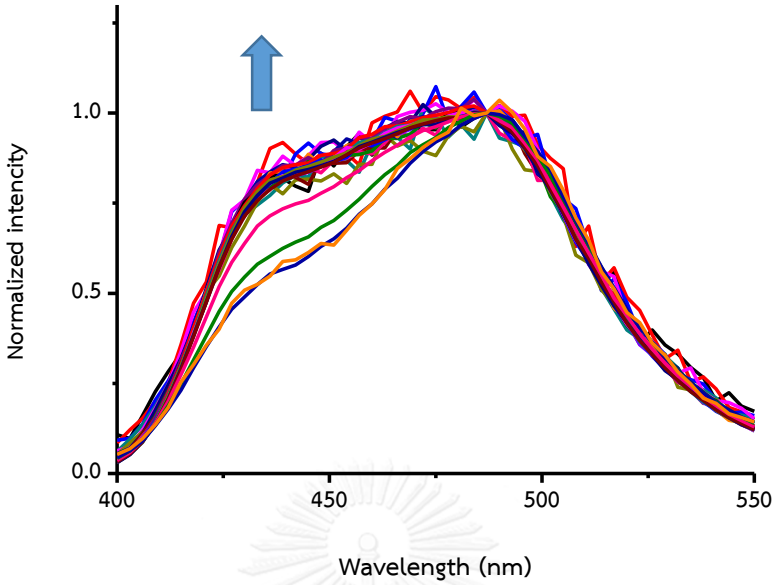

Figure 2.14 Time-resolved emission spectra of complexation sensor **PBA** (1 μM) + **CA** (30 μM) in the presence of 100 μM of DA in HEPES buffer solution pH 7.4 upon the normalized intensity of emission band at 487 nm corresponding to sensor **CA**.

To investigate on selectivity of combination sensors (**CA** and **PBA**) toward biogenic amines, the addition of sensor **CA** to sensor **PBA** led to a decrease in emission of monomeric pyrene band. Upon addition of Lys, Tym or Glu into the mixture of **PBA** and **CA**, the fluorescence spectra were similar to the mixture of **CA** and **PBA**. In the presence of DA or NE, the large quenching of **PBA** monomeric band with significant enhancement of emission band at 487 nm assigned to sensor **CA** was concomitantly observed. Interestingly, the excimer band at 451 nm was still observed upon the addition of EPI as shown in Figure 2.15. These result strongly supported the non-FRET

process in the presence of EPI. As an observation of the emission band at 466 nm, the combination of sensors provided a high discrimination of EPI from other catecholamine compounds (Figure 2.16).

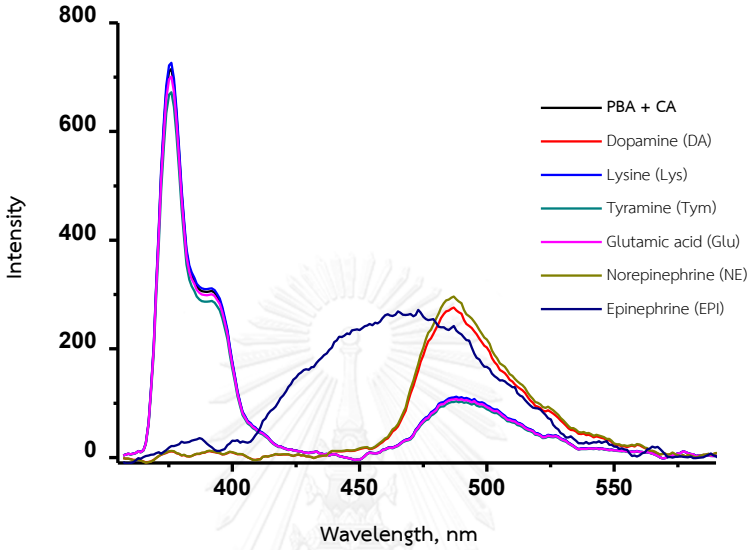

Figure 2.15 Fluorescence spectra of sensors **PBA** (1 μM) and **CA** (30 μM) in HEPES buffer in the presence of various biogenic amines.

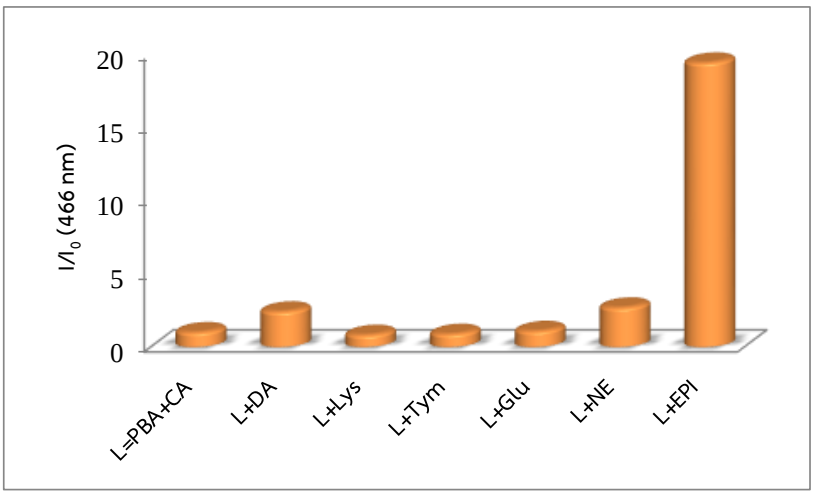

Figure 2.16 Relative fluorescence intensities at 466 nm of the mixed sensors **PBA** (1 μM) and **CA** (30 μM) in the presence of various biogenic amines.

The successful discrimination of EPI stems from the reaction between amine moieties on the catecholamine side chain with the aldehyde based coumarin to form iminium species. Only primary amines based DA and NE can react with aldehyde group of sensor **CA**. Thus, DA and NE properly act as guest linkers between sensors **PBA** and **CA** and induce FRET-on process from sensor **PBA** to sensor **CA** resulting in an enhancement of emission band centered at 487 nm. The ESI-MS spectrum was measured to confirm the intermolecular self-assembled reaction of two sensors and guest as illustrated in Figure 2.17. The intense peak at m/z of 609.97 was observed which clearly supported the purposed structure of **PBA-DA-CA** complex as show in Figure 2.18.

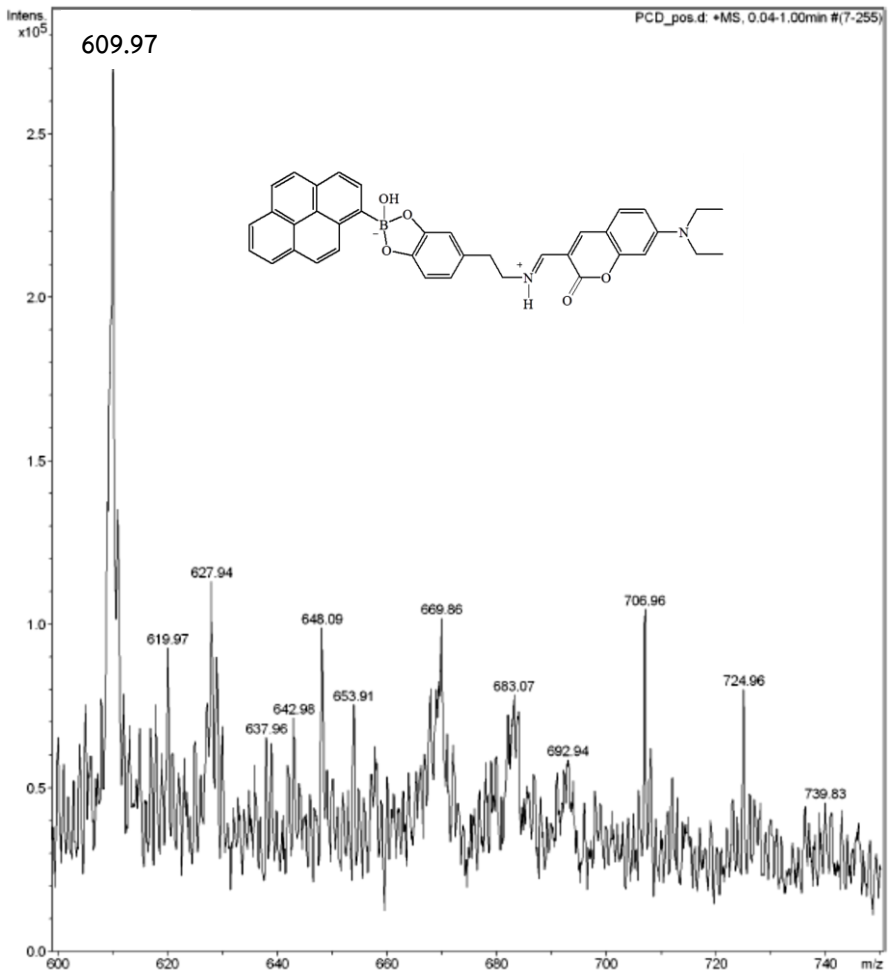

Figure 2.17 ESI-MS spectrum of **PBA-DA-CA** complex.

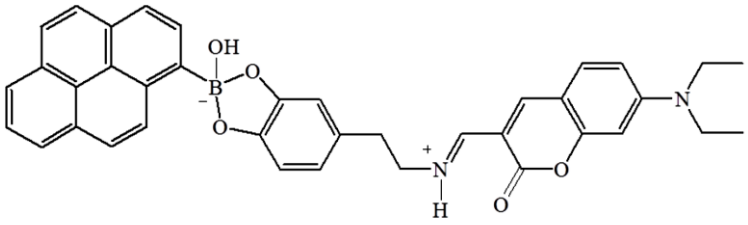

Figure 2.18 The proposed structure of an intermolecular assembled complex between **PBA-DA-CA.**

Moreover, the fluorescence titration of the combination sensors **PBA** and **CA** toward DA displayed a decreasing in fluorescence intensity of monomeric pyrene with an enhancement of emission band at 487 nm corresponding to **CA** emission band upon an increment of DA (Figure 2.19). The detection limit of DA by this sensory system was examined from fluorescence titration by monitoring the emission band at 487 nm as presented in Figure 2.20. The result revealed the detection limit of the combination sensors toward DA to be 1.41 μM with linear relationship in the concentration range from 16.7 to 47.4 μM.

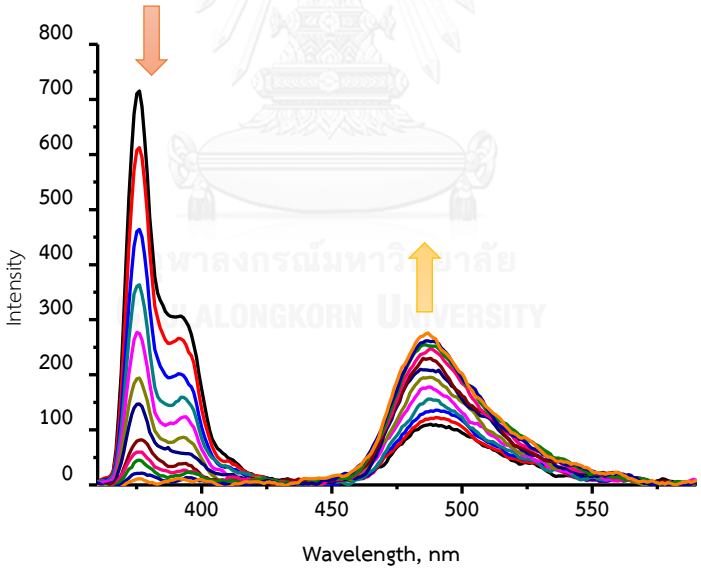

Figure 2.19 Fluorescence titration of the combined sensors **PBA** (1 μM) and **CA** (30 μM) toward DA in HEPES buffer solution pH 7.4.

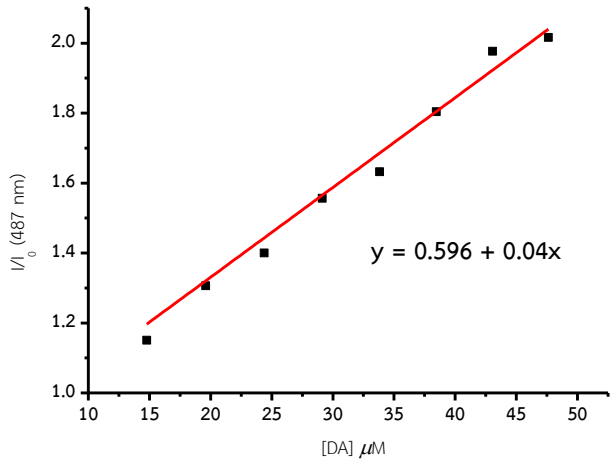

Figure 2.20 Calibration curve of combination probes **PBA** (1 μM) and **CA** (30 μM) toward DA in HEPES buffer solution pH 7.4.

In the case of EPI sensing, the fluorescence titration of the combination probes showed dramatically decrease in monomeric band of pyrene with concomitant fluorescence enhancement at centered 451 nm belonging to excimer band of **PBA** upon increasing in concentration of EPI as shown in Figure 2.21. The detection limit of combined sensors **PBA** and **CA** toward EPI was examined by following the enhancement of emission band at 451 nm providing 0. 69 μM with the linear relationship in the concentration range of 2.0-56.0 μM as illustrated in Figure 2.22.

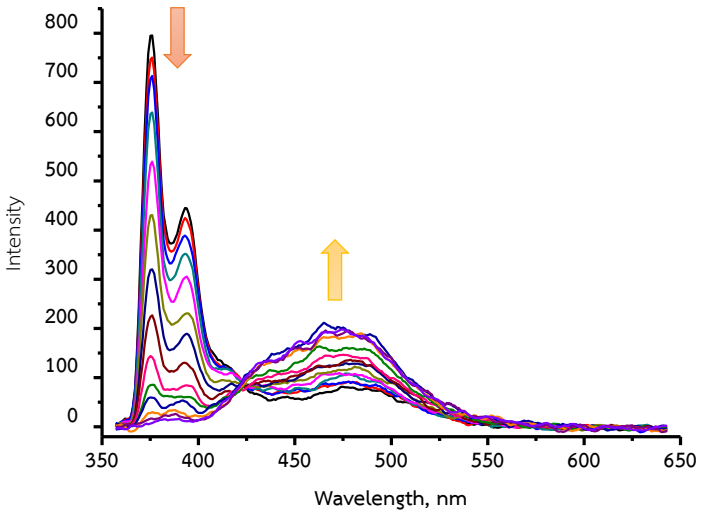

Figure 2.21 Fluorescence titration of combination probes **PBA** (1 μM) and **CA** (30 μM) toward EPI in HEPES buffer solution pH 7.4.

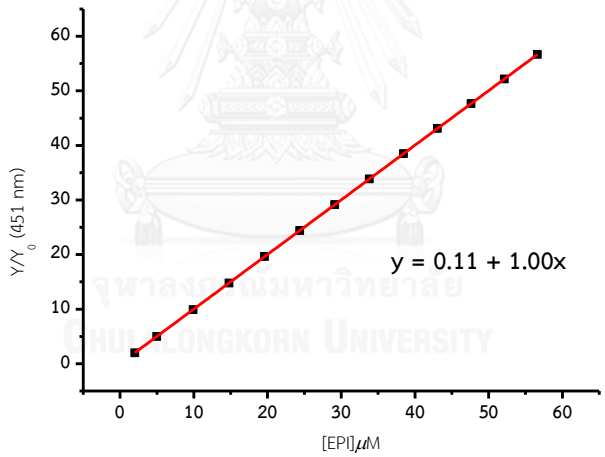

Figure 2.22 Calibration curve of combination probed **PBA** (1 μM) and **CA** (30 μM) toward EPI in HEPES buffer solution pH 7.4.

2.2.5 Applications of Combination sensors PBA and CA toward catecholamine

The combination sensor system (**PBA** and **CA**) was applied to be a naked-eye sensors in aqueous solution and solid support under exposure to the 356 nm UV-

visible light. The solution of combined probes illustrated sky blue color and was changed to green color belonging to emitting light of **CA** upon adding of DA into mixture sensors. In comparison with single fluorescence sensor system (**PBA**), the **PBA** solution in the presence of DA exhibited the blue brightness assigned to the excimer band of **PBA**. In the case of sensor **CA**, the green luminescence remained unchanged although sensor **CA** is able to form an iminium ion with primary amine of DA as shown in Figure 2.23.

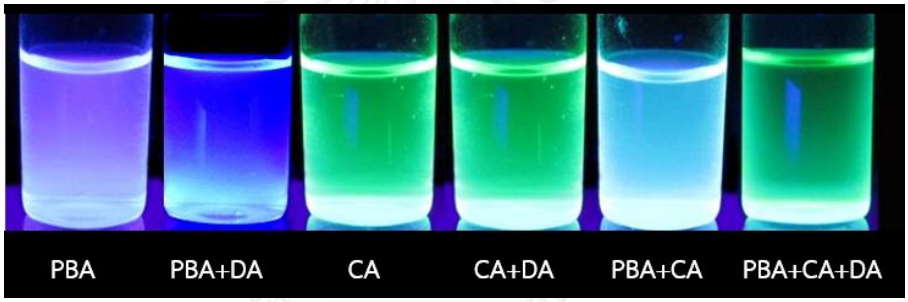

Figure 2.23 Photographs of the solution of sensors **PBA**, **CA** and combination of sensors **PBA** and **CA** in the presence and absence of DA.

On the solid support, the mixture solution of sensors **PBA** and **CA** was painted in the word "P", "C", "PC" and "PCD" by using a paintbrush. All fabricated paper were immersed in solution of DA. The result showed green luminescence color of the fabricated paper with mixture of sensors **PBA** and **CA** as labeled PCD upon exposure to DA under the 356 nm UV-visible light as illustrated in Figure 2.24.

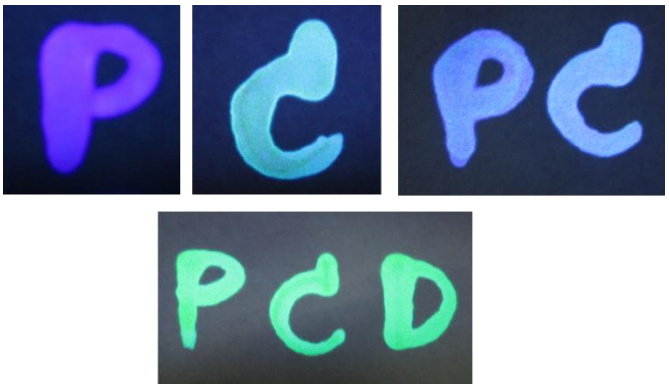

Figure 2.24 Photographs of the fluorescence images of sensor **PBA**; P, sensor **CA**; C, the mixture of sensors **PBA** and **CA** in the absence of DA; PC and in the presence of DA; PCD.

In addition, this proposed self-assembled complex sensing system was applied to determine the concentration of DA in real urine samples. The calibration curve of combination sensors **PBA** and **CA** toward DA in synthetic urine was firstly examined by following the fluorescence intensity at 487 nm in varying concentration of DA. The calibration curved provided the linear range from 4.97-27.39 μM of DA concentration (Figure 2.25). Then, the 14.78 μM sample DA was spiked into real urine samples and the amount of DA was determined from two spike urine samples by using the intermolecular assembly approach of sensors **PBA** and **CA**. The acceptable values of %recoveries from the spike sample with DA were observed as presented in Table 2.3. Average %recoveries of the spike samples of DA from the solution of sensors **PBA** and

CA were 106.0. This result revealed a good analytical characteristics of the sensor in DA detection.

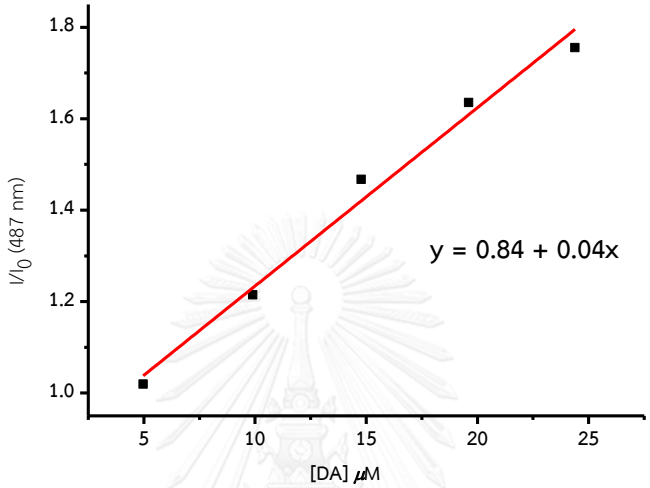

Figure 2.25 Calibration curve of combination probes **PBA** (1 μM) and **CA** (30 μM) toward spike DA into synthetic urine under HEPES buffer solution pH 7.4.

Table 2.3 Determination of DA in real urine samples from combination sensors **PBA** and **CA**.

experiment	Sample 1			
	Amount of DA			
	Added (μM)	Recovery (μM)	Average (μM)	% recovery
1	14.78	11.63	15.87 ± 4.44	107.4
2	14.78	15.51		
3	14.78	20.49		
Sample 2				
experiment	Amount of DA			
	Added (μM)	Recovery (μM)	Average (μM)	% recovery
1	14.78	13.57	15.46 ± 2.58	104.6
2	14.78	14.4		
3	14.78	18.4		

Chapter III

Histamine Sensor

3.1 Introduction

A poisoning biogenic amine such as histamine (Him) is normally found in a postmortem of the muscle in fish, such as tuna, salmon. The poisoning compound was easily produced from bacteria by decarboxylation of an essential amino acid, histidine (His), consequence the quantity of Him in food is commonly regarded as one of the biomarker in food quality for monitoring food quantity during food production, storage and transportation. Ingestion food-borne contains high levels of Him lead to a variety symptoms including nausea, vomiting, diarrhea, red rash, oral burning sensation and itching of the skin. For this reason, the United States Food and Drug Administration (FDA) have established Him index at 50 ppm for fish spoilage based on the assessment of poisoning cases. The suggested safety levels for histamine content in seafood are consumption <50 ppm and possibly toxic for human consumption of 50-500 ppm. Therefore, the analytical determination of Him is an important topic in clinical and food chemistry.

Due to the prominence of Him level in food safety, an effective separation technique, such as gas chromatography (GC) or gas chromatography mass spectrometry (GC- MS) , high performance liquid chromatography (HPLC is widely used for determination of Him. However, the aforementioned methods are generally tedious, laborious, and, most importantly, expensive for routine detection cause the molecular sensing of Him plays a pivotal role in biochemistry and molecular biology.

Specific discrimination of histidine (His) and histamine (Him) is a challenge task for sensing purpose, in particularly optical detection. Most of reports concerned the ligand exchanged sensing approach of metal complexes, especially Ni^{2+} and Cu^{2+}, with Him and following by the UV-Vis or fluorescence spectroscopy. There are very few reports demonstrating the covalent reaction between ligand and Him or His. Kielland and coworker have fantastically reported the histamine sensing by the other sensing mechanism employing reaction of mesoionic acid fluoride or histamine blue (**HB**) with

amino acid group by self-catalytic reaction of imidazole group in biogenic amines. However, most of previous fluorescent chemosensors afford high sensitivity in the quantitative but nonspecific selectivity for His and Him due to both compounds comprising similar functional group of amine and imidazole, which provide the same sensing mechanism.

To obvious discrimination of similar functional biogenic amines, there are a numerous reports regarding nanoporous silica (**NPS**) for serving a high selective fluorescence sensing for biogenic amines. The selectivity stems from functionalized surface of materials with steric molecules or gatekeeper resulting in a different kinetic reaction of each biogenic amine. Concerning the discrimination of each biogenic amine, many reports regarding fluorescent chemosensors showed a nonspecific binding among Him and His. None of fluorescence chemosensors for biogenic amines sensing employed the Fluorescence Resonance Energy Transfer (FRET) process as a tool in detection. This approach brings us to design the donor fluorescence sensor for biogenic amines loaded into **NPS** which modify by proper acceptor fluorophore for providing the significant emission changes via the FRET process. Herein, we demonstrated a highly selective fluorescence compound for determination of Him by loading **HB** into **NPS** which modified surface by fluorescein dye for preventing an infiltration of His to react with **HB**.

3.2 Experiment

3.1.1 Synthesis of Histamine blue (HB)

HB was synthesized according to the published procedure [55]. Briefly, TFAA (0.393 mL, 2.78 mmol) and isocyanide (0.253 mL, 2.78 mmol) were added to a solution of isoquinoline (360 mg, 2.78 mmol) in anhydrous CH_2Cl_2 (5 mL) at – 30 °C. The reaction was stirred for 3 min at this temperature, and then the cooling bath was removed and the reaction mixture was stirred for 14 h at room temperature. A saturated solution of Na_2CO_3 (10 mL) was added and the mixture was extracted with dichloromethane (2x5mL). The combined organic extract was washed with brine (10 mL) and then dried over Na_2SO_4. The silica and Na_2SO_4 were added to the organic extracts and stirring for 1 h and then were filtered through Celite. The precipitate was washed with AcOEt, and the collected filtrates were combined. The solvent was removed under reduced pressure and the residue was washed with Et_2O (10 mL) to yield the product as a brown solid. The structure of **HB** was confirmed by ^{1}H NMR spectroscopy. The chemical shifts (δ) values of **HB** were listed. ^{1}H NMR (400 MHz, $CDCl_3$): δ = 9.28 (d, *J* = 6.8 Hz, 1 H), 8.04 (d, *J* = 8.4 Hz, 1 H), 7.96 (d, *J* = 8.0 Hz, 1 H), 7.83 (m, *J* = 7.2, 8.0 Hz, 1 H), 7.76 (m, *J* = 8.4, 7.2 Hz, 1 H), 7.56 (d, *J* = 7.2 Hz, 1 H), 5.31 (s, 2 H), 3.80 (s, 3 H) ppm. ^{13}C NMR (100 MHz, $CDCl_3$): δ = 167.8, 157.1, 152.9, 135.0, 133.3, 131.6, 129.8, 128.9, 124.1, 122.3, 116.6, 116.4, 90.7, 53.5, 43.4 ppm.

3.1.2 HB loaded in silica nanoparticles (HB-NPS and HB-SNS)

HB loaded nanoparticles was prepared by dispersion 1 g of synthesized nanoparticles (**NPS** or **SNS**) in 5 mL EtOH. The solution of 100 mg **HB** in 1 ml ethanol was added in the solution of silica nanoparticles (NPS or SNS) and stirred for 48 hours at room temperature. The 200 µL aminopropyltriethoxy-silane (APTEOS) was added in to the mixture and stirred at 60 °C for 24 h. The particles were recovered by centrifugation at 10,000 rpm at 25°C for 20 min. The pellet was washed with ethanol and water for 3 times after that the particles were dried in the air.

3.1.3 Modification of silica nanoparticles (HB-NPS@FC)

To develop the selectivity of a fluorescence sensor, fluorescein (**FC**) was modified on the surface of silica by following procedure [56-59]. 1 g of **HB-NPS** dispersed in 5 mL EtOH, was added by fluorescein isothiocyanate (1 mg) and the mixture solution was stirred for 12 h under nitrogen atmosphere and in the dark. The obtained **HB-NPS@FC** was centrifuged at 10,000 rpm for 20 min and washed with ethanol and water 3 times to remove unreacted chemical substance.

3.1.4 Loading efficiency and loading degree

The loading quantification was performed by determining the absorbance of the samples at 327 nm of **HB**. The 1 g of **NPS** dispersed in 5 mL EtOH was added by the solution of 100 mg **HB** in 1 ml ethanol. The mixture solution was

stirred at room temperature for 48 h. The mixture was centrifuged at 25 °C, 10,000 rpm for 20 min. The supernatant was collected. The concentration of **HB** was obtained from standard curve of **HB**. The loading efficiency and **NPS** loading degree were calculated using the equations presented below [60-63]:

Loading efficiency (%) = [(initial HB weight) - (HB weigth in supernatant)] / initial HB weight

Loading efficiency (%) = [(initial HB weight) - (HB weigth in supernatant)] / NPS initial weight

3.1.5 Spectroscopic measurement of complexation studies

All fluorescent experiments were measured in aqueous solution which was prepared by 0.05 M solution of PBS buffer (pH 7.0) in MilliQ water. 200 µL of 1 mM stock solutions of guests (DA, Lys, Tym, Glu, NE, EPI, His and Him) were added directly into 2.00 mL solution of receptor (1mg/mL) in a 1-cm quartz cuvette by micropipette. For fluorescence titration, stock solution of guest was added in portion via micropipette (2-250 µL) to a solution of 2.00 mL of sensor (1mg/mL) in a cuvette. After each addition, the mixture was stirred prior to measurement under the excitation wavelength at 340 nm.

3.1.6 Determination of the detection limit of HB-NPS@FC with Him

Typically, stock solution of **HB-NPS@FC** (1mg/mL) was dispersed in 0.5 M PBS buffer (pH 7.0) in Milli-Q water. Fluorescence spectra of **HB-NPS@FC** were monitored for 10 times and all data were used to calculate the standard deviation (SD). The stock solution of Him (1×10^{-3} M) was added in portions (2-240 µL) to the solution of **HB-NPS@FC** and then fluorescence spectra of each

portion were recorded under the excitation wavelength of 340 nm for 3 times. All data were used to construct the calibration curve for calculation of the detection limit.

3.1.7 Determination of Him in fish samples

The fish samples including tuna and salmon were purchased from a local supermarket and were kept in a refrigerator until analysis. The accurately weighed amount of samples around 50 g was homogenized with 250 mL of 0.05 M phosphate buffer solution of pH 7.0. The homogenate was centrifuged at 25 ^{o}C, 5000 rpm for 10 minutes. The resulting clear solution of 100 µL supernatant was transferred to a 10 mL volumetric flask and diluted with the phosphate buffer solution to make the final determination.

3.1.8 Determination of Him recovery

Recovery assay was performed for examining the selectivity by adding the known concentration of Him into fish samples. Each sample was first analysed separately with standard Him solution at a concentration of 5.5, 26.5 and 50 ppm. A mixed sample was added into the solution of **HB-NPS@FC** (1 mg/mL) then the fluorescence spectra were recorded with the excitation wavelength at 340 nm. Then, the recoveries were calculated from fluorescence intensity at 525 nm by using equation;

$$y = 3.85 + 1.7x$$

When y = fluorescence intensity at 525 nm

x = concentration (μM)

3.2 Result and Discussions

3.2.1 Conceptual design for histamine sensing

Specific determination of histidine (His) and histamine (Him) is a challenge task for sensing purpose, in particularly optical detection. Most of reports concerned the ligand exchanged sensing approach of metal complexes, especially Ni^{2+} and Cu^{2+}, with Him using the UV-Vis or fluorescence spectroscopy. There are very few reports demonstrating the covalent reaction between ligand and Him or His. Kielland and coworkers [55] have fantastically reported the histamine sensing by the reaction of mesoionic acid fluoride or histamine blue (**HB**) with amino acid group by self-catalytic reaction of imidazole group in biogenic amines (Figure 3.1).

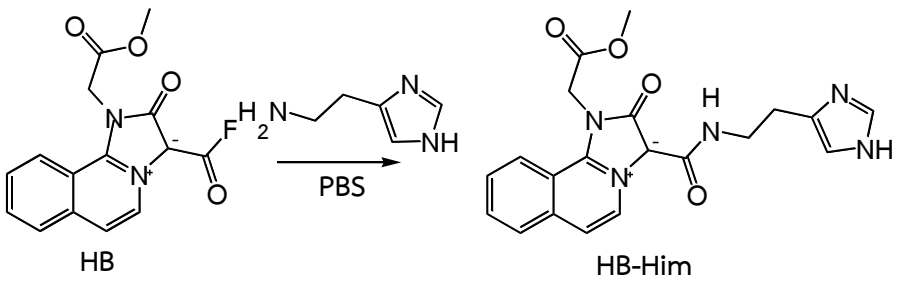

Figure 3.1 The complexation of **HB** and histamine (**HB**-Him) **[55]**

However, most of previous fluorescent chemosensors afford high sensitivity in the quantitative determination but the specific selectivity for His and Him (Figure 3.2) has been rare in the report due to both compounds comprising similar functional group of amine and imidazole, which provided the same sensing mechanism as shown in Figure 3.3.

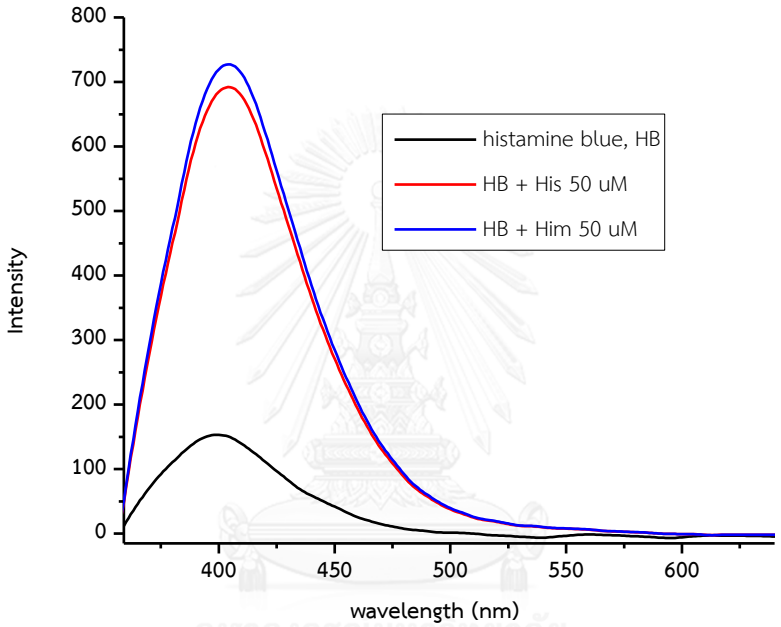

Figure 3.2 The fluorescence of **HB** (1 μM) in the presence of His and Him in PBS buffer solution pH 7.0.

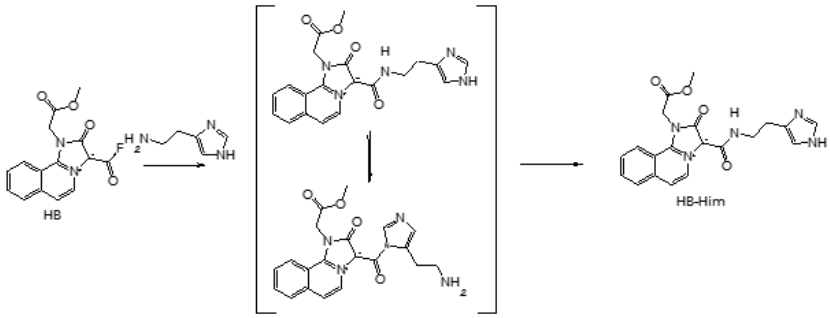

Figure 3.3 The possible mechanism of **HB** reacts with histamine (Him) **[55]**

To improve the discrimination of similar functional biogenic amines, we attempt to apply the nanoporous silica (**NPS**) for serving a high selective fluorescence sensing for biogenic amines. The selectivity stems from functionalized surface of materials with steric molecules or gatekeeper resulting in a different kinetic reaction of each biogenic amine. Concerning the discrimination of each His and Him, many reports regarding fluorescent chemosensors showed a nonspecific binding among Him and His. None of fluorescence chemosensors for biogenic amines sensing employed the fluorescence energy transfer (FRET) as a tool of detection. This approach brings us to design the donor electron fluorescence sensor for biogenic amines loaded into **NPS** and the proper electron acceptor fluorophore was modified on the surface of **NPS** resulting in significant emission changes via the FRET process. Herein, we demonstrated a highly selective fluorescence system for determination of Him by loading sensor **HB** into **NPS** which modified surface by fluorescein dye for preventing His to react with **HB** doped in **NPS**, as shown in Figure 3.4.

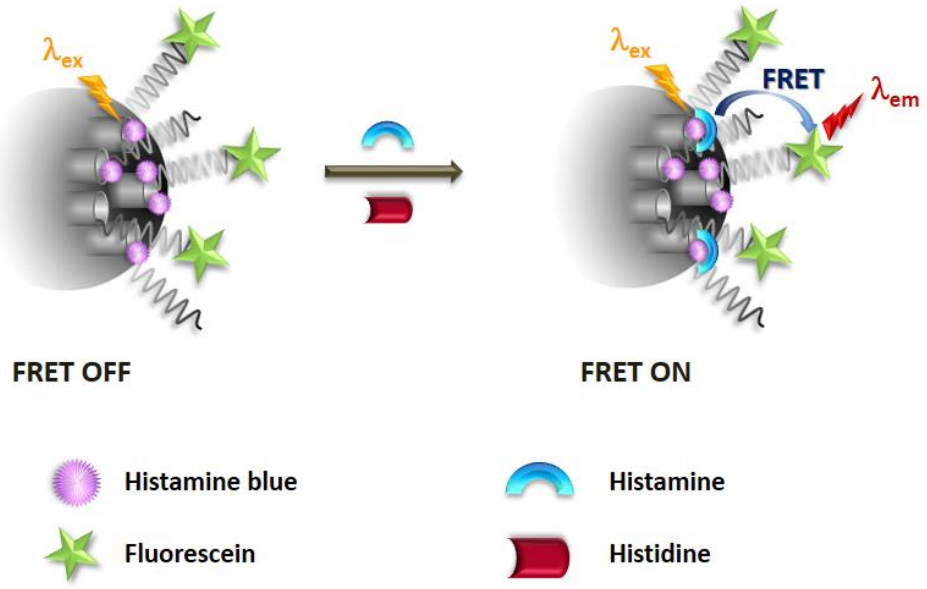

Figure 3.4 The conceptual of fluorescence sensor for Him detection.

Deeply considering the molecular structure of Him baring amine and imidazole in their structure, **HB** sensor can covalently bind with amine group by the self-catalytic reaction via imidazole. Thus, only **HB** sensor can be used to separate among biogenic amines that contain imidazole from the other biogenic amines (Figure 3.2). Since both of His and Him have a similar chemical structure containing both of amine and imidazole in their structure. Therefore, **HB** sensor could not discriminate the Him from His. Thus the obvious discrimination of Him and His by **HB** is a challenge task. However, the chemical structure of His contains the additional carboxylic acid on the side chain while Him consist of only amine on side chain. This gave the slightly fluorescence response as shown in Figure 3.5.

Histamine (Him) Histidine (His)

Figure 3.5 The molecular structure of Him and His.

The totally different charge of the target molecule bring us to design the sensory system comprising the charge gate selector on the surface of silicon nanoparticles. We selected the fluorescein dye (**FC**) performing both of the acceptor fluorophore part and gate selector for screening the specific guest through the porous of SNP. Because **FC** contains carboxylic group similar to His and the carboxylic group normally forms carboxylate ion in aqueous solution. We hypothesized that the

negative carboxylate group of **FC** could repulsion with the negative carboxylate based His. Thus, **FC** might be a filter to screen out His and allow only Him passing through the pore of NPS. Moreover, the absorption band of **FC** overlaps with the emission spectrum of **HB-Him** complexation. In our concept, the **HB** sensor acting as the donor fluorophore part which was loaded into the pore of silica nanoporous. The specific of Him can pass through the gate selector of **FC** modified on the surface of SNP and react with **HB** loaded in the pore resulting in FRET-on spectrum.

3.2.2 Synthesis of NPS@FC

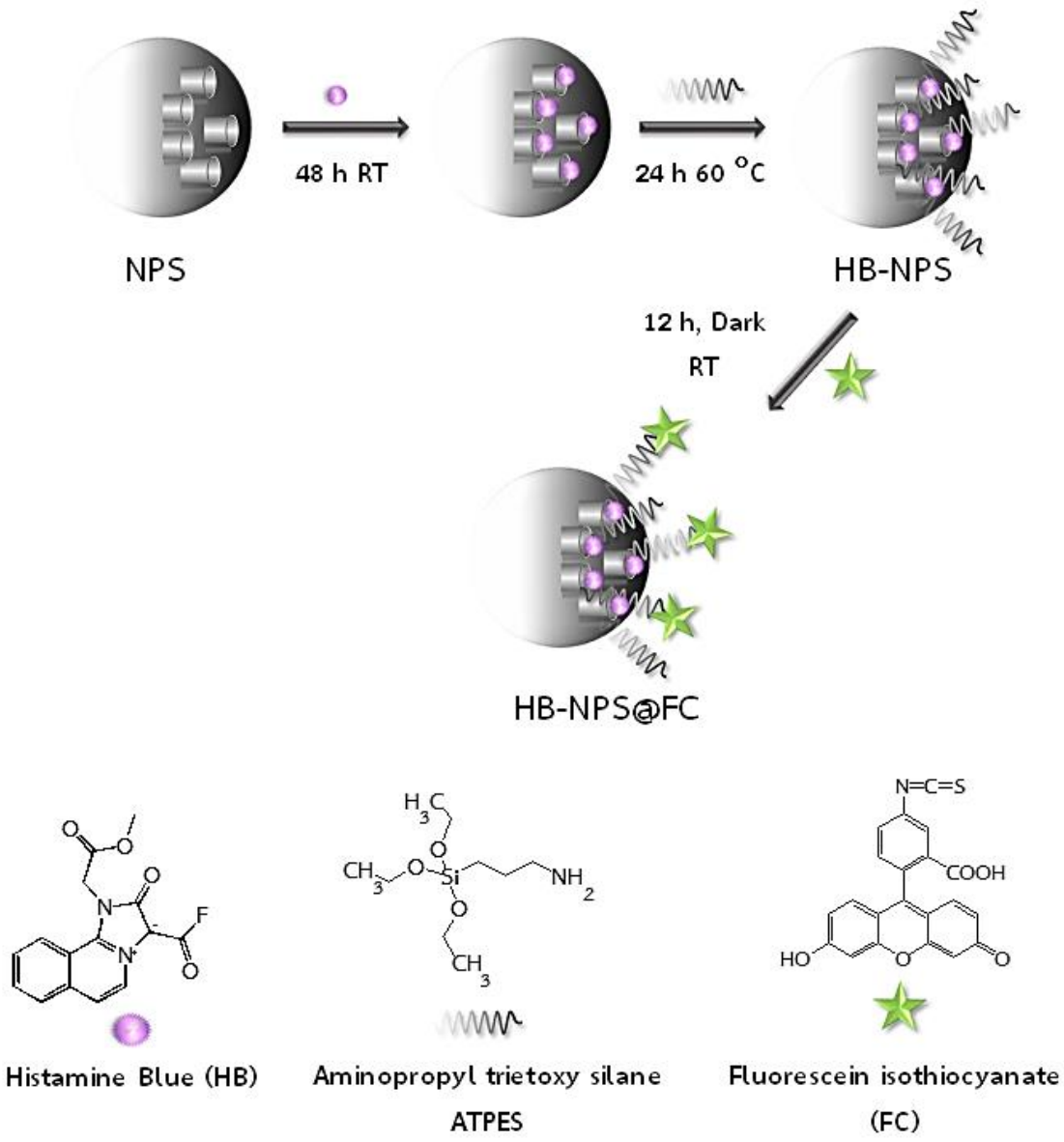

Figure 3.6 The synthesis pathway of **HB-NPS@FC**.

The sensor **HB-NPS@FC** was initially synthesized by loading **HB** sensor into nanoporous silica (NPS) by under stirring the mixture NPS and sensor **HB** in ethanol at room temperature for 48 h and then the ATPES was suddenly modified on the surface

of NPS as shown in Figure 3.6. Then, the **HB** doped in NPS was purified by centrifugation several times. To verification of HB loading into NPS, the HB-loading efficiency values of sensor HB should be firstly inspect by UV-vis spectroscopy. The **HB**-loading efficiency was examined from equation 3.1 and the result revealed the percent loading of 8%. The successful HB-loading was validated by reaction with Him which followed by fluorescence spectroscopy. Since reaction between **HB** and Him provided the fluorescence respond in PBS buffer. Herein, the fluorescent spectrometry was used to confirm the sensor **HB** loaded into NPS as shown in Figure 3.7.

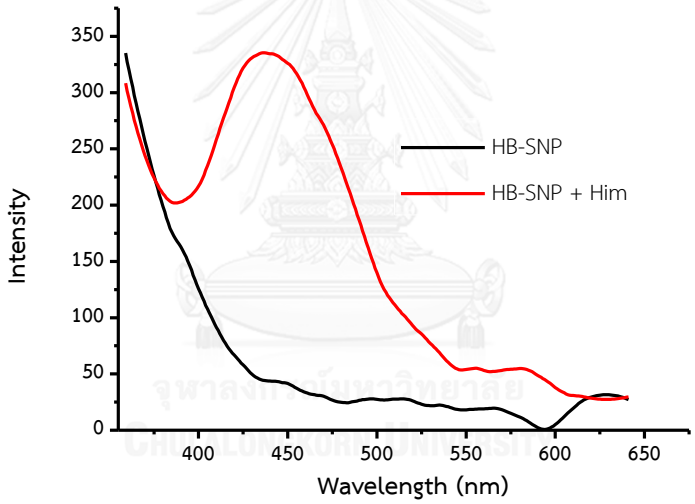

Figure 3.7 Fluorescence spectra of **HB-NPS** (1 mg/mL) in PBS buffer solution pH 7.0 in the presence of Him.

After sensor **HB** was loaded in NPS, the **FC** was then modified on the surface of NPS. The reaction was carried out in the dark place at room temperature to avoid the decomposition of **FC** dye. After the reaction completed, the solution of sensor **HB-NPS@FC** was centrifuged several times to ensure the removed of unreacted **FC**.

The product **HB-NPS@FC** was easily monitored by the colour changing of NPS from white to yellow.

3.2.3 Sensing properties of HB doped nanoporous silica (HB-NPS)

In the presence of Him, the fluorescence spectra of **HB-NPS** exhibited an enhancement in emission band at 436 nm assigned to the amide product obtained from reaction between **HB** and Him. Similarly, this emission band was also observed in the presence of His as shown in Figure 3.8. The emission band of **HB** with non-imidazole biogenic amines including DA, Lys, Tym, Glu, NE, and EPI remained unchanged. This result implied that non-imidazole biogenic amines cannot react with **HB** via imidazole self-catalytic reaction as shown in Figure 3.3. Moreover, the appearance of emission band at 436 evidently confirmed the **HB** loaded in the porous silica nanoparticles.

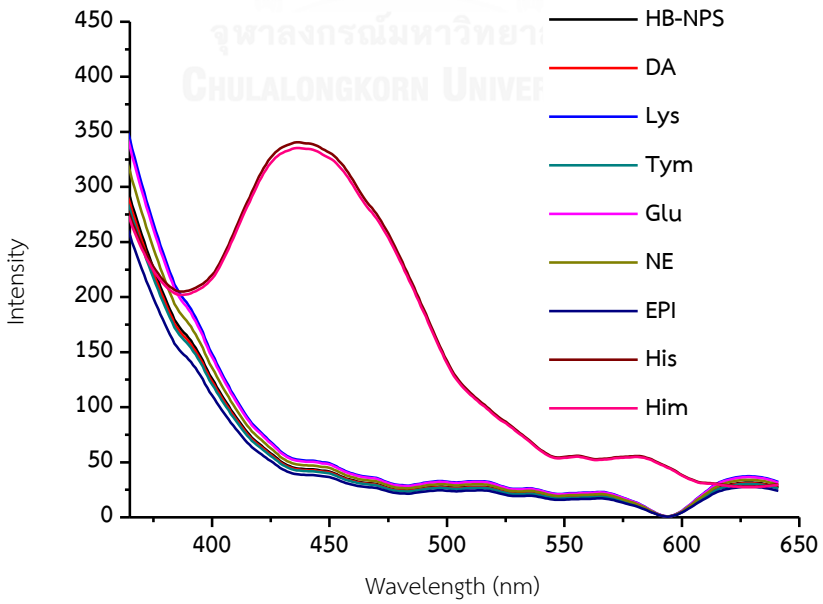

Figure 3.8 Fluorescence spectra of **HB-NPS** (1 mg/mL) in PBS buffer solution pH 7.0 in the presence of various biogenic amines.

3.2.4 Sensing properties of HB-NPS@FC

Comprehensive high selective detection of Him leads to the most engrossing sensing approach for clinical and food chemistry. To enhance the specific detection of Him, we attempted to design materials based on **HB-NPs**. As particular hypothesis of surface screening is attractive approach for screening out the interference, we chose the fabrication of the fluorescein (**FC**) acting not only the gate filter but also the proper electrons acceptor part coupling with **HB-NPs**. The characteristic fluorescence spectra of **HB-NPS@FC** in the presence of Him exhibited an enhancement of emission band at 526 nm corresponding to emission band of **FC** (Figure 3.9). Upon the addition of His and other biogenic amine, both emission band of 526 and 436 nm were disappeared. This result revealed the **FC** is a proper gate filter to allow only Him passing to react with **HB** in porous nanosilica.

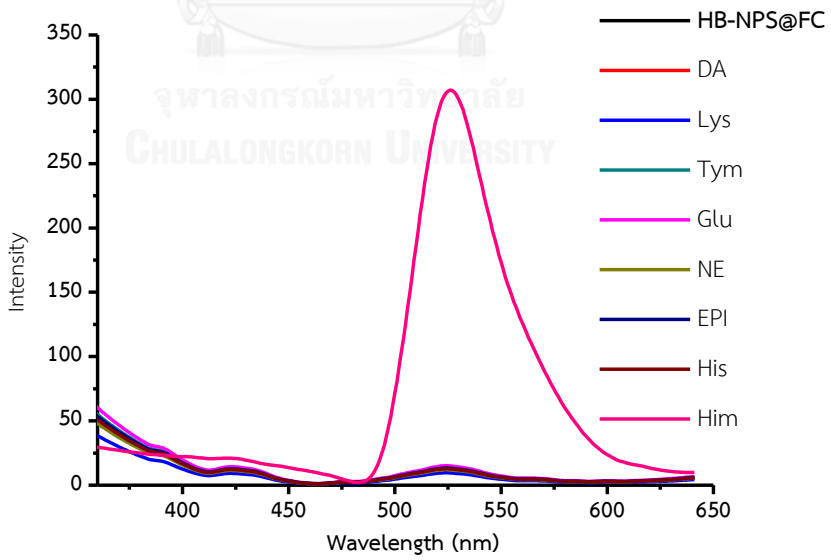

Figure 3.9 Fluorescence spectra of **HB-NPS-FC** (1 mg/mL) in PBS buffer solution pH 7.0 in the presence of various biogenic amines.

To confirm the elimination of interference His by charge repulsion, the pH profile of **HB** sensing toward His and Him was investigated. The reaction between sensor HB toward His and Him were studied on the range of pH from 5.5 - 9.17. The result showed high fluorescence intensity at 436 nm assigned to the emission band of amide product in all pH. It can be explained that the both of His and Him could reacted with sensor **HB** in all pH as shown in Figure3.10. From this result revealed the reaction between of HB with Him and His is pH independent. In the case of sensor **HB-NPS@FC,** His and Him detection was monitored emission band at 526 nm. The addition of Him provided emission band at 526 nm assigned to emission band of **FC** in all pH as shown in Figure 3.11. However, in the presence of His, this emission band was observed at pH lower 6.2. At this pH value, the structure of His contains ammonium and carboxylate ions (pKa from 6.02 – 9.17). Mover, the monoanion of **FC** is form at this pH (pKa = 6.31) [64, 65]. Then, this implied that at pH higher pKa of **FC** the carboxylic acid of **FC** was depronated to form anion species which obstructed the penetration of His due to electrostatic repulsion between carboxylated group of His and negative charge of **FC** on the surface of silica. As mentioned above, the reaction between **HB** and amine group base biogenic amines has to pass the self- catalyzed imidazole. Thus, the disappearance of emission band of **FC** and **HB** for case of other biogenic amine confirmed no reaction of **HB** and other biogenic amine which do not contain the imidazole group. As the result of sensing, **FC** was a suitable modification compound on the surface of NPS which allowed Him to penetrate through the porous and react with **HB** resulting in high selective detection of Him at pH higher than 6.2.

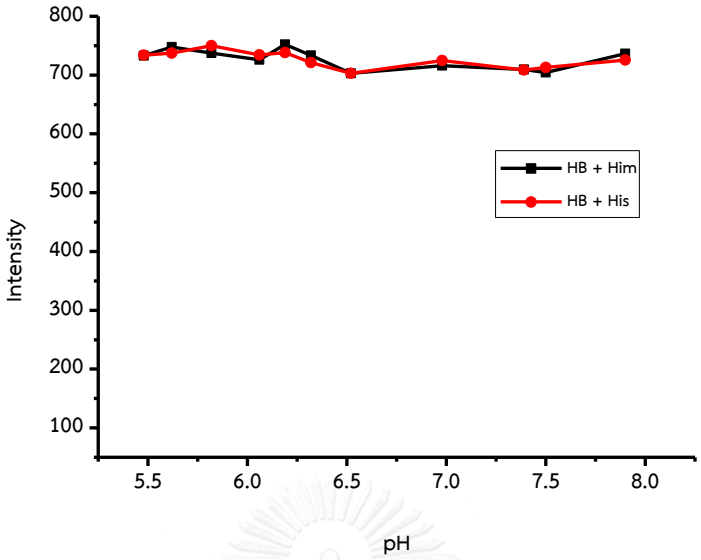

Figure 3.10 The sensing ability of **HB** toward His and Him under monitoring of emission band at 436 nm in various pH.

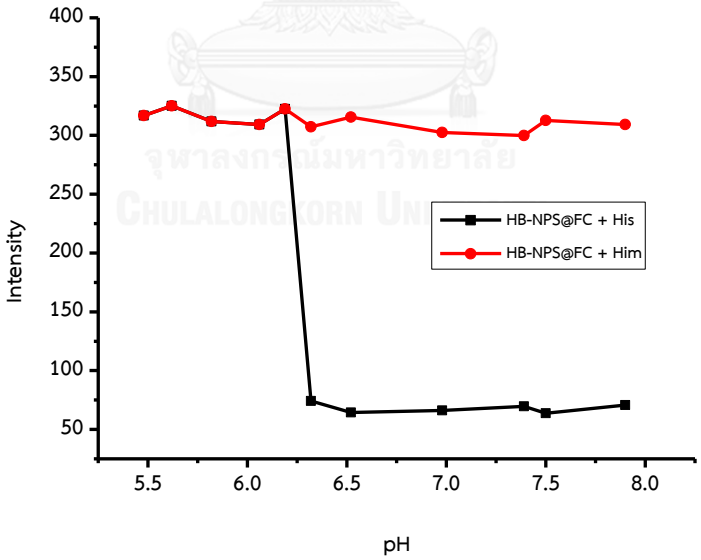

Figure 3.11 The sensing ability of **HB-NPS@FC** toward His and Him under monitoring of emission band at 526 nm in various pH.

3.2.5 Energy transfer mechanism

From the previous result, the emission band at 526 corresponding to **FC** was obviously observed. This emission band was stemmed by the resonance fluorescence energy transfer from **HB** to **FC.** To confirm the mechanism of FRET, time-resolved FRET (trFRET) technique was examined. Firstly, the time resolved emission band at 436 nm was normalized exhibit an increase fluorescence band at 526 nm upon time increasing as shown in Figure 3.2.11. The normalization of emission band at 526 nm illustrated the decrease fluorescence intensity at 436 nm and shown in Figure 3.2.12. This result revealed that fluorescence intensity at 436 nm of the **HB**⊂Him product amide product decrease with concomitant increase at 526 nm of **FC**. This is a strong evident for FRET mechanism in our detection system.

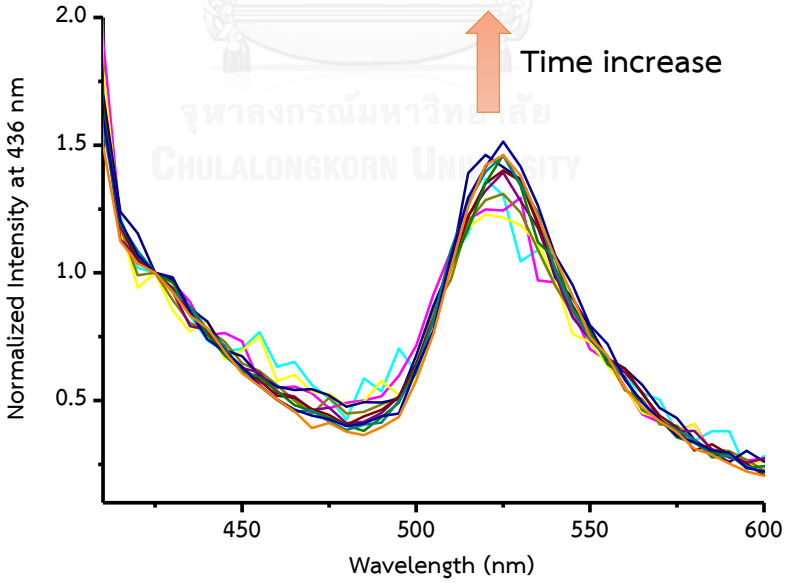

Figure 3.12 Time-resolved emission spectra of sensor **HB-NPS-FC** (1 mg/mL) in PBS buffer solution pH 7.0 upon the normalized intensity of emission band of sensor **HB**.

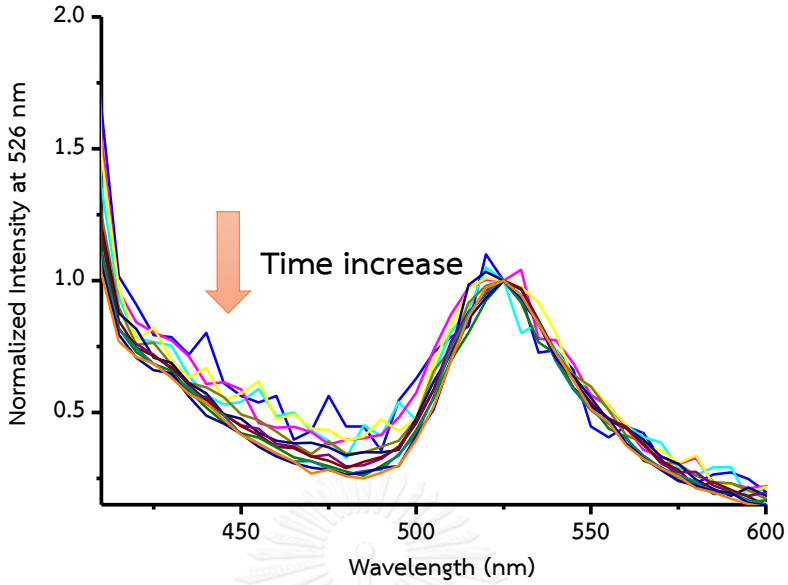

Figure 3.13 Time-resolved emission spectra of sensor **HB-NPS-FC** (1 mg/mL) in PBS buffer solution pH 7.0 upon the normalized intensity of emission band of sensor **FC**.

3.2.6 Determination of Him

Regarding to a specific detection of Him, the limit of detection (LOD) of **HB-NPS@FC** toward Him was evaluated by fluorescence titration in phosphate buffer pH 7.4. Upon increasing of Him concentration, the fluorescent intensity at 526 nm was gradually increased as shown in Figure 3.14. This result provided the detection limit of 9.29 μM under the linear relationship in the concentration range from 48 – 180 μM for Him (Figure 3.15).

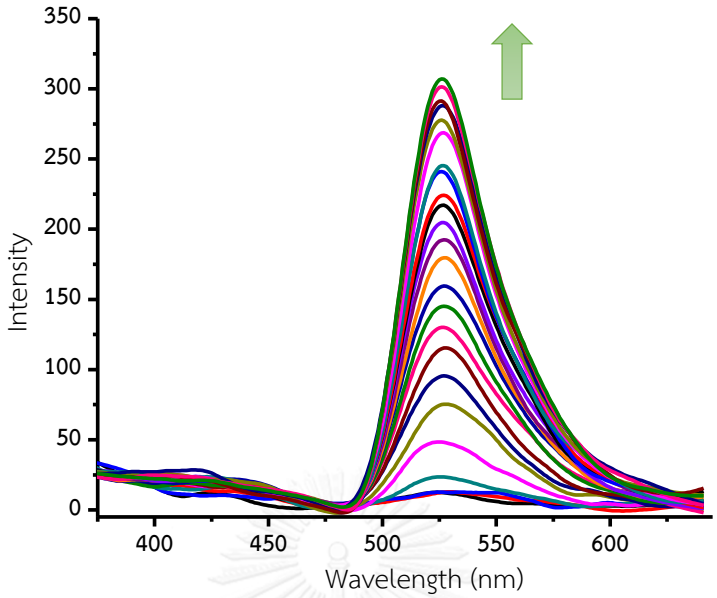

Figure 3.14 Fluorescence titration of **HB-NPS@FC** (1mg/mL) in PBS buffer solution pH 7.0 with various concentrations of Him.

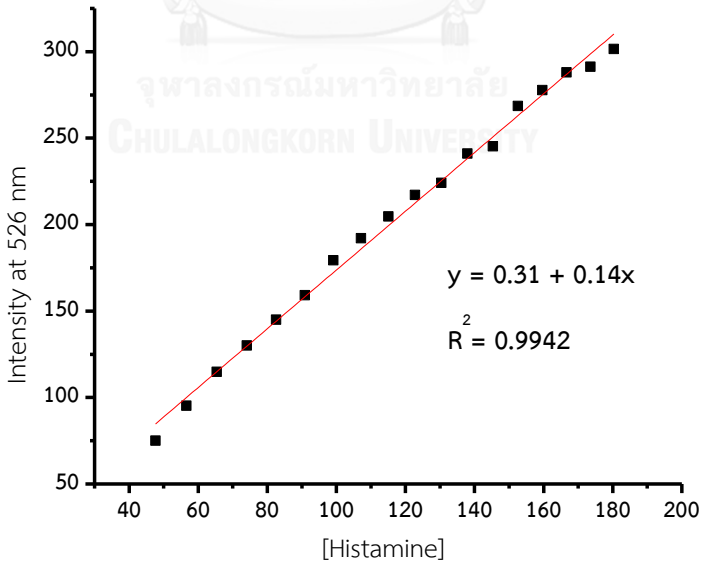

Figure 3.15 Calibration curve of fluorescence probe **HB-NPS@FC** (1 mg/mL) toward Him under PBS buffer solution pH 7.4.

Furthermore, the highly selective sensor was applied to determine the amount of Him in real salmon and tuna samples. Firstly, the calibration curves of sensors **HB-NPS@FC** toward Him in the medium of salmon and tuna were examined by following the fluorescence intensity at 526 nm in varying concentration of Him. The calibration curves provided the linear range of 22-339 ppm and 22-180 ppm of Him for salmon and tuna, respectively, as illustrated in Figure 3.16 and 3.17. The Him concentration of 26.5, 50 and 59.5 ppm was spiked into real salmon and tuna samples. The %recovery of Him was evaluated by monitoring the emission band at 526 nm. The result showed an acceptable value of %recoveries of 106.43 and 99.00 for Him detection in real samples of salmon and tuna, respectively, as presented in Table 3.1. This revealed a good analytical detection of the prepared **HBNPs@FC** sensor for Him.

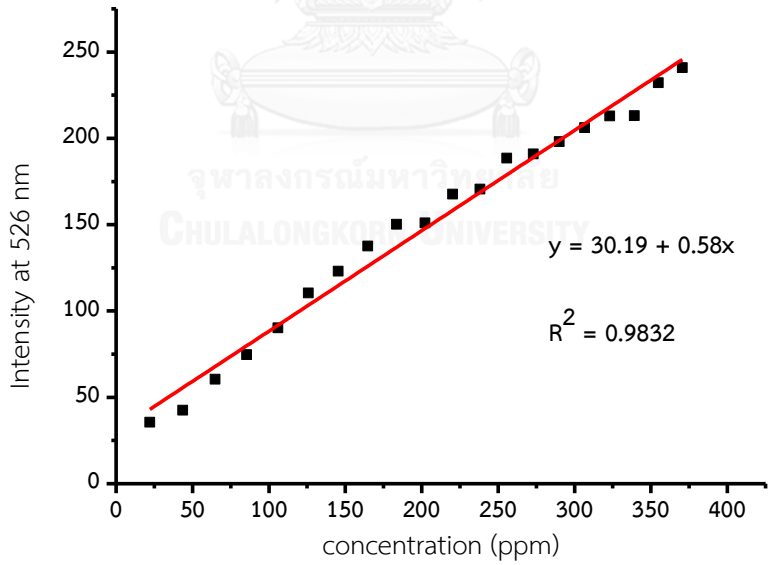

Figure 3.16 Calibration curve of **HB-NPS@FC** (1 mg/mL) toward spike Him into real salmon sample under PBS buffer solution pH 7.4.

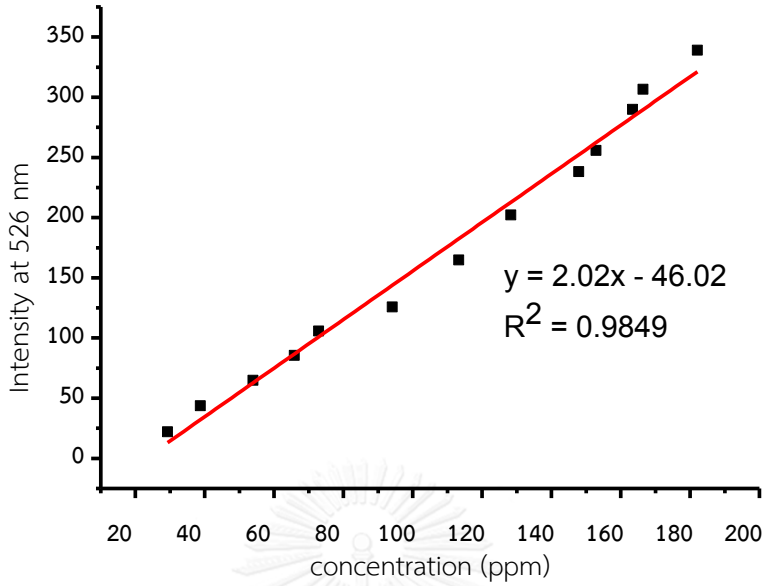

Figure 3.17 Calibration curve of **HB-NPS@FC** (1 mg/mL) toward spike Him into real tuna sample under PBS buffer solution pH 7.4.

Table 3.1 Determination of Him in real salmon and tuna samples by **HB-NPS@FC** in PBS solution pH 7.4.

Sample	Him added (ppm)	Recovery	%recovery
Salmon	26.5	29.23±0.49	110.3
	50.5	52.80±0.24	104.6
	59.5	62.13±0.91	104.4
Tuna	26.5	27.01±3.34	101.9
	50.5	49.82±5.92	98.7
	59.5	57.38±4.40	96.4

Chapter IV

Copper Sensor devices

4.1 Introduction

A long-standing challenge in the area of point-of-care (POC) diagnosis has been development of functional simple and inexpensive platforms for reproducible and rapid quantitative assays of analytes in variety of environments. The key of quantitative POC assay should be inexpensive, be easy to operate, and provide rapid and high precision without the requirement of specialized electronic devices to measure the output of the assay. To achieve this goal, measurement of time often is performed using a timer that is external to the platform of the assay. Notable examples reported by Gregory and co-worker, demonstrated quantitative assays based on hydrophobic oligomers- to- hydrophllic switch of hydrogen- peroxide- responsive. However, the oligomers need many steps for synthesis and provide a high limited of detection in the range of millimolar of analyst. Herein, we describe an approach for substantially improving the sensitive model assay by using small molecule and also reducing the waste from synthesis and saving cost.

In 2012, Kulchat and coworker have reported the molecular sensor (**FBA**) which contained spirolactam fluorescein unit and boronic acid for Cu^{2+} detection in aqueous solution. The sensing mechanism of **FBA** toward Cu^{2+} was found that Cu^{2+} perform a catalyst for the hydrolysis reaction of **FBA** to yield fluorescein as product and the rate of the reaction was depended on the concentration of copper. After hydrolysis reaction, the hydrophobicity of **FBA** sensor was changed from hydrophobic to hydrophilic compound. From this discovery, we hypothesized that **FBA** sensor could be developed to determine the concentration of Cu^{2+} in microfluidic devices.

4.2 Experiment

4.1.1 Initial prototypes of 3D microfluidic devices with flow rate of water

The 3D paper-based microfluidic device (23 mm wide x 26 mm long x 0.9 mm) was constructed by stacking alternating layers of wax-pattern paper and patterned double-side adhesive tape which contained four layers of paper and tree layers of tapes. Layer 1 of the device contained an adding water sample region on the hydrophilic conduit and a detection zone as shown in Figure 4.1. Layer 3 contained tree hydrophilic regions of 7 mm diameter disk which was pre-deposited by 7 µL of 0.1 mM yellow dye on left and right of hydrophobic regions. All prepared papers were dried before assembling the device. Layer 5 contained two hydrophilic region disks which were pre-deposited by **FBA** on the left hydrophilic region. The central hydrophilic region of this layer contained conduit 7 mm diameter x 28 mm long to separate the sample evenly into the left and right. The layer 7 contained two conduits of 7 mm diameter x 28 mm long which was deposited by 20 µL of 0.1 M pH 7.1 HEPES buffer solution and then was dried prior to assembling the device. The layers 2, 4 and 6 were the patterned tapes baring a 7 mm diameter hole that was filled with a 180 um thick disk of Watman Chromatography Paper No. 1.

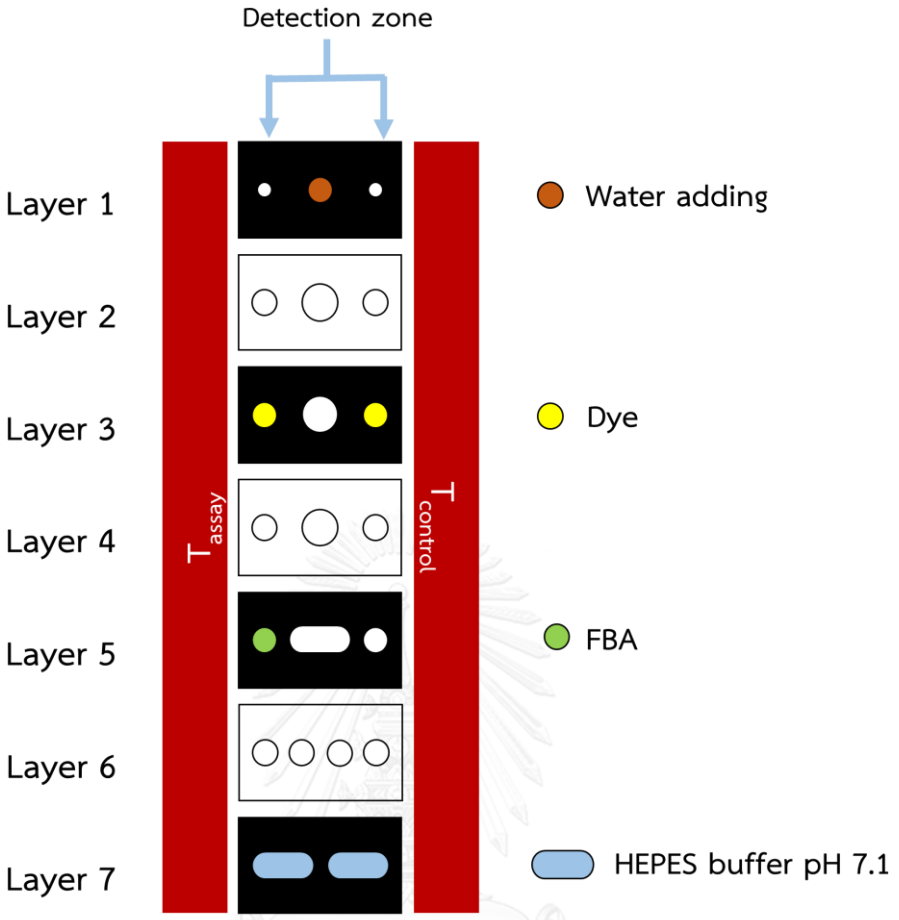

Figure 4.1 The 3D picture of device and the chemical pre-deposited in each layer for measuring the effect of amount of **FBA** toward flow-through time rate of water.

4.1.2 Prototypes of 3D microfluidic devices for detection of copper ions

The device was constructed from Watman Chromatography Paper No. 1 with 9 layers (five layers of paper and four layers of tape) with 23 mm wide x 26 mm long x 0.9 mm thick (Figure 4.2). The structure of this paper based device was similar to the previous one in the layers 1-4. For layer 5, **FBA** was doped in the sample detection hole and control hole. The central disk of hydrophilic region in layer 5 was designed to connect with conduit 7 mm diameter x 28 mm long of layer 7 to separate the

sample into the left and right zone of the device. To get rid of Cu^{2+} ion interacting with **FBA** on the control zone, NaOH was doped on the right hand side of paper hole. As the basic knowledge, Cu^{2+} ion interacts with NaOH to provide $Cu(OH)_2$ precipitate causing no interaction between Cu^{2+} ion and **FBA** on the layer 5. However, the insertion of NaOH layer made an increasing of ionic strange on the control zone. To normalize the ionic strange factor, the assay zone of layer 7 on left side of device was deposited by NaCl. The two disks of the left and right side on layer 7 were pre-deposited by 5 µL 1 mM of NaCl and NaOH, respectively, and were dried prior to assembling the device. The layer 9 contained two conduits of 7 mm diameter x 28 mm long which was pre-deposited by 20 µL of 0.1 M pH 7.1 HEPES buffer solution. The layers 2, 4, 6 and 8 were the patterned tape that contained a 7 mm diameter hole which was filled with a 180 µm thick disk of Watman Chromatography Paper No. 1.

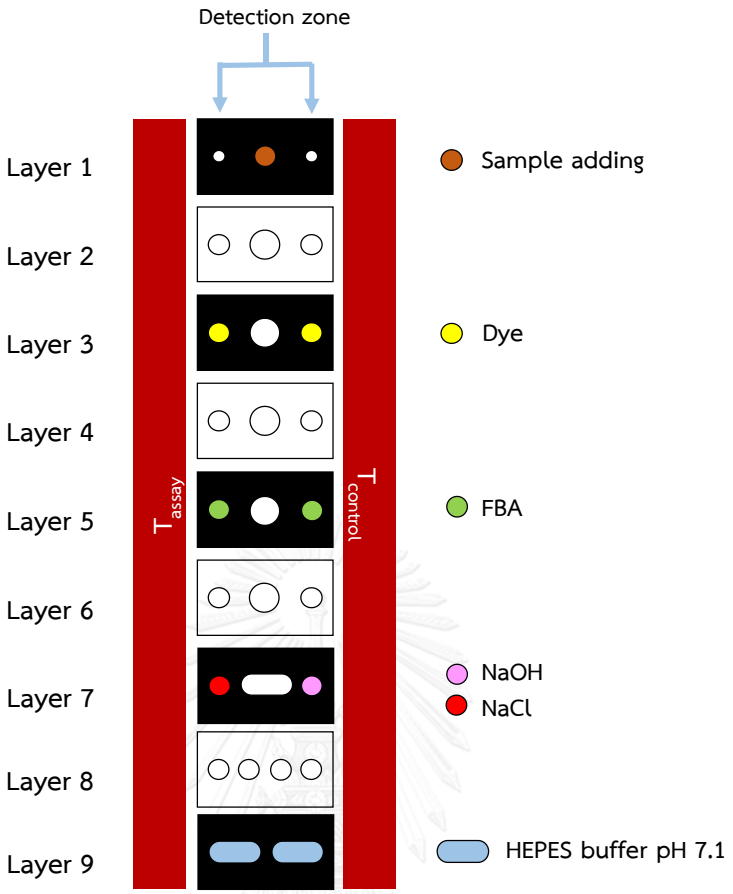

Figure 4.2 The 3D picture of device and the chemical pre-deposited in each layer for assay Cu^{2+} ions.

4.1.3 Effect of amount of FBA toward copper ions detection

4.1.4 Prototype for detection of copper ions in blood

The device was constructed from Watman Chromatography Paper No. 1 with 9 layers (five layers of paper and four layers of tape) with 23 mm wide x 26 mm long x 0.9 mm thick. The structure of this paper based device was similar to the previous one in Figure 4.2 exception in layer 1 and hole of tape in layer 2. For layer 1, the central of hydrophilic region of blood sample added hole was enlarged from 7 mm to be 15 mm

because blood sample has a higher viscosity than aqueous sample. Therefore, a high volume of hole was required for the blood solution to easily pass through the end of device. Moreover, blood sample contains white blood cell, red blood cell, protein, and plasma. Thus, the blood filter paper was inserted in layer 2 to filtrate the protein and blood cell and to allow only plasma passing through the device as shown in Figure 4.3. For layers 5, 30 μg/mm^2 **FBA** was doped in the sample detection hole and control hole. The central disk of hydrophilic region in layer 5 was designed to connect with conduit 7 mm diameter x 28 mm long of layer 7 to separate the plasma sample into the left and right zone of the device. To get rid of Cu^{2+} ion interacting with **FBA** on the control zone, layer 7 was pre-deposited by NaOH solution on the right hand side of paper hole for elimination of copper in control zone and the ionic strange was normalized by the pre-deposited NaCl disk in the assay zone (left side of the device) and the paper was dried prior to assembling the device. The layer 9 contained two conduits of 7 mm diameter x 28 mm long which was pre-deposited by 20 μL of 0.1 M pH 7.1 HEPES buffer solution and was dried by air. The layers 2, 4, 6 and 8 were patterned tape that contained a 7 mm diameter hole with a 180 um thick disk of Watman Chromatography Paper No. 1.

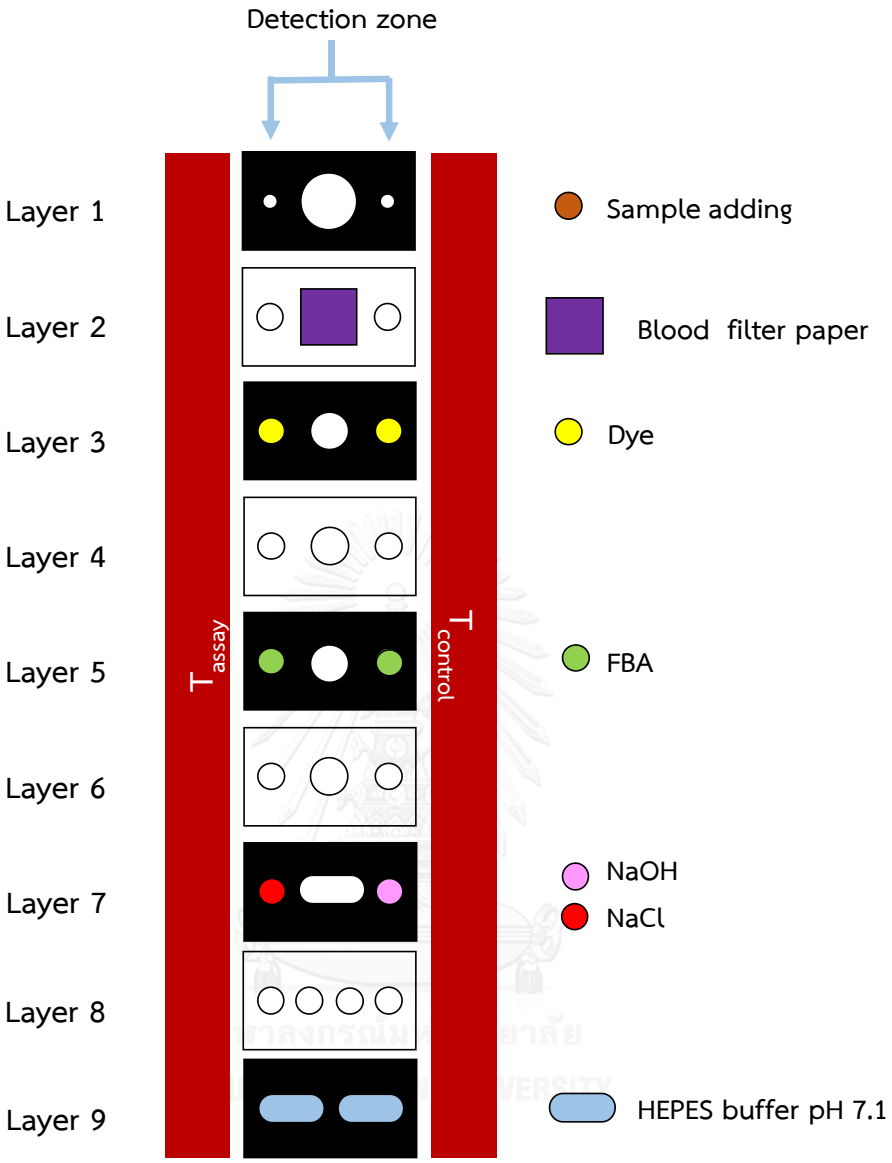

Figure 4.3 The 3D picture of device and the chemical pre-deposited in each layer for measuring the concentration of copper in blood.

4.2 Result and discussion

4.2.1 The effect of concentration of FBA toward flow-through rate of water

In 2012, Kulchat and coworkers [66] have reported the molecular sensor (**FBA**) which containing of spirolactam fluorescein unit and boronic acid for Cu^{2+} ion detection in aqueous solution. The sensing mechanism of **FBA** toward Cu^{2+} ion was found that Cu^{2+} ion performed a catalyst for the hydrolysis reaction of **FBA** to yield fluorescein as product (Figure 4.4a and 4.4b). After hydrolysis reaction, the hydrophobicity of **FBA** sensor was changed to be hydrophilic compound. From this finding, we hypothesized that **FBA** sensor could be developed to determine the concentration of Cu^{2+} ion in microfluidic devices.

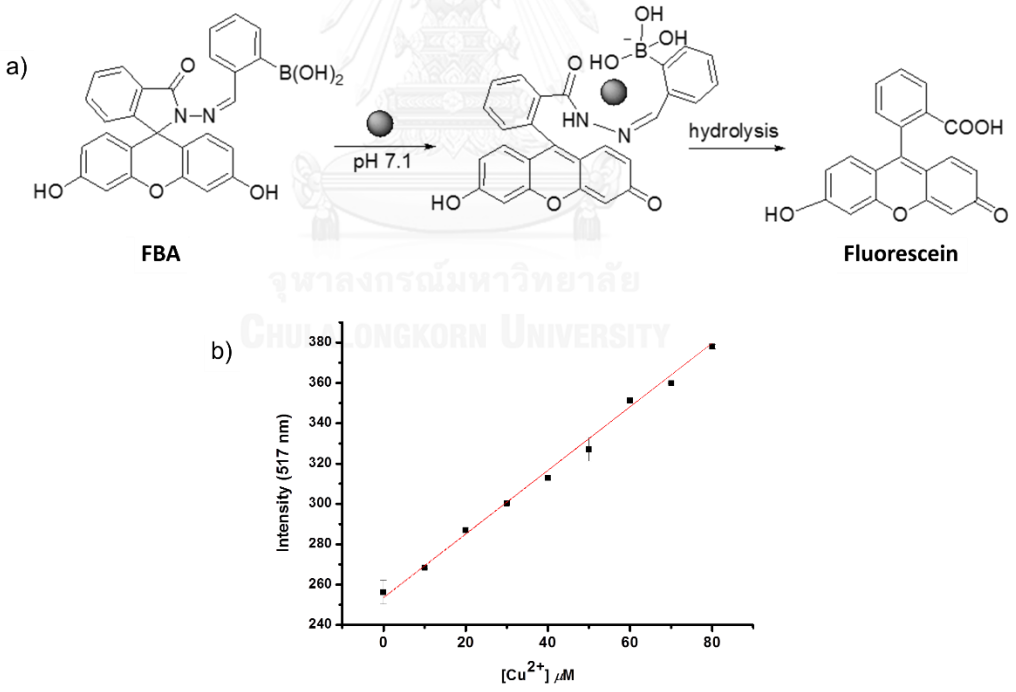

Figure 4.4 (a) The copper catalyzed hydrolysis of **FBA** (b) The fluorescence intensity at 517 nm of 5 μM **FBA** in the presence of various concentration of Cu^{2+} ion (5% Ethanol in HEPES buffer pH 7.1).

Based on the hydrolysis reaction of **FBA**, we expected that when Cu^{2+} ion passed through the 3D microfluidic device and hydrolyzed the **FBA** doped on the paper to give the hydrophilic fluorescein which directly effected on the flow-through rate of sample. Hydrophilic compound inverted from hydrophobic compound of dye would enhance the flow-through rate of sample through the device and make a wet of detection region and a consequent color appeared on the detection region. The time required to wet the detection region corresponds to the concentration of the analyte. Firstly, the relationship between amounts of **FBA** and the flow-through rate of water was investigated from the first design (Figure 4.1). After the adding 120 µL of water on layer 1, the water wicked down through the device in z direction and passed through the central disks of layer 3 and conduited on layer 5 to separate the sample into the left and the right of the device before passing through layer 7 under gravity force. When the sample wicked through layer 7 of the devices, the pre-deposited HEPES buffer on this layer was redissolved and adjusted the pH value of the sample at approximately 7.1 to protect the rapid hydrolysis of **FBA** in the absence of Cu^{2+} ions. In layer 7, the central conduit can also separate the sample evenly into the left and the right hand side of the device before moving up in opposite z direction under the capiraly force. This arrangement on the left side allowed the sample to react with **FBA** in layer 5 and to pass through layer 3. The yellow dye moved through the end of device on layer 1 resulting in the appearance of yellow spot on the top layer in the detection zone. Since wicking rate in porous media typically relates to temperature, humidity, and sample viscosity on the sample distribution [67, 68], we, thus, designed the strategy to offer a step forward on the goal of quantitative point-of-care assays without using auxiliary instruments. The control region on the right-hand channel (Figure

4.5) which was fabricated the same of reagents as the sampling zone. When **FBA** affected to flow-through rate of water, the difference time requirement for appearance of yellow color on the top layer of control zone (right-hand of the device) called $T_{control}$ and the assay zone (T_{assay}, left-hand of device) on layer 1 would be observed. The affected factors (temperature, humidity, and sample viscosity) toward sample distribution rates were normalized by measuring the time required for the control zone (right-hand of the device) and assay zone (the left-hand of the device) called $T_{measurement}$. Since, the **FBA** deposited in assay zone on layer 5 could retard the flow-through rate of water while the control zone was not be deposited by **FBA**. The appearance of yellow spot on the detection zone of layer 1 in control zone was faster than in assay zone. Consequently, the measurement time ($T_{measurement}$) is the different time of the assay time (T_{assay}) and the control time ($T_{control}$) for the sample passing through the device from the beginning to the end of the device. The relationship between $T_{measurement}$, $T_{control}$, and Tassay is depicted in eq 4.1.

$$T_{measurement} = T_{assay} - T_{control} \qquad (4.1)$$

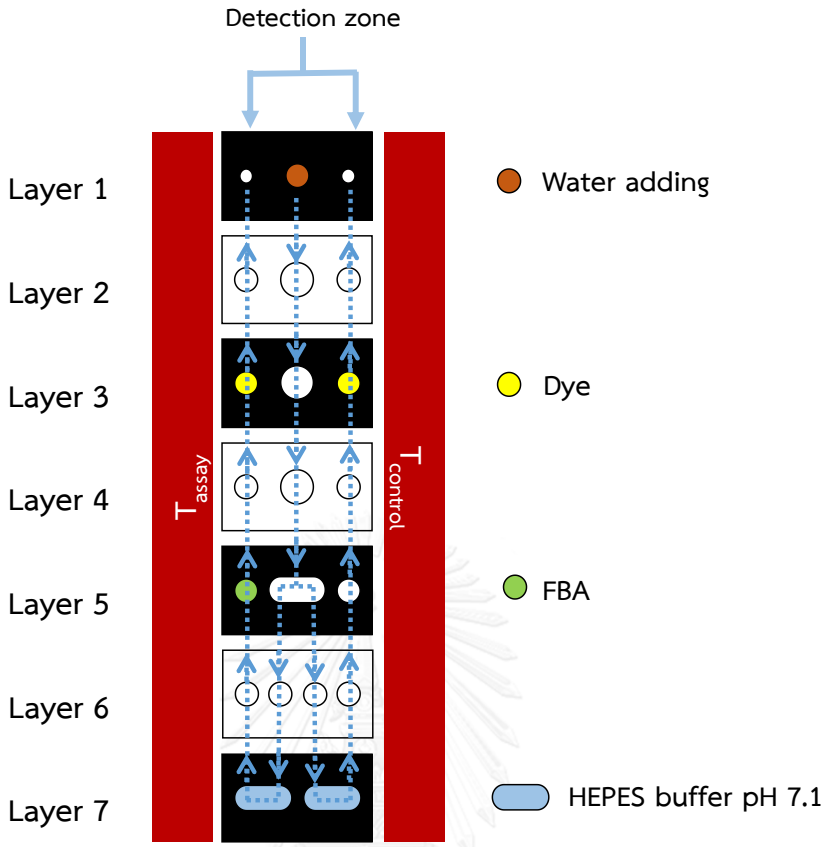

Figure 4.5 The flow-through pathway of water from the entrance to the end of the 3D microfluidic device.

To verify the effect of amount of **FBA** toward flow-through rate, the amount of **FBA** in the left-hand disk in layer 5 was examined from 0-45 µg/mm^2 but the disk of the control region without **FBA** on layer 5 was constant. After adding 120 µL pure water to the device, the result exhibited the increasing of $T_{measurement}$ upon the increment of amount of **FBA** as shown in Table 4.1 and Figure 4.6. It suggested that **FBA** would retard the flow-through rate of water and it revealed that the proper amount of 45 µg/mm^2 of **FBA** in layer 5 gave the largest decrease of flow-through rate of water.

Table 4.1 The time measurement of flow-through water from the microfluidic device Figure 4.1.

H2O	Amount of PBA per volume of paper					
	0 mg/mm3	9 mg/mm3	18 mg/mm3	27 mg/mm3	36 mg/mm3	45 mg/mm3
Time measurement (sec)	203	223	227.5	1480.5	1906.5	2113.5
	216.5	227.5	194.5	1246	2081.5	2160.5
	206.5	210	385	1620.5	1980.5	2210
	201	234.5	304	1513	2060	2053
	222.5	248.5	318	1452.5	1907	2160.5
Average	209.9	228.7	285.8	1462.5	1987.1	2139.5
S.D.	8.25	14.22	75.73	136.76	82.43	59.18

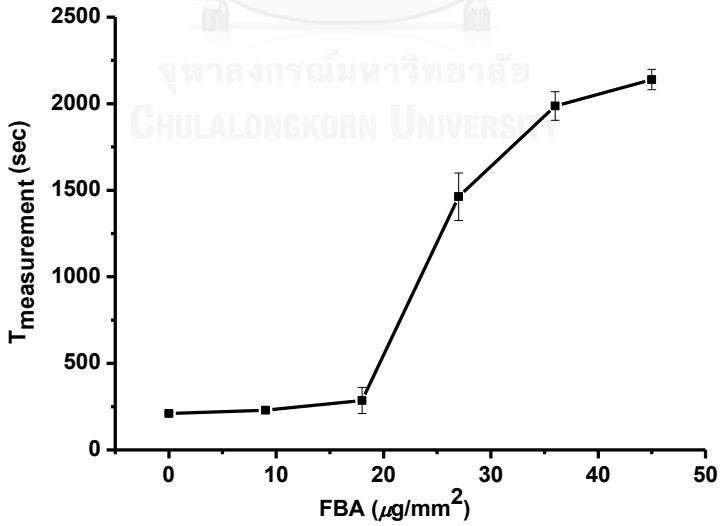

Figure 4.6 The effect of **FBA** amount toward $T_{measurement}$ of water with the flow-through rate from the beginning to the end of the device.

4.2.2 The effect of concentration of copper toward flow-through rate

From the designed device in Figure 4.1, the result showed that the pre-deposited **FBA** could retard the flow-through rate of water and the suitable amount of **FBA** at 45 μg/mm^2 exhibited an effective retard of the flow-through rate of water. Then, we continuously adopted the 45 μg/mm^2 of **FBA** to investigate the effect of copper ions toward the flow-through rate by using the device which was constructed as shown in Figure 4.2.

In the case of copper solution, sample solution was added on the control hole of layer 1 and wicked down through to layer 6 of the device (Figure 4.7) in z direction. When the copper solution passed to layer 7, it was separated into the left and right hand sides of the device before passing through the holes in layer 8 by gravity force. Then, the sample wicked through layer 9 of the devices. The pre-deposited HEPES buffer on this layer was re-dissolved to control pH of the sample to be approximately 7.1. In layer 9, the central conduit also separated the sample evenly into the assay zone (left side of the device) and the control zone (right side of the device) before moving up in the opposite z direction by the capiraly force. This arrangement allowed the sample passing through the different deposited substance of control and assay zone in layer 7. In the control zone, the sample passed through the pre-deposited NaOH disk on right-hand channel disk of the device to precipitate the copper hydroxide in sample solution. Then, the sample solution without free Cu^{2+} ion passed to layer 5 and could not hydrolyte the **FBA** on the control zone. From this design, the copper ion solution in the assay zone passed through layer 5 and catalyzed the hydrolysis reaction of **FBA** in layer 5 (as the reaction shown in Figure 4.4) as a result of an increase

of flow-through rate of sample. The period time of assay zone was shorter than that of control zone. The T_{assay} and $T_{control}$ were recorded when the yellow color was observed on the detection zone of layer 1. Since, the copper ion in the assay zone could hydrolyze **FAB** to provide the hydrophilic products which enabled to quickly pass through layer 5. The factors of sample distribution rates were normalized by the relationship between Tmeasurement, Tcontrol, and Tassay as depicted in eq 4.2.

$$T_{measurement} = T_{control} - T_{assay} \qquad (4.2)$$

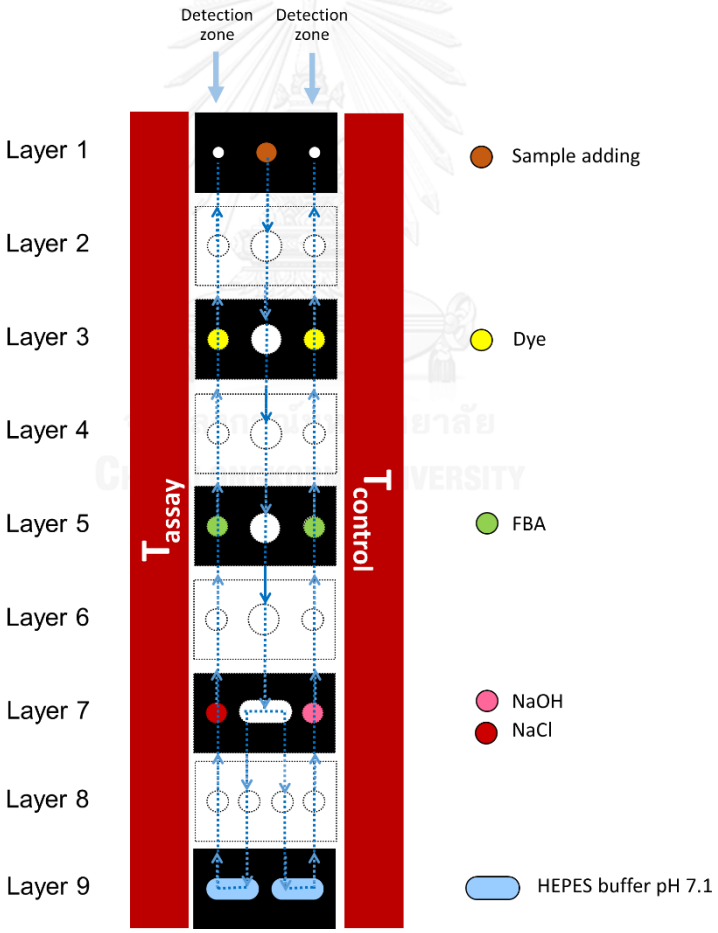

Figure 4.7 The flow-through pathway of Cu^{2+} ions from the entrance to the end of the 3D microfluidic device.

The $T_{measurement}$ of the device (as constructed in Figure 4.2) was obtained by using the amount of 45 μg/mm^2 of **FBA**. The results showed that the $T_{measurement}$ was increased upon the increment of copper as shown in Figure A3 and Table A3. The limit of detection (LOD) of Cu^{2+} ion detection by this device under the linear range of 5 – 100 μM was 38.77 μM.

4.2.3 The effect of the quantity of FBA on the limit of detection (LOD)

To create the general assay device, the device was actually needed to increase the sensitivity of the system to detect copper ions in vary low concentration. For previous report, Gregory and co-workers discovered that a relationship between the LOD of analyst in sample and quantity of pre-deposited molecule on the paper can reduce the flow-through rate of analytes. To increase the sensitivity of the device for detection of analyte at low concentration, the optimization of quantity of pre-deposited **FBA** in layer 5 (Figure 4.2) was investigated. The experiment was designed by varying amount of pre-deposited **FBA** concentration on the disk in layer 5 in the range of 10-70 μg/mm^2. The relationships of time measurement ($T_{meansurment}$) obtained from the experiment and the concentration of Cu^{2+} ion at the different amounts of **FBA** deposited on paper of 10, 25, 30, 45, 55 and 70 μg/mm^2 were illustrated in Figures A1-A6 and Tables A1-A6, respectively. The calibration curves provided the detection limit of Cu^{2+} ion over the various amount of **FBA** deposited on paper at 10, 25, 30, 45, 55 and 70 μg/mm^2 of 19.42, 13.56, 11.36, 38.77 42.98 and 42.78, respectively. The relationship between LOD and quantities of **FBA** pre-deposited in layer 5 exhibited a

parabolic feature as shown in Figure 4.8 and Table 4.2. The optimized of detection limit for Cu^{2+} ion detection was achieved by the quantity of 30 μg/mm^2 **FBA**. A high amount of **FBA** deposited on layer 5 over 30 μg/mm^2 showed high limit of detection (45, 55 and 70 μg/mm^2). It can be explained that the high concentration of **FBA** possibly obstructed a small amount of hydrophilic compound obtained by the hydrolysis reaction of **FBA** at low concentration of Cu^{2+} ion. Thus the devices needed a high concentration of copper ion to allow the hydrolyzed compound passing through the device. Consequently, high amount of pre-deposited **FBA** in layer 5 provided a high LOD for copper ion detection. Alternatively, a small amount of pre-deposited **FBA** at 10 and 25 μg/mm^2 on layer 5 preferentially allows the hydrophilic compound passing through the device causing a high flow-through rate. (Figure A1-A2 and Table A1-A2) Clearly, the optimized quantity of **FBA** per area of paper was definitely important for improving the sensitivity of the assay. The dynamic range and the sensitivity of the assay for Cu^{2+} ion in each quantity of **FBA** were summarized in Table 4.2.

Table 4.2 The effect of quantity of **FBA** in the sensitivity and dynamic range of assay for copper (II) ions

Quantity of **FBA** in layer 5	Dynamic range of Cu^{2+}(μM)	LOD (μM)
10	10-75	19.42
25	10-60	13.56
30	5-95	11.36
45	5-95	38.77
55	10-100	42.98
70	10-100	42.78

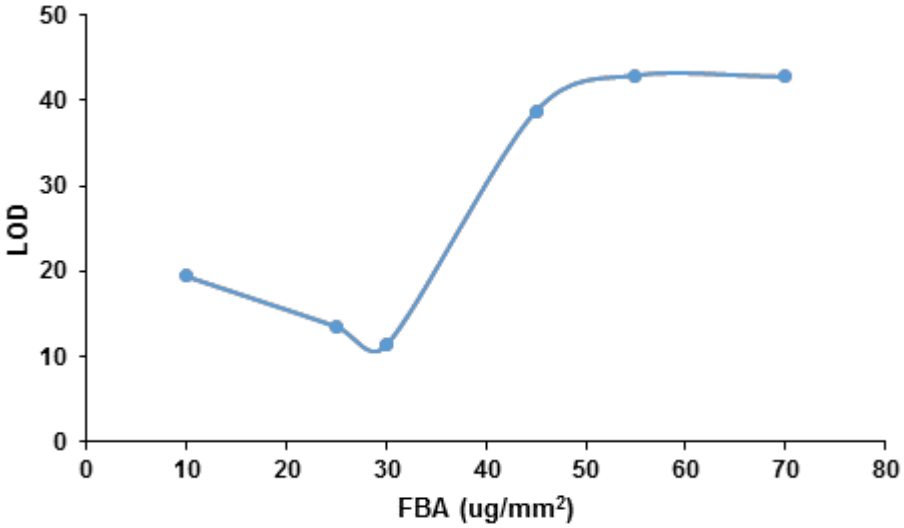

Figure 4.8 The amount of **FBA** effects to limit of detection for determination of copper ions.

4.2.4 The Application of 3D microfluidic device for measurement of Cu^{2+} ion in blood sample

Since the device enabled to utilized for quantitative detection of copper (II) ions by measuring $T_{measurement}$ of the sample. The detection limit was depended on the amount of doped **FBA** on the device. We would apply this paper-based device to detect copper (II) ions in the real blood sample by the designed device in Figure 4.3. Our purpose is to develop the easy device of Cu^{2+} ions sensing in a real blood sample without centrifugation to separate white blood cell, red blood cell, protein, and plasma. We attended to design a new paper device by inserting the additional blood filter paper for removing white and red blood cell and protein from the blood sample. Consequently, the required plasma of blood sample was allowed to pass through the paper-based device. Interestingly, the suitable plasma passing through paper-based device would provide the color change on the detection zone in case of the presence of Cu^{2+} ion in blood sample. Then, the device comprised the blood filter paper for separation of plasma from blood cell and protein. Furthermore, the sample added area would be enlarged to support the higher volume of sample as shown in Figure 4.9. The challenges of this work is to design the easily paper-based device for detection of analyte in blood sample without the centrifugation and the avoidance of coagulation of blood cell in paper-based device. Therefore, the heparin was added into blood sample to prolong blood coagulation. Moreover, the volume of blood sample and type of blood filter papers including LF1, MF1, VF1 and VF2, were

optimized to offer a good $T_{measurement}$ values as shown in Table 4.3. The result revealed that 100 and 150 µL of blood volume could not be determined for assay copper (II) ions in blood sample. It was possibly blood coagulation and/or the plasma volume in blood sample was not enough to pass through the beginning to the end of the device. In the case of higher volume of sample, blood sample could pass to the end of the device. Considering the filter papers for measurement, LF1 showed the lowest $T_{measurement}$ in 300 µL of blood volume. Then, it is notably that the 300 µL of blood volume and LF1 were selected for further determination of Cu^{2+} ion in blood sample. From the table 4.4 and titration curves in Figure 4.11, the $T_{measurement}$ was gradually increased upon the increment of Cu^{2+} ion. The calibration curve in Figure 4.12 provided the linear range from 10-100 µM of copper ions concentration. This system was developed to the analytical application by measuring % recoveries of Cu^{2+} ion which was spiked in the blood sample. The result showed an acceptable value of 103.38% recovery (Table 4.5). It could be concluded that this paper-based device offers an excellently promising detection of copper (II) ions in real times sample.

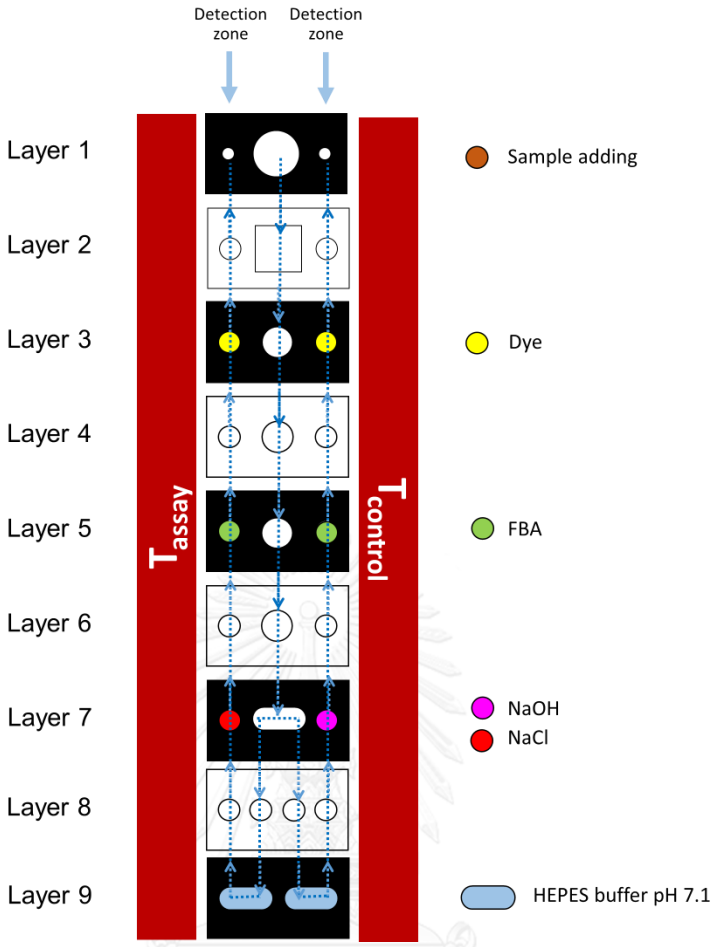

Figure 4.9 The flow-through pathway of blood sample from the entrance to the end of the 3D microfluidic device.

Table 4.3 The $T_{measurement}$ of the device (as prepared in Figure A4) by varying of blood filter paper and blood volume.

Blood volume (μL)	Time measuring (min)			
	LF1	MF1	VF1	VF2
100	ND	ND	ND	ND
150	ND	ND	ND	ND
200	23	31	ND	ND
250	19	21	ND	ND
300	13	15	30	38

Table 4.4 The detection of copper ions in blood sample by using the device in Figure 4.3

30 µg/mm3	[Cu2+]/ µM						
	0	10	50	100	150	250	500
Time measurement (Dt)	22	39	91	167	167	212	219
	13.5	33.5	94.5	117.5	177.5	191	251
	12	22	79	142	191	215	224.5
	10	35	105	165.5	175	196.5	237
	8	19.5	92	148.5	187	212	214.5
	7.5	29	73.5	166.5	201.5	208	217
	13.5	34	105	134	171	181.5	213
	10.5	19.5	80	151	196	211	210.5
	12	40	104.5	139.5	182.5	178	206
	23	27	75.5	159	187	219	234.5
Average	13.2	29.85	90	149.05	183.55	202.4	222.7
STD	5.308274	7.663224	12.4231	16.20434	11.04901	14.60936	14.07559

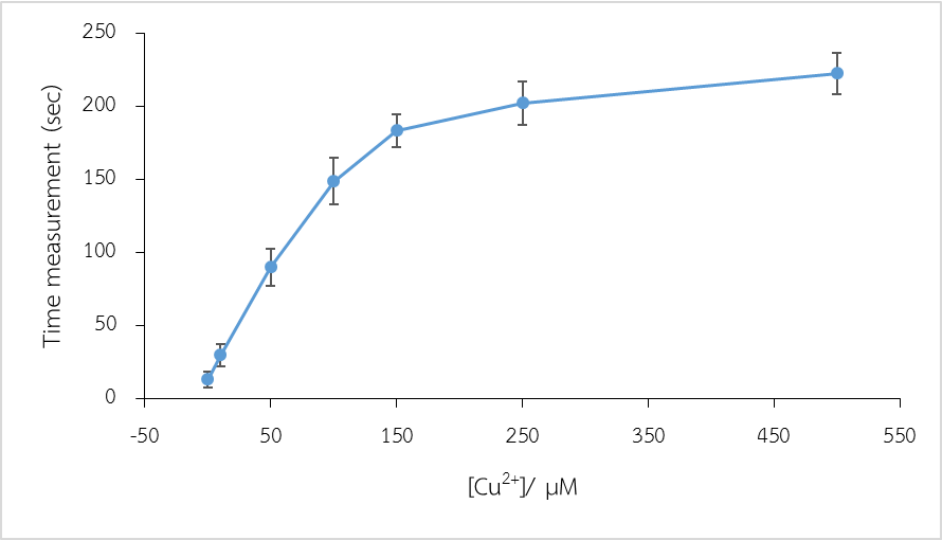

Figure 4.10 The graph showed the relationship between $T_{measurement}$ and concentration of Cu^{2+} ion.

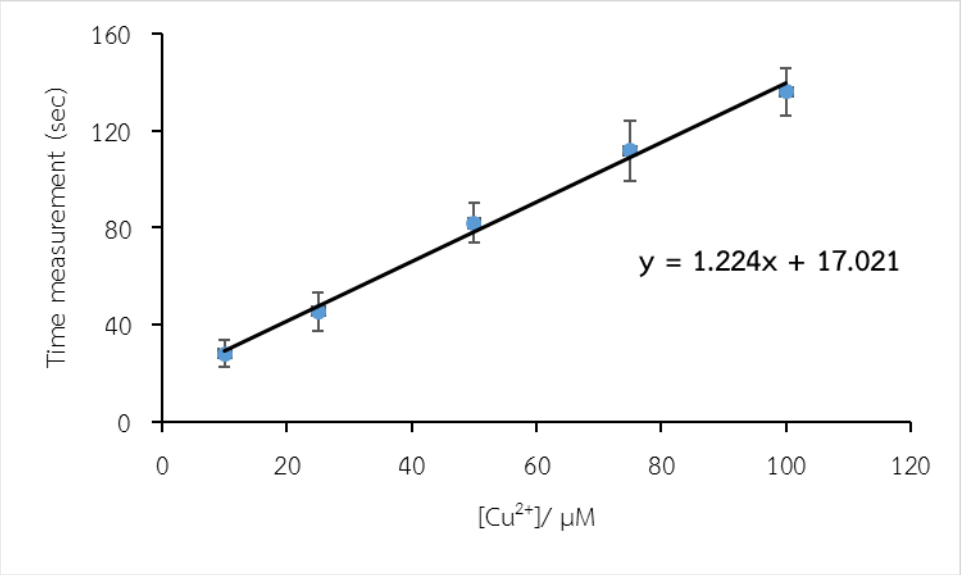

Figure 4.11 The calibration curve of $T_{measurement}$ from the device (Figure 4.3) toward spike Cu^{2+} ion into blood sample.

Table 4.5 Determination of Cu^{2+} in blood samples from the device in Figure 3.3.3.

Experiment	Amount of Cu^{2+}			
	Added (μM)	Recovery (μM)	Average (μM)	% recovery
1	13.22	13.18	13.67 ± 0.2	103.4
2	13.22	13.25		
3	13.22	13.24		

Chapter V

Conclusions

For catecholamine sensing, a new sensing approach based on the assembled complexes of two fluorescence sensors inducing the FRET process for high discrimination of catecholamines have successfully developed. Firstly, the sensor **PBA** showed an excellent covalent binding between boronic acid and catechol groups of catecholamine provided the high selectivity of catecholamine over other biogenic amines. For two sensing elements, the additional sensor **CA** could discriminate EPI from other catecholamines. Based on a basic reaction of sensor **PBA** and the catechol group as well as sensor **CA** and primary amines of catecholamine, the catecholamine induces the intermolecular assembled complexes between sensors **PBA** and **CA** by properly coupled fluorescence chemosensors via the FRET-on process. On the basis of these findings, the possibility of the intermolecular assembled sensors based on non-complicated sensory molecules by using a specific guest as a linker highlighted a powerful tool for sensing purposes in real time analysis in the field of medical diagnosis.

In the case of histamine sensing, we have successfully developed a new fluorescence sensors based on the **HB** doped in nanoporous silica and surface modification with **FC** to provide FRET process and highly discriminate among biogenic amines. The case of a non-surface modification (**HB-NPS**) sensing offered the promising

selectivity of His and Him over other biogenic amines by the imidazole self-catalytic reaction between **HB** added in NPS and amine group of biogenic amines. For **HB-NPS@FC** sensing, the negative charge of **FC** at pH over 6.2 could screen His from analytical detection of Him. The self-catalytic reaction of sensor **HB** with biogenic amines and negative charge selection afforded the highly selective fluorescence sensor for Him via FRET-On process. To apply the **HB- NPS@FC** in food chemistry, the fluorescence chemosensor displayed a good quantitative determination of Him in real fish samples with real time analysis. On the discovery of highly selective Him detection, the couple of sensor and surface selector is a good candidate for powerful specific detection of Him in the field of clinical diagnosis and food chemistry.

In the microfluidic devices, we described a new designed 3D microfluidic device based on switching hydrophobic **FBA** to hydrophilic product. The use of this assay device in detection was completed in few minutes, and the readout was simple measurements of time to quantify the amount of copper analyte in a sample. The device was designed to two parts. The first part is assay zone that composed of buffer, NaCl, food coloring and **FBA.** The second part is the control zone that was designed to normalize the affected factors (temperature, humidity, and sample viscosity) toward sample distribution rates. The control zone was deposited by NaOH for removing Cu^{2+} from sample. The good detection limit for detection of Cu^{2+} ion was achieved by depositing the quantity of 30 μg/mm^2 **FBA**.

For application, the device was applied to detect copper ions in the real blood sample. The result provided the linear range from 10- 100 μM of copper ions concentration. This system was applied to measure %recoveries of the spike samples of copper to the blood sample and the result showed an acceptable value of 103.38% recovery. Thus, this highlighted a powerful paper-based device in real time analysis for Cu^{2+} ion determination in diagnosis task.

REFERENCES

[1] Paris, I., et al. Copper neurotoxicity is dependent on dopamine-mediated copper uptake and one-electron reduction of aminochrome in a rat substantia nigra neuronal cell line. Journal of Neurochemistry 77(2) (2001): 519-529.

[2] Gingrich, J.A. and Caron, M.G. Recent Advances in the Molecular Biology of Dopamine Receptors. Annual Review of Neuroscience 16(1) (1993): 299-321.

[3] Bravo, E.L., Tarazi, R.C., Gifford, R.W., and Stewart, B.H. Circulating and Urinary Catecholamines in Pheochromocytoma. New England Journal of Medicine 301(13) (1979): 682-686.

[4] Taylor, S.L., Stratton, J.E., and Nordlee, J.A. Histamine Poisoning (Scombroid Fish Poisoning): An Allergy-Like Intoxication. Journal of Toxicology: Clinical Toxicology 27(4-5) (1989): 225-240.

[5] Bartholomew, B.A., Berry, P.R., Rodhouse, J.C., Gilbert, R.J., and Murray, C.K. Scombrotoxic fish poisoning in Britain: features of over 250 suspected incidents from 1976 to 1986. Epidemiology and Infection 99(3) (1987): 775-782.

[6] Bjornsdottir-Butler, K., Jones, J.L., Benner, R., and Burkhardt Iii, W. Development of a real-time PCR assay with an internal amplification control for detection of Gram-negative histamine-producing bacteria in fish. Food Microbiology 28(3) (2011): 356-363.

[7] Sparks, S.N. and Millard, S. Speech and language characteristics of genetic syndromes. Journal of Communication Disorders 14(5) (1981): 411-419.

[8] Suchi, M., Harada, N., Wada, Y., and Takagi, Y. Molecular cloning of a cDNA encoding human histidase. Biochimica et Biophysica Acta (BBA) - Gene Structure and Expression 1216(2) (1993): 293-295.

[9] Swi Chang, T.M. Artificial cells with emphasis on bioencapsulation in biotechnology. in El-Gewely, M.R. (ed.)Biotechnology Annual Review, pp. 267-295: Elsevier, 1995.

[10] Tada, K. and Nihei, K. Founders of Child Neurology in Japan – Keiya Tada. Brain and Development 26(3) (2004): 143-145.

[11] Tada, K., et al. Intellectual development in patients with untreated histidinemia: A collaborative study group of neonatal screening for inborn errors of metabolism in Japan. The Journal of Pediatrics 101(4) (1982): 562-563.

[12] Silva, C.C.G., Da Ponte, D.J.B., and Dapkevicius, M.L.N.E. Storage Temperature Effect on Histamine Formation in Big Eye Tuna and Skipjack. Journal of Food Science 63(4) (1998): 644-647.

[13] Kanki, M., Yoda, T., Ishibashi, M., and Tsukamoto, T. Photobacterium phosphoreum caused a histamine fish poisoning incident. International Journal of Food Microbiology 92(1) (2004): 79-87.

[14] Maue, M. and Schrader, T. A Color Sensor for Catecholamines. Angewandte Chemie 117(15) (2005): 2305-2310.

[15] Liu, C.-H., Yu, C.-J., and Tseng, W.-L. Fluorescence assay of catecholamines based on the inhibition of peroxidase-like activity of magnetite nanoparticles. Analytica Chimica Acta 745 (2012): 143-148.

[16] Bai, H.-Y., Campo, F.J.D., and Tsai, Y.-C. Sensitive electrochemical thrombin aptasensor based on gold disk microelectrode arrays. Biosensors and Bioelectronics 42 (2013): 17-22.

[17] Yoon, J. and Czarnik, A.W. Fluorescent chemosensing of catechol and catecholamines in water. Bioorganic & Medicinal Chemistry 1(4) (1993): 267-271.

[18] Frattini, V. and Lionetti, C. Histamine and histidine determination in tuna fish samples using high-performance liquid chromatography: Derivatization with o-phthalaldehyde and fluorescence detection or UV detection of “free” species. Journal of Chromatography A 809(1–2) (1998): 241-245.

[19] He, H.-Z., Wang, M., Chan, D.S.-H., Leung, C.-H., Qiu, J.-W., and Ma, D.-L. A label-free G-quadruplex-based luminescent switch-on assay for the selective detection of histidine. Methods 64(3) (2013): 205-211.

[20] Shi, F., Liu, S., and Su, X. Dopamine functionalized–CdTe quantum dots as fluorescence probes for l-histidine detection in biological fluids. Talanta 125 (2014): 221-226.

[21] Zhang, L.-Y. and Sun, M.-X. Determination of histamine and histidine by capillary zone electrophoresis with pre-column naphthalene-2,3-dicarboxaldehyde derivatization and fluorescence detection. Journal of Chromatography A 1040(1) (2004): 133-140.

[22] Sapsford, K.E., Berti, L., and Medintz, I.L. Materials for Fluorescence Resonance Energy Transfer Analysis: Beyond Traditional Donor–Acceptor Combinations. Angewandte Chemie International Edition 45(28) (2006): 4562-4589.

[23] Sun, Y., Wallrabe, H., Seo, S.-A., and Periasamy, A. FRET Microscopy in 2010: The Legacy of Theodor Förster on the 100th Anniversary of his Birth. ChemPhysChem 12(3) (2011): 462-474.

[24] Banwell, M.G., Hungerford, N.L., and Jolliffe, K.A. Synthesis of the Sialic Acid (–)-KDN and Certain Epimers from (–)-3-Dehydroshikimic Acid or (–)-Quinic Acid. Organic Letters 6(16) (2004): 2737-2740.

[25] Secor, K.E. and Glass, T.E. Selective Amine Recognition: Development of a Chemosensor for Dopamine and Norepinephrine. Organic Letters 6(21) (2004): 3727-3730.

[26] Azath, I.A. and Pitchumani, K. Flavone modified-β-cyclodextrin as a highly selective and efficient fluorescent chemosensor for Cu2+ ions and l-histidine. Sensors and Actuators B: Chemical 188 (2013): 59-64.

[27] Mikulski, D., Basinski, K., Gasowska, A., Bregier-Jarzebowska, R., Molski, M., and Lomozik, L. Experimental and quantum-chemical studies of histamine complexes with copper(II) ion. Polyhedron 31(1) (2012): 285-293.

[28] Seto, D., Soh, N., Nakano, K., and Imato, T. An amphiphilic fluorescent probe for the visualization of histamine in living cells. Bioorganic & Medicinal Chemistry Letters 20(22) (2010): 6708-6711.

[29] Wu, P. and Yan, X.-P. Ni2+-modulated homocysteine-capped CdTe quantum dots as a turn-on photoluminescent sensor for detecting histidine in biological fluids. Biosensors and Bioelectronics 26(2) (2010): 485-490.

[30] Li, Z.a., Lou, X., Li, Z., and Qin, J. A New Approach to Fluorescence "Turn-On" Sensing of α-Amino Acids. ACS Applied Materials & Interfaces 1(2) (2009): 232-234.

[31] Attia, M.S., Diab, M., and El-Shahat, M.F. Diagnosis of some diseases related to the histidine level in human serum by using the nano optical sensor Eu–Norfloxacine complex. Sensors and Actuators B: Chemical 207, Part A (2015): 756-763.

[32] Bhatnagar, D., Kumar, V., Kumar, A., and Kaur, I. Graphene quantum dots FRET based sensor for early detection of heart attack in human. Biosensors and Bioelectronics 79 (2016): 495-499.

[33] Ganiga, M. and Cyriac, J. FRET based ammonia sensor using carbon dots. Sensors and Actuators B: Chemical 225 (2016): 522-528.

[34] Maniyazagan, M., et al. Rhodamine based "turn–on" molecular switch FRET–sensor for cadmium and sulfide ions and live cell imaging study. Sensors and Actuators B: Chemical 238 (2017): 565-577.

[35] Puthiyedath, T. and Bahulayan, D. A click-generated triazole tethered oxazolone-pyrimidinone dyad: A highly selective colorimetric and ratiometric FRET based fluorescent probe for sensing azide ions. Sensors and Actuators B: Chemical 239 (2017): 1076-1086.

[36] Qin, J.-c., Yang, Z.-y., Wang, G.-q., and Li, C.-r. FRET-based rhodamine–coumarin conjugate as a Fe3+ selective ratiometric fluorescent sensor in aqueous media. Tetrahedron Letters 56(35) (2015): 5024-5029.

[37] Lewis, G.G., Robbins, J.S., and Phillips, S.T. Point-of-Care Assay Platform for Quantifying Active Enzymes to Femtomolar Levels Using Measurements of Time as the Readout. Analytical Chemistry 85(21) (2013): 10432-10439.

[38] Lewis, G.G., Robbins, J.S., and Phillips, S.T. Phase-Switching Depolymerizable Poly(carbamate) Oligomers for Signal Amplification in Quantitative Time-Based Assays. Macromolecules 46(13) (2013): 5177-5183.

[39] Lewis, G.G., DiTucci, M.J., and Phillips, S.T. Quantifying Analytes in Paper-Based Microfluidic Devices Without Using External Electronic Readers. Angewandte Chemie International Edition 51(51) (2012): 12707-12710.

[40] Feuster, E.K. and Glass, T.E. Detection of Amines and Unprotected Amino Acids in Aqueous Conditions by Formation of Highly Fluorescent Iminium Ions. Journal of the American Chemical Society 125(52) (2003): 16174-16175.

[41] Exner, O. Calculating equilibrium constants from spectral data: Reliability of the Benesi-Hildebrand method and its modifications. Chemometrics and Intelligent Laboratory Systems 39(1) (1997): 85-93.

[42] Kádár, M., Biró, A., Tóth, K., Vermes, B., and Huszthy, P. Spectrophotometric determination of the dissociation constants of crown ethers with grafted acridone unit in methanol based on Benesi-Hildebrand evaluation. Spectrochimica Acta Part A: Molecular and Biomolecular Spectroscopy 62(4–5) (2005): 1032-1038.

[43] Ding, Y.-r., Xiao, N.-y., and Xia, Y.-f. Short-period fluctuation analysis of the new BIH LOD series. Chinese Astronomy and Astrophysics 12(4) (1988): 334-338.

[44] Ipe, D.S. and Ulett, G.C. Evaluation of the in vitro growth of urinary tract infection-causing gram-negative and gram-positive bacteria in a proposed synthetic human urine (SHU) medium. Journal of Microbiological Methods 127 (2016): 164-171.

[45] Lee, S.K., Choi, M.G., Choi, J., and Chang, S.-K. Fluorescence signaling of Zn2+ levels in synthetic urine by dipicolylamine-armed hydroxynaphthalimide. Sensors and Actuators B: Chemical 207, Part A (2015): 303-307.

[46] Ninnemann, A.L., Lechner, W.V., Borges, A., and Lejuez, C.W. Synthetic cannabinoids to avoid urine drug screens: Implications for contingency management and other treatments for drug dependence. Addictive Behaviors 63 (2016): 72-73.

[47] Akkaya, E.U., Huston, M.E., and Czarnik, A.W. Chelation-enhanced fluorescence of anthrylazamacrocycle conjugate probes in aqueous solution. Journal of the American Chemical Society 112(9) (1990): 3590-3593.

[48] Huang, X. and Zacharia, N.S. Facile Assembly Enhanced Spontaneous Fluorescent Response of Ag+ Ion Containing Polyelectrolyte Multilayer Films. ACS Macro Letters 3(10) (2014): 1092-1095.

[49] Huston, M.E., Akkaya, E.U., and Czarnik, A.W. Chelation enhanced fluorescence detection of non-metal ions. Journal of the American Chemical Society 111(23) (1989): 8735-8737.

[50] Huston, M.E., Haider, K.W., and Czarnik, A.W. Chelation enhanced fluorescence in 9,10-bis[[(2-(dimethylamino)ethyl)methylamino]methyl]anthracene. Journal of the American Chemical Society 110(13) (1988): 4460-4462.

[51] Kwon, J.Y., et al. A Highly Selective Fluorescent Chemosensor for Pb2+. Journal of the American Chemical Society 127(28) (2005): 10107-10111.

[52] Yoon, J. and Czarnik, A.W. Fluorescent chemosensors of carbohydrates. A means of chemically communicating the binding of polyols in water based on chelation-enhanced quenching. Journal of the American Chemical Society 114(14) (1992): 5874-5875.

[53] Bao, X., et al. A new selective fluorescent chemical sensor for Fe3+ based on rhodamine B and a 1,4,7,10-tetraoxa-13-azacyclopentadecane conjugate and its imaging in living cells. Sensors and Actuators B: Chemical 208 (2015): 54-66.

[54] Dong, W.-K., Akogun, S.F., Zhang, Y., Sun, Y.-X., and Dong, X.-Y. A reversible “turn-on” fluorescent sensor for selective detection of Zn2+. Sensors and Actuators B: Chemical 238 (2017): 723-734.

[55] Kielland, N., Vendrell, M., Lavilla, R., and Chang, Y.-T. Imaging histamine in live basophils and macrophages with a fluorescent mesoionic acid fluoride. Chemical Communications 48(59) (2012): 7401-7403.

[56] Deze, E.G., et al. Metal loaded nanoporous silicas with tailor-made properties through hyperbranched polymer assisted templating approaches. Microporous and Mesoporous Materials 235 (2016): 107-119.

[57] Li, J., Xu, L., Zheng, N., Wang, H., Lu, F., and Li, S. Biomimetic synthesized bimodal nanoporous silica: Bimodal mesostructure formation and application for ibuprofen delivery. Materials Science and Engineering: C 58 (2016): 1105-1111.

[58] Mohammadi Ziarani, G., Badiei, A., Aslani, Z., and Lashgari, N. Application of sulfonic acid functionalized nanoporous silica (SBA-Pr-SO3H) in the green one-pot synthesis of triazoloquinazolinones and benzimidazoquinazolinones. Arabian Journal of Chemistry 8(1) (2015): 54-61.

[59] Zarezadeh-Mehrizi, M. and Badiei, A. Highly efficient removal of basic blue 41 with nanoporous silica. Water Resources and Industry 5 (2014): 49-57.

[60] Bi, Y., et al. Facile large-scale preparation of mesoporous silica microspheres with the assistance of sucrose and their drug loading and releasing properties. International Journal of Pharmaceutics 500(1–2) (2016): 77-84.

[61] Dai, J.-T., et al. Enhancement of gemcitabine against pancreatic cancer by loading in mesoporous silica vesicles. Chinese Chemical Letters.

[62] Geng, H., et al. Hollow mesoporous silica as a high drug loading carrier for regulation insoluble drug release. International Journal of Pharmaceutics 510(1) (2016): 184-194.

[63] Xu, G., Shen, X., Dai, L., Ran, Q., Ma, P., and Cai, K. Reduced bacteria adhesion on octenidine loaded mesoporous silica nanoparticles coating on titanium substrates. Materials Science and Engineering: C 70, Part 1 (2017): 386-395.

[64] Alvarado-González, M., Orrantia-Borunda, E., and Glossman-Mitnik, D. Computational note on the calculation of the pKa of fluorescein. Journal of Molecular Structure: THEOCHEM 869(1–3) (2008): 105.

[65] Batistela, V.R., et al. pKa determinations of xanthene derivates in aqueous solutions by multivariate analysis applied to UV–Vis spectrophotometric data. Spectrochimica Acta Part A: Molecular and Biomolecular Spectroscopy 79(5) (2011): 889-897.

[66] Kulchat, S., Chaicham, A., Ekgasit, S., Tumcharern, G., Tuntulani, T., and Tomapatanaget, B. Self-assembled coordination nanoparticles from nucleotides and lanthanide ions with doped-boronic acid-fluorescein for detection of cyanide in the presence of Cu2+ in water. Talanta 89 (2012): 264-269.

[67] Li, L., Nikiforidis, G., Leung, M.K.H., and Daoud, W.A. Vanadium microfluidic fuel cell with novel multi-layer flow-through porous electrodes: Model, simulations and experiments. Applied Energy 177 (2016): 729-739.

[68] Li, L., Zheng, K., Ni, M., Leung, M.K.H., and Xuan, J. Partial modification of flow-through porous electrodes in microfluidic fuel cell. Energy 88 (2015): 563-571.

Appendix

Table A.1. Time measurement for copper ions detection from the device (Figure 4.2) with the pre-deposited **FBA** at 10 μg/mm^2.

10 μg/mm^2 of FBA	[Cu^{2+}]/ μM							
	0	10	25	40	50	60	75	100
Time measurement (Δt)	10.5	22.5	13.5	47	41.5	41.5	76	52.5
	5.5	12	13.5	37.5	48.5	48	75.5	76
	5	26.5	27.5	29	52	40	52.5	65
	3.5	21.5	36	23.5	59.5	47.5	60.5	75.5
	1.5	12	26	32.5	33	52	69.5	80.5
	2.5	13.5	17	30.5	58	58.5	76	69.5
	1	15.5	21	29	33	59.5	48.5	76
	16.5	16.5	19	45.5	35.5	47.5	58	81
	2.5	13	17	56	56	58	76	49
	2	11.5	33.5	36.5	38	40.5	57	52.5
Average	5.05	16.45	22.4	36.7	45.5	49.3	64.95	67.75
S.D.	4.884499	5.257006	8.009716	10.031063	10.53302	7.487768	10.82808	12.30007

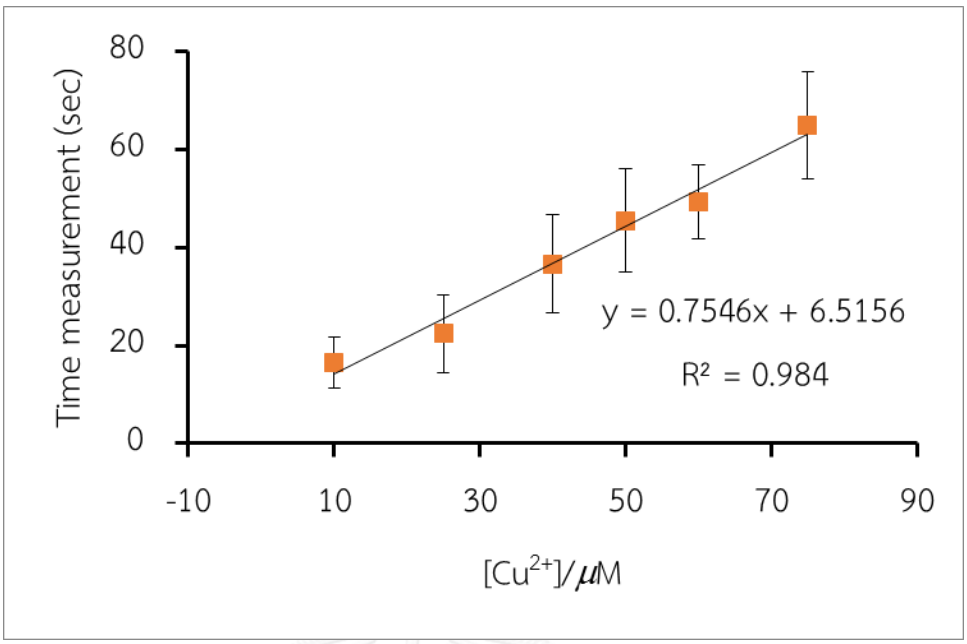

Figure A.1 The calibration curve of $T_{measurement}$ from the device (Figure 4.2) with the pre-deposited **FBA** at 10 μg/mm^2 toward copper ions in sample.

Table A.2 Time measurement for copper ions detection from the device (Figure 4.2) with the pre-deposited **FBA** at 25 μg/mm^2.

25 μg/mm^2 of FBA	[Cu^{2+}]/ μM							
	0	10	25	40	50	60	75	100
Time measurement (Δt)	2	2	17	21	44.5	31	78	103
	3	1.5	18	33	34	44.5	81	96
	10.5	3	5.5	26.5	27	27	90	77
	1	3	24	15	26.5	35.5	72.5	78.5
	1.5	11	7	16.5	28.5	47	97.5	80.5
	2.5	7.5	11	20	24	42	76	83.5
	8	2.5	17.5	32	31.5	45.5	91.5	95.5
	2.5	1	7.5	15.5	39.5	26	90.5	72
	3	2.5	24.5	29	41	39	74.5	102
	4.5	6.5	7.5	29	36.5	28	74.5	98
Average	3.85	4.05	13.95	23.75	33.3	36.55	82.6	88.6
S.D.	3.055505	3.218436	7.166473	6.953217	6.933013	8.135826	8.937437	11.45717

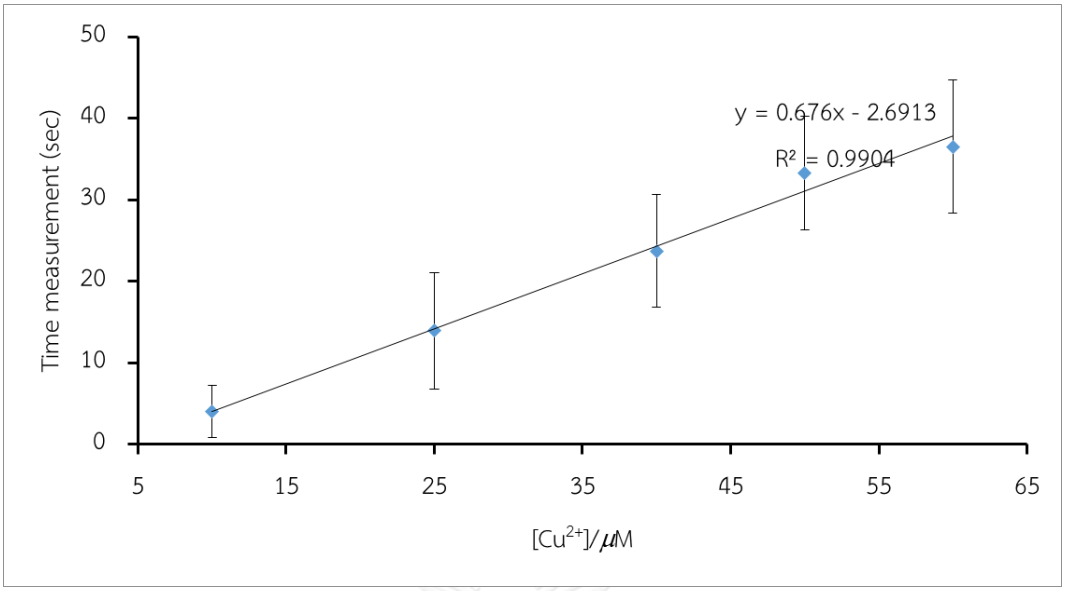

Figure A.2 The calibration curve of $T_{measurement}$ from the device (Figure 4.2) with the pre-deposited **FBA** at 25 μg/mm^2 toward copper ions in sample.

Table A.3 Time measurement for copper ions detection from the device (Figure 4.2) which pre-deposited amount of **FBA** 30 μg/mm^2

30 μg/mm^2	[Cu^{2+}]/ μM					
	0	10	25	50	75	100
Time measurement (Δt)	8	22.5	31.5	37	65.5	82.5
	10	12	42	50.5	69	95
	9	15.5	28.5	34	71	87
	10.5	16.5	31	53	57	94.5
	4	15.5	51	51.5	73.5	46.5
	6	12.5	31.5	36	69	102.5
	11	26	34	53	75.5	72
	6	28	29.5	41.5	63	88.5
	9.5	19.5	26.5	48	52.5	76
	3.5	28.5	46	44.5	66	79
Average	7.75	19.65	35.15	44.9	66.2	82.35
S.D.	2.710576	6.240771	8.24638	7.36282	7.161626	15.6951

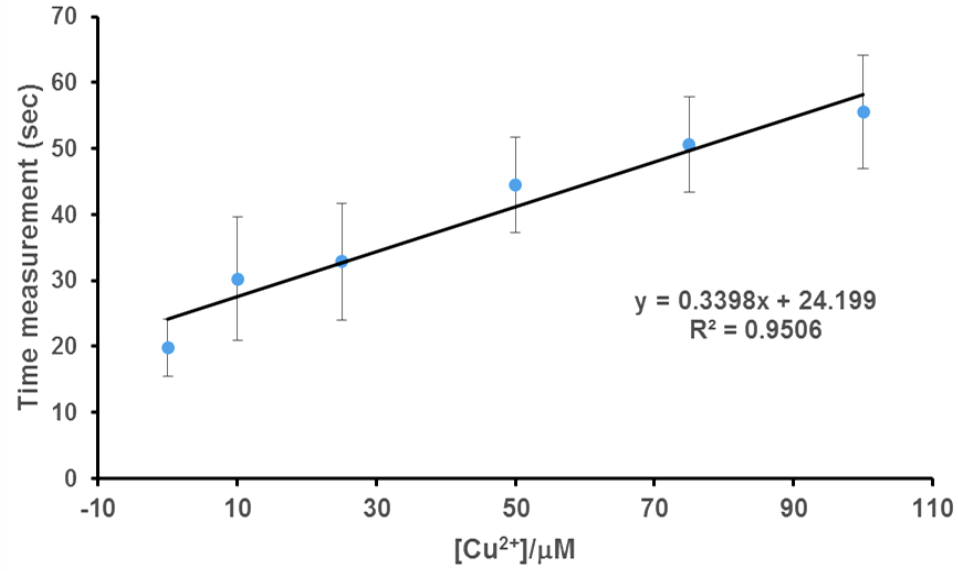

Figure A.3 The calibration curve of $T_{measurement}$ from the device (Figure 4.2) toward copper ions in sample.

Table A.4 Time measurement for copper ions detection from the device (Figure 4.2) with the pre-deposited **FBA** at 45 μg/mm^2.

45 μg/mm^2	[Cu^{2+}]/ μM							
	0	10	25	50	75	100	500	1000
Time measurement (Δt)	17.5	46.5	46	52	44	52.5	95	76
	15.5	30	37	48.5	53.5	65	80.5	119.5
	12.5	24.5	32	34	43.5	47.5	87	111.5
	21.5	28.5	33	44.5	51	50.5	97.5	82
	21	42	40	52	51	46.5	106.5	86.5
	24.5	21.5	44.5	42.5	42.5	60.5	90.5	103
	27	17	21.5	54	65	72	95.5	83.5
	19.5	24.5	22	35.5	46.5	48	106.5	96
	16.5	30	25	45	59.5	51.5	104.5	105.5
	22.5	38	27.5	37	50	61	85.5	110
Average	19.8	30.25	32.85	44.5	50.65	55.5	94.9	97.35
S.D.	4.391912	9.331101	8.9102	7.230337	7.242045	8.621678	9.103723	14.72724

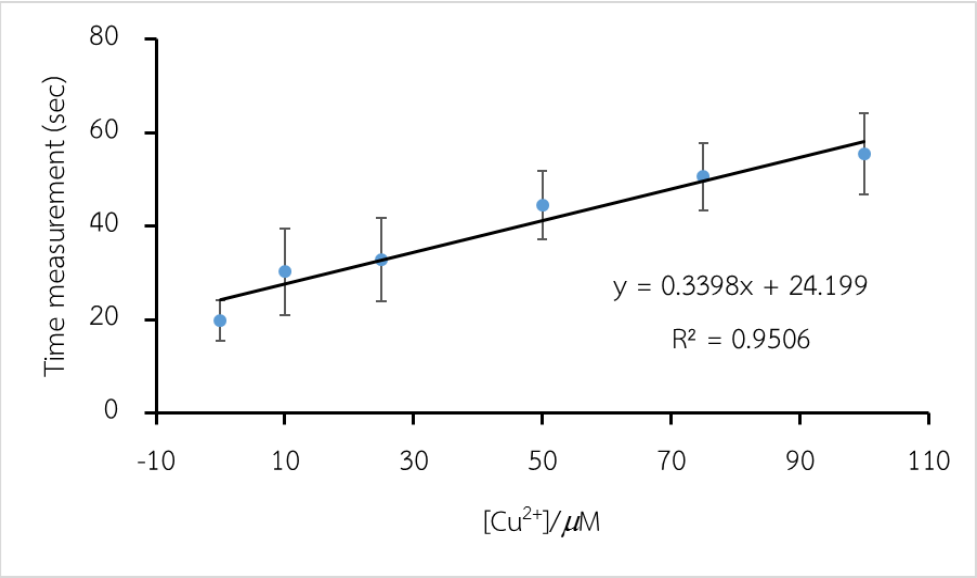

Figure A.4 The calibration curve of $T_{measurement}$ from the device (Figure 4.2) with the pre-deposited **FBA** at 45 μg/mm^2 toward copper ions in sample.

Table A. 5 Time measurement for copper ions detection from the device (Figure 4. 2) with the pre-deposited **FBA** at 55 μg/mm^2.

55 μg/mm^2 of **FBA**	[Cu^{2+}]/ μM					
	0	10	25	50	75	100
Time measurement (Δt)	23	46	39.5	54	64	90
	33	40.5	53	44.5	67.5	65
	24.5	53	54	63	58.5	87.5
	22	33	44.5	68.5	63.5	61.5
	20	43	34.5	55.5	55	70.5
	18	38.5	32	56	57	90.5
	21	52.5	56	47.5	69.5	87
	13	41	45.5	55	53.5	62.5
	18	42.5	57.5	37.5	79	85
	15.5	35.5	53.5	54.5	56	88.5
Average	20.8	42.55	47	53.6	62.35	78.8
S.D.	5.518655	6.533886	9.216531	8.831132	7.993226	12.30221

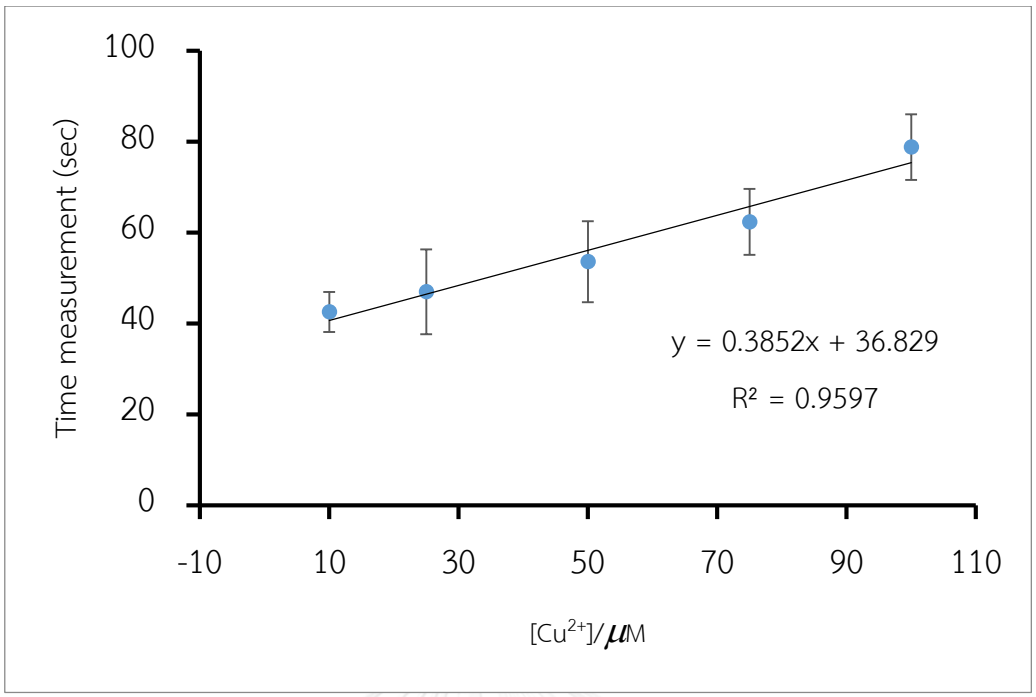

Figure A.5 The calibration curve of $T_{measurement}$ from the device (Figure 4.2) with the pre-deposited **FBA** at 55 μg/mm^2 toward copper ions in sample.

Table A. 6 Time measurement for copper ions detection from the device (Figure 4. 2) with the pre-deposited **FBA** at 70 μg/mm^2.

70 μg/mm^3	[Cu^{2+}]/ μM					
	0	10	25	50	75	100
Time measurement (Δt)	12	61	64	67.5	80.5	82.5
	28.5	57	58.5	66	72.5	81
	15	45.5	61.5	77.5	76	84
	27.5	44.5	59.5	72	88.5	81.5
	24.5	52.5	41.5	61.5	77.5	78.5
	18	38	47	66.5	80	100.5
	26.5	53.5	46	78	70	93.5
	21.5	41	55	77.5	66.5	71.5
	16	39	47.5	69	80	89
	20.5	53.5	61	58	67.5	76.5
Average	21	48.55	54.15	69.35	75.9	83.85
S.D.	5.700877	8.001562	7.944425	6.896255	6.842677	8.482171

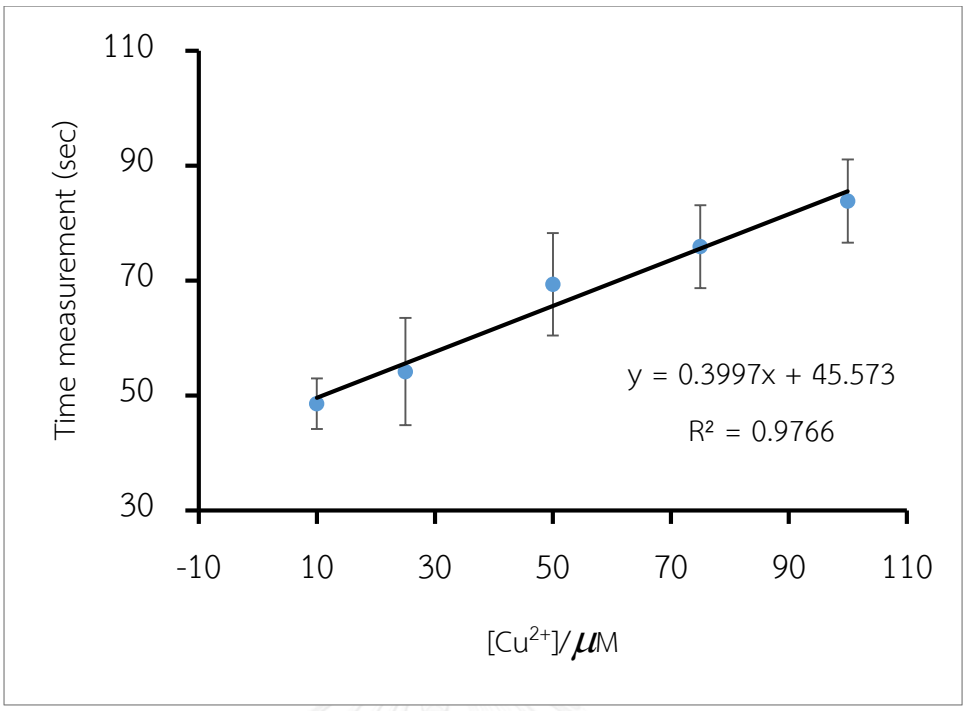

Figure A.6 The calibration curve of $T_{measurement}$ from the device (Figure 4.2) with the pre-deposited **FBA** at 70 μg/mm^2 toward copper ions in sample.

VITA

Mister Anusak Chaicham was born on October 30, 1983 in Chaiyaphum, Thailand. He graduated with a high school diploma from Phukhieo, Chaiyaphum in 2001. He received his Bachelor's degree of Science in Chemistry from Khonkean University in 2005. Since 2006, he has been a graduate student at the Department of Chemistry, Chulalongkorn University and become a member of the Supramolecular Chemistry Research Unit under supervision of Assistant Professor Dr. Boosayarat Tomapatanaget. He continue to study in Ph.D at the Department of Chemistry, Chulalongkorn University under supervision of Assistant Professor Dr. Boosayarat Tomapatanaget. Since 2016, he has been a graduate student at the Department of Chemistry, Chulalongkorn University.